UNIVERSITÉ DU QUÉBEC À MONTRÉAL

SPATIAL AND TEMPORAL VARIATIONS IN CLIMATE TRENDS FROM BOREHOLE TEMPERATURE DATA

DISSERTATION

PRESENTED

AS PARTIAL REQUIREMENT

OF THE DOCTORATE OF ENVIRONMENTAL SCIENCES

BY

CAROLYNE PICKLER

MAY 2017

UNIVERSITÉ DU QUÉBEC À MONTRÉAL

VARIATIONS SPATIALES ET TEMPORELLES DES TENDANCES CLIMATIQUES DÉDUITES DES PROFILS DE TEMPÉRATURE DU SOUS-SOL

THÈSE

PRÉSENTÉE

COMME EXIGENCE PARTIELLE

DU DOCTORAT EN SCIENCES DE L'ENVIRONNEMENT

PAR

CAROLYNE PICKLER

MAI 2017

ACKNOWLEDGEMENTS

The works presented in this dissertation represent the blood, sweat, and tears of three plus years of work. I would like to thank my supervisors, Dr. Hugo Beltrami and Dr. Jean-Claude Mareschal, for giving me the opportunity to undertake this adventure. From field work to analysis to article writing and reviewing, I have learnt so much from both of you. Furthemore, I would like to thank the UQÁM Faculty of Science, NSERC and the NSERC-CREATE Training program in Climate Science based at St. Francis Xavier University for the financial support.

The geophysics lab has also been a huge source of motivation throughout this endeavour. They have motivated me, distracted me and forced me to watch the horrible sloth short. A big thanks to the geophysics crew: Jean-Claude, Fiona, Lidia, Ignacio, Dr. Francesco Fish Geophysical Experiment, Arlette (our honorary geophysicist) and Fernando. Without your friendship, support, dances, sarcastic comments, and food/liquor, I wouldn't have survived, let alone loved this experience. A big thanks also to the SAQ, who provided the much needed libation for Friday afternoon geophysics parties.

Finally, I would like to thank my friends and family for their unconditional support and ability to put up with my craziness. Erica, thanks for listening to my rants and always understanding my klutzy moments. To my family, my parents, Andy, and Mr. Baby Bear, thanks for always cheering me on and the moral/immoral support. To my favourite Spaniard, Fernando, thanks for always making me laugh and smile and understanding every step of this crazy process.

FOREWORD

This dissertation is presented as three scientific articles that have been co-authored by my supervisors, Dr. Hugo Beltrami and Dr. Jean-Claude Mareschal. The first article entitled *Laurentide Ice Sheet basal temperatures at the Last Glacial Cycle as inferred from borehole data* has been published in *Climate of the Past* on 22 January 2016. The second article, *Climate trends in northern Ontario and Quebec from borehole temperature profiles*, has also been published in *Climate of the Past* on 16 December 2016. The third article is in preparation. The format of the published and submitted articles has been modified to satisfy the presentation criteria for Université du Québec à Montréal dissertations.

TABLE OF CONTENTS

LIST OF TABLES

LIST OF FIGURES

LIST OF ABBREVIATIONS AND ACRONYMS

BP	Before Present
CE	Common Era
CMIP5	Coupled Model Intercomparison Project Phase 5
DTS	Digital Optic-Fibre Temperature Sensing
GCM	General Circulation Model
GRACE	Gravity Recovery and Climate Experiment
GST	Ground Surface Temperature
GSTH	Ground Surface Temperature History
HCO	Holocene Climatic Optimum
LGC	Last Glacial Cycle
LGM	Last Glacial Maximum
LIA	Little Ice Age (1500-1800)
NOAA	National Oceanic and Atmospheric Administration
PMIP3	Paleoclimate Modelling Intercomparison Project Phase III
SAT	Surface Air Temperature
SVD	Singular Value Decomposition

RÉSUMÉ

Nous avons étudié le régime thermique du sous-sol et déterminé les variations du climat passé en utilisant la méthode de reconstruction de l'histoire de la température à la surface du sol à partir de profils de température mesurés dans des forages. Cette thèse, divisée en trois chapitres sous forme d'articles scientifiques, porte sur la reconstitution de l'histoire des températures à la surface du sol dans l'est et le centre du Canada et au nord du Chili sur des échelles de temps allant du dernier cycle glaciaire aux 500 dernières années.

Le premier article reconstitue les températures à la base de la calotte glaciaire Laurentide depuis le dernier cycle glaciaire jusqu'à 100 ans avant présent (AP). Treize profils profonds de température ($\geq$ 1500 m) ont été mesurés dans l'est et le centre du Canada, une région qui était couverte par la partie sud de la calotte glaciaire Laurentide. La reconstitution de la température à la surface du sol pour 100-100000 années AP montre des températures entre -1,4-3,0°C au cours du dernier maximum glaciaire, $\sim$ 20 ka. Ces température représentent donc les températures basales de la calotte glaciaire. Ces températures sont proches du point de fusion de la glace et démontrent qu'un écoulement rapide de la glace à la base était possible. Cela aurait pu entraîner une instabilité dans la calotte glaciaire car de grandes quantités d'eau pouvait être transportées depuis l'intérieur. Cependant, la couche de glace a persisté pendant $\sim$30000 ans avant son effondrement au cours de l'Holocène. Par conséquent, des températures basales proches du point de fusion de la glace n'impliquent pas nécessairement que les calottes de glace sont instables et près de l'effondrement.

Le deuxième article concerne les tendances climatiques pour les 500 dernières années dans le nord de l'Ontario et du Québec. Les histoires de température à la surface du sol de cette région sont reconstituées à partir de 18 profils de température provenant de 10 sites. Ces sites se trouvent dans la région peu échantillonnée entre 51°N- 60°N de chaque côté de la baie James. Des histoires de températures à la surface du sol similaires sont reconstituées pour les 10 sites et montrent un réchauffement climatique récent de 1-2 K pour les 150 dernières années, ce qui est en accord avec les reconstitutions plus au sud et dans l'est et le centre du Canada. Les résultats concordent aussi avec les reconstitutions disponibles de données indirectes. Nous avons trouvé un refroidissement associé avec le petit âge glaciaire

que pour un seul site. Par ailleurs, les cartes de pergélisol localisent ces forages dans une région de pergélisol discontinu, mais le pergélisol n'a pas été rencontré lors de l'échantillonnage. À l'exception du site Nielsen Island, les histoires de température à la surface du sol suggèrent également que le pergélisol était absent de la région pour les 500 dernières années. Cela pourrait être le résultat d'un décalage entre la température du sol et la température de l'air en raison de la couverture de neige dans la région et/ou l'interpolation de la température de l'air utilisée pour estimer la probabilité de présence de pergélisol dans ces régions en l'absence de mesures de températures à la surface du sol.

Le troisième article reconstitue le climat des 500 dernières années dans le nord du Chili à partir de 31 profils de température mesurés dans des forages. Il y a des tendances différentes entre les régions échantillonnées. Michilla, une région sur la côte nord du Chili, ne montre ni réchauffement ni refroidissement, tandis que la région du nord-centre suggère un réchauffement très récent de 1,9 K, à partir ~20 ans AP, suivant d'un refroidissement entre ~20-150 ans AP. L'ordre de grandeur du réchauffement est en accord avec les reconstitutions de température à la surface du sol pour le Pérou et les régions de climat semi-aride de l'Amérique du Sud mais ~1.5-2 fois plus grand que celles des données météorologiques, des reconstitutions climatiques pour le centre du Chili et le sud de l'Amérique du Sud et des températures de surface moyennes multi-modèles du millénaire passé (Paleoclimate Modelling Intercomparison Project Phase III pour le Coupled Model Intercomparison Project Phase 5). Des différences temporelles pour ce réchauffement sont observées et aucune méthode ne montre la période de refroidissement à partir ~20-150 ans AP déduite à partir des profils de température du nord du Chili. Ces différences suggèrent une tendance régionale distincte dans le nord du Chili mais pour confirmer ces conclusions nous devrons obtenir d'autres ensembles de données et d'effectuer d'autres reconstitutions.

MOTS-CLÉS: Histoires de température à la surface du sol, inversion, paléoclimats, profils de température du sous sol, régime thermique du sol.

ABSTRACT

Ground surface temperature histories reconstructed from borehole temperature-depth profiles are used to determine the past climate on varying spatial and temporal scales and study the ground thermal regime. This dissertation is presented as three articles reconstructing ground surface temperature histories on time scales from the last glacial cycle to the past 500 years in eastern and central Canada and northern Chile.

The first article reconstructs the basal temperatures of the Laurentide Ice Sheet from the last glacial cycle to 100 years BP. Thirteen deep ($\geq$1500 m) borehole temperature-depth profiles were measured in eastern and central Canada, a region that was covered by the southern portion of the Laurentide Ice Sheet. The ground surface temperature reconstructions for 100-100,000 years BP yield temperatures during the last glacial maximum, $\sim$20 ka, between -1.4-3.0°C. As the region was covered by the Laurentide Ice Sheet during this period, they represent the basal temperatures of the ice sheet. These temperatures near the pressure melting point of ice demonstrate that basal flow and fast flowing ice streams were possible. This could lead to ice sheet instability as large quantities of water could be transported from the interior. However, the ice sheet persisted for $\sim$30,000 years before collapsing during the Holocene. Therefore, basal temperatures near the melting point of ice do not solely indicate that ice sheets are unstable and on the verge of collapse.

The climate trends for the past 500 years in northern Ontario and Quebec are examined in the second article. The ground surface temperature histories from 18 borehole temperature-depth profiles from 10 sites in northern Ontario and Quebec were reconstructed. These sites lie in the poorly sampled region between 51°N-60°N on either side of James Bay. Similar ground surface temperature histories are reconstructed from the regions with a recent climate warming for the past 150 years of 1-2 K, agreeing with reconstructions for the southern portion of eastern and central Canada and available proxy data. However, a cooling period associated with the little ice age is only found at one site. Furthermore, permafrost maps locate these boreholes in a region of discontinuous permafrost but permafrost was not encountered during sampling. With the exception of Nielsen Island, the ground surface temperature histories also suggest that the region was

void of permafrost for the past 500 years. This could be the result of an offset between ground and surface air temperatures due to snow cover in the region and/or air surface temperature interpolation used in permafrost models being unsuitable to represent the spatial variability of ground temperatures.

The third article reconstructs the climate of the past 500 years in northern Chile from 31 borehole temperature-depth profiles located in two regions, northern coastal Chile and north-central Chile. Trends differ between sampled regions, which is not surprisings since they are over 500 km apart. The ground surface temperature history of Michilla, in northern coastal Chile, shows no warming or cooling signal. The north-central Chile ground surface temperature history has a very recent warming signal of 1.9 K, starting ~20 years BP, preceded by a cooling from ~20-150 years BP. The magnitude of this warming signal agrees with ground surface temperature reconstructions for Peru and the semiarid regions of South America but is ~1.5-2 times greater than that found in meteorological data, climate reconstructions from other proxies for central Chile and southern South America and multi-model mean surface temperatures from the past millennium simulations of the Paleoclimate Intercomparison Modelling Project Phase III for the Coupled Model Intercomparison Project Phase 5. Differences are observed in the timing of the warming and the cooling period from ~20-150 years BP in north-central Chile is only inferred from the ground surface temperature history. A regional trend for northern Chile that cannot be resolved on the gridpoint scale could explain these differences. However, more data sets and reconstructions are needed to confirm these conclusions and determine the long-term climatic trends in northern Chile.

KEYWORDS: ground surface temperature histories, inversion, paleoclimate, borehole temperature-depth profiles, ground thermal regime.

INTRODUCTION

With evidence for increasing global temperatures, there is concern about the consequences climate change will have on society and natural ecosystems. Models of Earth's climate, such as those from general circulation models (GCMs), allow for the study of various future climate scenarios. However, these models must be calibrated and tested against paleoclimate data and reconstructions to assess their robustness. These paleoclimate data and reconstructions also provide insight to how past climate responded to different forcings, indicating how future climate might respond to increases in carbon dioxide in the atmosphere. As the meteorological record extends back, at best, 150 years, proxy climate indicators are necessary to resolve past climate trends. Pollen, tree rings, oxygen isotopes in ice cores and deep sea sediments, corals and borehole temperature data are some examples of proxy climate indicators. Different parameters characterizing the climate can be reconstructed from these climate-dependent natural phenomenon (Bradley, 1999). The width of tree rings, which depend on temperature and precipitation during the growth season, are measured to infer past climate. Pollen assemblages found in sediment cores from lakes, ponds, or oceans indicate the type of vegetation present during the period of sedimentation and allow scientists to infer the local climate. Seasonal variations in temperature and precipitation can be tracked by variations in the ratio of oxygen isotopes ($\delta^{18}O$). The ratio of oxygen isotopes in deep sea sediment depends on oceanic temperature and on the total volume of ice caps and glaciers. In ice cores, the ratio of oxygen isotopes depends on the temperature of the air above the glaciers when snow accumulated. Borehole temperature data are obtained by measuring how temperature varies

with depth in a borehole, which is used to determine ground surface temperature (GST) history. Proxy climate indicators have different advantages, disadvantages, uncertainties, and spatial and temporal resolutions. High resolution proxies, such as tree-rings, can resolve seasonal to decadal changes but have difficulty resolving long-term climate trends. On the other hand, low resolution proxies (ex. borehole temperature data) resolve multi-decadal to centennial trends and highlight long-term climate trends. In this thesis, we use borehole temperature data to reconstruct past climate and its variability.

Borehole climatology assumes that GST and surface air temperature (SAT) are coupled. Model simulations (García-García *et al.*, 2016) and comparison of borehole temperature data with records from nearby meteorological stations (Harris and Chapman, 1998; Beltrami, 2001) have confirmed this hypothesis. The first attempt at inferring climate from these temperature data was made by Hotchkiss and Ingersoll (1934), who estimated the timing of the last glacial retreat from temperature measurements in the Calumet copper mine in northern Michigan. However, it was only in the 1970s that systematic studies were conducted (e.g., Cermak, 1971; Sass *et al.*, 1971; Vasseur *et al.*, 1983). With concern about climate change in the 1980s, studies estimating recent ground temperature changes (<300 years) became widespread (Lachenbruch and Marshall, 1986; Lachenbruch, 1988). Numerous high-resolution temperature measurements in shallow mining exploration boreholes (a few hundred meters), primarily made for heat flux studies, are available for studies of recent climate variations (<500 years) and led to many local, regional, and global studies (e.g., Huang *et al.*, 2000; Harris and Chapman, 2001; Gosselin and Mareschal, 2003; Beltrami and Bourlon, 2004; Pollack and Smerdon, 2004; Chouinard *et al.*, 2007; Jaume-Santero *et al.*, 2016). The global reconstruction of Huang *et al.* (2000) used temperature data from 616 boreholes. However, the geographical coverage of these is very uneven, with several subconti-

nents void of data and reconstructions. Furthermore, the majority of these studies focus on recent climate trends (<500 years) since there are very few deep (≥1500 m) boreholes available to reconstruct on longer timescales.

The objective of this work is to expand the spatial and temporal scale of climate studies based on borehole temperature data. This will require the addition of borehole temperature data and reconstructions in regions void of data so far and, with deeper boreholes, provide insight to their long-term climatic trends. Firstly, we expanded the timescale and measured deep boreholes (≥1500 m) in eastern and central Canada to reconstruct the climate of the Last Glacial Cycle (LGC), a period ~120,000-12,000 years BP when large ice sheets covered most of the northern regions in the Northern Hemisphere. Secondly, we reconstructed the climate of the past 500 years in northern Ontario and Québec. This region on both sides of James Bay was previously void of borehole temperature data and reconstructions. Finally, we examined the climate trends for the last 500 years in northern Chile. Along with a lack of northern Chile borehole GST reconstructions, the South American continent has seen very few paleoclimate reconstructions.

0.1 GST reconstructions from borehole temperature data

Earth's subsurface thermal regime is governed by the outflow of heat from the interior and persistent temporal variations in GST. In homogeneous rock, assuming negligible heat production, and without GST variations, temperature increases linearly with depth. Long-term persistent GST variations propagate into the subsurface and are recorded as perturbations to this linear quasi-steady state geotherm (e.g., Hotchkiss and Ingersoll, 1934; Birch, 1948; Beck, 1977). The extent to which they are recorded is proportional to their duration and amplitude and decreases with the time when they occurred. For periodic oscillations in sur-

face temperature, the thermal perturbation propagates downward as a damped wave. Its amplitude decreases exponentially with depth over a length scale, δ (skin depth), such that $\delta = \sqrt{\kappa T/\pi}$: where T is the period and κ is the thermal diffusivity ($\sim 10^{-6} m^2 s^{-1}$ or $\sim 31.5 m^2 yr^{-1}$). This damping allows for the preservation of the long-term climatic signal by removing the high-frequency variability present in meteorological records.

Reconstructing the GST history from borehole temperature data consists of an inverse geophysical problem. The inversion involves solving for $K + 2$ unknown parameters for each depth where temperature is measured: (1) the long-term surface temperature or the reference surface temperature (T_o), (2) the steady-state heat flux or the reference heat flux (q_o), and (3) the GST changes (ΔT_k) for K time intervals. Different techniques have been utilized to obtain GST histories from borehole temperature data (e.g., Vasseur *et al.*, 1983; Nielsen and Beck, 1989; Shen and Beck, 1991; Mareschal and Beltrami, 1992; Clauser and Mareschal, 1995; Mareschal *et al.*, 1999b). Here, singular value decomposition is used as it has a straightforward application to GST reconstructions and reduces the impact of noise and errors on the solution (Lanczos, 1961). Further details can be found in Mareschal and Beltrami (1992), Clauser and Mareschal (1995), Beltrami and Mareschal (1995), and Beltrami *et al.* (1997).

0.2 Measuring borehole temperature data

Several methods exist to measure borehole temperature. The conventional method involves lowering a calibrated thermistor attached to a cable into a borehole and measuring resistance (i.e. temperature), at fixed depth intervals or continuously. This results in temperature measurements with a precision better than 0.005 K and an accuracy on the order of 0.02 K. An alternative method is digital optic-fibre

temperature sensing (DTS), which is based on the measurement of a backscattered laser light pulse through a fibre-optic cable (Förster *et al.*, 1997; Förster and Schrötter, 1997). This results in the instantaneous measurement of the entire profile once the cable has been completely lowered into the borehole and yields temperature measurements with a precision of 0.3°C. A detailed description of this methodology can be found in Förster *et al.* (1997), Förster and Schrötter (1997), Hausner *et al.* (2011) and Suárez *et al.* (2011). When available, core samples are obtained to measure thermal conductivity, usually by the method of divided bars (Misener and Beck, 1960), and heat production.

0.3 Suitability of borehole temperature data for climate studies

We have applied several selection criteria to retain only borehole temperature data suitable for climate studies. Changes in surface conditions, such as vegetation or snow cover, can alter the assumed GST and SAT coupling and therefore must be taken into consideration when determining the suitability for climate. Topography is known to distorts the temperature isotherms (Jeffreys, 1938). A positive topography leads to a reduced temperature gradient and an apparent warming signal (Blackwell *et al.*, 1980; Lewis and Wang, 1992). Sites with significant topography must be excluded. Proximity to lakes is also known to distort temperature isotherms. This occurs when the mean distance between a lake and a borehole is less than the depth of the borehole, resulting in a warming or cooling signal depending on the dip and azimuth of the hole (Lewis and Wang, 1992). The time period of interest must be considered to ensure that only boreholes deep enough are retained. The suitable depth (z) is determined by the scaling relationship $z \approx 2\sqrt{t\kappa}$, where κ is thermal diffusivity and t is time. Finally, profiles are visually examined to ensure that there are no discontinuities in the profile or signs of water flow. When a profile meets the selection criteria, it can be used to determine the

GST history.

0.4 Application of GST reconstructions

The results of this dissertation are presented in three distinct chapters as three scientific articles. The first and second articles have been published in Climate of the Past and the third is in preparation. A brief overview of each article follows.

0.4.1 Basal temperatures of the Laurentide Ice Sheet

The first article reconstructs the GST history for 100 to 100,000 years BP in eastern and central Canada. During the LGC, ~120,000-12,000 years BP, the Laurentide Ice Sheet covered almost all of Canada. Thirteen deep ($\geq$ 1500 m) borehole temperature-depth profiles were measured in eastern and central Canada from the region covered by the southern portion of the Laurentide Ice Sheet and used to determine the GST history from 100 to 100,000 years BP. The Laurentide Ice Sheet persisted over 30,000 years with its largest extent during the Last Glacial Maximum (LGM), ~20,000 years BP. The examination of basal conditions during the LGM elucidate the basal conditions of a stable ice sheet and provide insight to the fate and stability of the present-day ice sheets, Antarctica and Greenland.

The GST histories show basal temperatures near the pressure melting point of ice (-1.4°C to 3.0°C) during the LGM. This indicates the possibility of basal melt and fast flowing ice streams. These processes are hypothesized to play a key role in glacial terminations as they can transport large quantities of water from the interior, leading to a thin, climatically vulnerable ice sheet (Marshall and Clark, 2002). Since the ice sheet persisted for over 30,000 years, our results indicate that basal temperatures near the pressure melting point of ice do not necessarily imply

that an ice sheet is unstable and on the verge of collapse.

0.4.2 Climate in northern Ontario and Québec for the past 500 years

The second article involves determining the GST histories for the past 500 years in northern Ontario and Québec. Many studies have been undertaken in the Canadian Arctic and the southern portion of eastern and central Canada (southern portion of Superior Province) but the region between 50°N and 60°N has remained void of GST histories (e.g., Beltrami and Taylor, 1995; Huang *et al.*, 2000; Harris and Chapman, 2001; Gosselin and Mareschal, 2003; Beltrami and Bourlon, 2004; Majorowicz *et al.*, 2004; Pollack and Smerdon, 2004; Chouinard *et al.*, 2007; Jaume-Santero *et al.*, 2016). We analyzed twenty-five borehole temperature-depth profiles measured in northern Ontario and Québec, on either side of James Bay, between 50°N and 60°N and reconstructed the GST for the past 500 years to examine the long-term climate trends in the region. Furthermore, permafrost maps locate this region is a zone of discontinuous permafrost and isolated patches of permafrost (Brown, 1979). This allows for the investigation of whether borehole temperature data and GST histories can be useful tools for permafrost studies.

The GST histories for northern Ontario and Québec show a warming of 1.5±0.8 K for the last 150 years. This agrees with the warming of ~1-2 K for the past 150 years reconstructed for the southern portion of the Superior Province. A little ice age (LIA) signal was observed at only one site, Otoskwin, in northern Ontario. This is surprising as paleoclimatic reconstructions from pollen data found their greatest little ice age signal, a cooling of 0.3°C, in northern Québec (Gajewski, 1988; Viau and Gajewski, 2009). This could be due to insufficient resolution since a cooling between 200 and 500 years BP is difficult to resolve in the presence of noise. It could also be associated with an early little ice age (Chouinard *et al.*, 2007) or be masked by physical effects (Gosselin and Mareschal, 2003).

Permafrost was not encountered during sampling of any of the 25 boreholes. As the majority lie in isolated patches of permafrost, these statistics do not allow us to draw any conclusions. However, researchers from the GEOTOP and the Institut de Physique du Globe de Paris sampled more than 60 boreholes in the sporadic discontinuous permafrost region of Manitoba and only encountered permafrost at one site. This points to disparities with permafrost maps and leads to questions about their robustness. Furthermore, the GST histories for the past 500 years remained well above freezing at all sites except Nielsen Island indicating a low probability of permafrost. This illustrates that borehole temperature data and GST histories could be useful in permafrost mapping and studies.

0.4.3 Climate trends in northern Chile

The third article focuses on reconstructing the climatic trends for the past 500 years in northern Chile. Many data sets and reconstructions are available for the Northern Hemisphere (e.g., Mann *et al.*, 1999; Moberg *et al.*, 2005; Rutherford *et al.*, 2005). However, these are lacking for the Southern Hemisphere, in particular South America, where knowledge of the past climate is limited (Huang *et al.*, 2000; Mann and Jones, 2003; IPCC, 2013). Thirty-one borehole temperature-depth profiles from northern Chile have been analyzed to reconstruct the climate of the past 500 years. The profiles suitable for climate lie in two regions: northern coastal Chile and north-central Chile

Differing trends were observed between the regions of northern coastal Chile and north-central Chile. This is not surprising as these two regions are over 500 km apart. The GST history of northern coastal Chile shows no warming or cooling. A climate signal, however, was observed in north-central Chile. Between 1500 and ~1800, no warming or cooling is found in the GST. A cooling of ~0.5

K was recorded between ~1800 and 1940, followed by a warming of ~2 K. The amplitude of this warming agrees with the GST history from borehole temperature data from two sites in Peru, at the northern edge of the Atacama Desert. But, no cooling signal is found in the Peruvian GST history. Meteorological data from north-central Chile show a pronounced cooling of ~2.5 K between 1950 and 1960. This could explain the cooling present in the north-central Chile GST history as a local feature. The north-central Chile GST history was also compared with data from the CRUTEM4, paleoclimate proxy reconstructions for central Chile and southern South America, and with climate model simulations. These comparisons show several differences: (1) the cooling signal is only present in the north-central Chile GST and (2) a greater warming signal (~2 K) is observed in the GST reconstructions. These differences could be attributed to the coarse gridding of the CRUTEM4 and climate simulation and their lack of resolution in central Chile and southern South America. More data and reconstructions are required to resolve the long-term climatic trends in northern Chile.

0.5 Originality and contribution

The three articles are original studies that have not been previously undertaken. While Chouinard and Mareschal (2009) have previously studied the basal temperatures of the Laurentide Ice Sheet, I have expanded their data set and reanalyzed all borehole temperature data. I have also compared inversions with the first order estimation of GST, a new technique. My results led to conclusions concerning the present-day ice sheets. My contribution has been key to the completion of these works. For the three articles, I processed the data, performed the analyses, and wrote the articles. Furthermore for the first and third article, I took part in the field work to obtain the borehole temperature-depth profiles. My directors, Hugo Beltrami and Jean-Claude Mareschal, have co-authored all three articles. Discussion with them throughout the work has been influencial in shaping it and they

played an important role in editing all the articles and responses to reviewers.

CHAPTER I

LAURENTIDE ICE SHEET BASAL TEMPERATURES AT THE LAST GLACIAL CYCLE AS INFERRED FROM BOREHOLE DATA

Manuscript published in Climate of the Past[1]

---

[1]Pickler, C., Beltrami, H., and Mareschal, J.C., 2016. Laurentide Ice Sheet basal temperatures at the Last Glacial Cycle as inferred from borehole data, Climate of the Past, 11, 3937-3971, doi:10.5194/cp-12-115-2016

Abstract

Thirteen temperature-depth profiles (≥1500 m) measured in boreholes in eastern and central Canada were inverted to determine the ground surface temperature histories during and after the last glacial cycle. The sites are located in the southern part of the region covered by the Laurentide Ice Sheet. The inversions yield ground surface temperatures ranging from -1.4 to 3.0°C throughout the last glacial cycle. These temperatures, near the pressure melting point of ice, allowed basal flow and fast flowing ice streams at the base of the Laurentide Ice Sheet. Despite such conditions, which have been inferred from geomorphological data, the ice sheet persisted throughout the last glacial cycle. Our results suggest some regional trends in basal temperatures with possible control by internal heat flow.

1.1 Introduction

The impact of future climate change on the stability of the present-day ice sheets in Greenland and Antarctica is a major concern of the scientific community (e.g. Gomez *et al.*, 2010; Mitrovica *et al.*, 2009). Satellite gravity measurements performed during the GRACE mission suggest that the mass loss of the Greenland and Antarctic glaciers has accelerated during the decade 2002-2012 (Velicogna and Wahr, 2013). Over the past two decades, mass loss from the Greenland Ice Sheet has quadrupled and contributed to a fourth of global sea level rise from 1992 to 2011 (Church *et al.*, 2011; Straneo and Heimbach, 2013). In 2014, two teams of researchers noted that the collapse of the Thwaites Glacier Basin, an important component holding together the West Antarctic Ice Sheet, was potentially underway (Joughin *et al.*, 2014; Rignot *et al.*, 2014). The collapse of the entire West Antarctic Ice Sheet would lead to rise in sea level by at least 3 m. The present observations of the ice sheet mass balance are important. However, to predict the effects of future climate change on the ice sheets, it is necessary to fully understand the mechanisms of ice sheet growth, decay, and collapse throughout the past glacial cycles. The models of ice sheet dynamics during past glacial cycles show that the thickness and elevation of the ice sheets and the thermal conditions at their base are key parameters controlling the basal flow regime and the evolution of the ice volume (Marshall and Clark, 2002; Hughes, 2009).

During the last glacial cycle (LGC), $\sim$ 120000-12000 yrs BP, large ice sheets formed in the Northern Hemisphere, covering Scandinavia and almost all of Canada (Denton and Hughes, 1981; Peltier, 2002, 2004; Zweck and Huybrechts, 2005). The growth and decay of ice sheets are governed mainly by ice dynamics and ice sheet-climate interactions (Oerlemans and van der Veen, 1984; Clark, 1994; Clark and Pollard, 1998). Ice dynamics are also strongly controlled by the underlying geolog-

ical substrate and associated processes (Clark *et al.*, 1999; Marshall, 2005). Clark and Pollard (1998) studied how the ice thickness and the nature of the geological substrate control flow at the base of the glacier. They showed that soft beds, beds of unconsolidated sediment at relatively low relief, result in thin ice sheets that are predisposed to fast ice flow when possible. Hard beds, beds of high relief crystalline bedrock, on the other hand, provide the ideal conditions for the formation of larger, thick ice sheets that experience stronger bed-ice sheet coupling and slow ice flow. Basal flow rate is also affected by the basal temperatures, which play a key role in determining the velocity. However, the ice sheet evolution models use basal temperatures that are poorly constrained because of the lack of direct data pertaining to thermal conditions at the base of ice sheets. The objective of the present study is to use borehole temperature depth data to estimate how the temperatures varied at the base of the Laurentide Ice Sheet during the last glacial cycle.

Temporal variations in ground surface temperatures (GST) are recorded by Earth's subsurface as perturbations to the "steady-state" temperature profile (e.g., Hotchkiss and Ingersoll, 1934; Birch, 1948; Beck, 1977; Lachenbruch and Marshall, 1986). With no changes in GST, the thermal regime of the subsurface is governed by the outflow of heat from Earth's interior resulting in a profile where temperature increases with depth. In homogeneous rocks without heat sources, the "equilibrium temperature" increases linearly with depth. When changes in ground surface temperature occur and persist, they are diffused downward and recorded as perturbations to the semi-equilibrium thermal regime. These perturbations are superimposed on the temperature-depth profile associated with the flow of heat from Earth's interior. For periodic oscillations of the surface temperature, the temperature fluctuations decrease exponentially with depth such that:

$$T(z,t) = \Delta T \exp(i\omega t - z\sqrt{\frac{\omega}{2\kappa}}) \exp(-z\sqrt{\frac{\omega}{2\kappa}}) \qquad (1.1)$$

where z is the depth, t is time, κ is the thermal diffusivity of the rock, ω is the frequency, and ΔT is the amplitude of the temperature oscillation. Long time persistent transients affect subsurface temperature to great depths. Hotchkiss and Ingersoll (1934) were the first to attempt and infer past climate from such temperature-depth profiles, specifically they estimated the timing of the last glacial retreat from temperature measurements in the Calumet copper mine in northern Michigan. Birch (1948) estimated the perturbations to the temperature gradient caused by the last glaciation and suggested a correction to heat flux determinations in regions that had been covered by ice during the LGC. A correction including the glacial-interglacial cycles of the past 400,000 years was proposed by Jessop (1971) to adjust the heat flow measurements made in Canada. It was only in the 1970s that systematic studies were undertaken to infer past climate from borehole temperature profiles (Cermak, 1971; Sass *et al.*, 1971; Beck, 1977). The use of borehole temperature data for estimating recent (<300 years) climate changes became widespread in the 1980s because of concerns about increasing global temperatures (Lachenbruch and Marshall, 1986; Lachenbruch, 1988). High precision borehole temperature measurements have been mostly made for estimating heat flux in relatively shallow (a few hundred meters) holes drilled for mining exploration. Such shallow boreholes are suitable for studying recent (<500 years) climate variations and the available data have been interpreted in many regional or global studies (e.g., Bodri and Cermak, 2007; Jaupart and Mareschal, 2011, and references therein). However, very few deep ($\geq$1500 m) borehole temperature data are available to study climate variations on the time scale of 10 to 100 kyr. Oil exploration wells are usually a few km deep but are not suitable because the temperature measurements are not made in thermal equilibrium and lack the required precision. Nonetheless a few deep mining exploration holes have been drilled, mostly in Precambrian Shields, where temperature measurements can be used for climate studies on the time scale of the LGC. In Canada, Sass *et al.*

(1971) measured temperatures in a deep (3000 m) borehole near Flin Flon, Manitoba, and used direct models to show that the surface temperature during the last glacial maximum (LGM), $\sim$ 20,000 yrs BP, could not have been more than 5 K colder than present. Other Canadian deep boreholes temperature profiles have since been measured revealing regional differences in temperatures during the LGM. From a deep borehole in Sept-Iles, Québec, Mareschal *et al.* (1999b) found surface temperatures to be approximately 10 K colder than present. This was confirmed by Rolandone *et al.* (2003b) who studied four deep holes and suggested that LGM surface temperatures were colder in eastern Canada than in central Canada. Chouinard and Mareschal (2009) examined eight deep boreholes located from central to eastern Canada and observed significant regional differences in heat flux, temperature anomalies and ground surface temperature histories. Majorowicz *et al.* (2014) have studied a 2,400m deep well near Fort McMurray, Alberta, penetrating in the basement. They interpreted the variations in heat flux as due to a 9.6 K increase in surface temparature at 13 ka. Majorowicz and Šafanda (2015) have revised this estimate to include the effect of the variations of heat productions with depth which is non negligible in granitic rocks with high heat production. They concluded that temperatures at the base of the ice sheet in Northern Alberta were about $-3°C$ during the LGM. On the other hand, studies of deep boreholes in Europe lead to different conclusions for the Fennoscandian Ice Sheet which covered parts of Eurasia during the LGC (e.g., Demezhko and Shchapov, 2001; Kukkonen and Jõeleht, 2003; Šafanda *et al.*, 2004; Majorowicz *et al.*, 2008; Demezhko *et al.*, 2013; Demezhko and Gornostaeva, 2015) . Kukkonen and Jõeleht (2003) analyzed heat flow variations with depth in several boreholes from the Baltic Shield and the Russian Platform and found a 8 ± 4.5 K temperature increase following the LGM. Demezhko and Shchapov (2001) studied a $\sim$ 5 km deep borehole in the Urals, Russia, and found a postglacial warming of 12-13 K with basal temperatures below the melting point of ice during the LGM. This

was confirmed by recent work indicating that temperatures in the Urals were $\sim -8°C$ at the LGM (Demezhko and Gornostaeva, 2015).

In this study, we shall examine all the deep borehole temperature profiles measured in central and eastern Canada in order to determine the temperature at the base of the Laurentide Ice Sheet, which covered the area during the LGC. The geographical extent of the study is confined to the southern portion of the Laurentide Ice Sheet because deep mining exploration boreholes have only been drilled in the southernmost part of the Canadian Shield.

1.2 Theory

For calculating the temperature-depth profile, we assume that heat is transported only by vertical conduction and that the temperature perturbation is the result of a time-varying, horizontally uniform, surface temperature boundary condition. The temperature at depth in the Earth, for a homogeneous half space with horizontally uniform variations in the surface temperature, can be written as:

$$T(z) = T_o + Q_o R(z) - \int_0^z \frac{dz'}{\lambda(z')} \int_0^{z'} H(z")dz" + T_t(z) \tag{1.2}$$

where T_o is the reference ground surface temperature ("steady-state"/long-term surface temperature), Q_o is the reference heat flux ("steady-state" heat flux from depth), $\lambda(z)$ is the thermal conductivity, z is depth, H is the rate of heat generation, and $T_t(z)$ is the temperature perturbation at depth z due to time-varying changes to the surface boundary condition. $R(z)$ is the thermal resistance to depth z, which is defined as:

$$R(z) = \int_0^z \frac{dz'}{\lambda(z')} \tag{1.3}$$

Thermal conductivity is measured on core samples, usually by the method of di-

vided bars (Misener and Beck, 1960). Radiogenic heat production is also measured on core samples. The temperature perturbation at depth z resulting from surface temperature variations can be written as (Carslaw and Jaeger, 1959):

$$T_t(z) = \int_0^\infty \frac{z}{2\sqrt{\pi\kappa t^3}} \exp\left(\frac{-z^2}{4\kappa t}\right) T_o(t)dt \tag{1.4}$$

where t is time before present, κ is thermal diffusivity and $T_o(t)$ is the surface temperature at time t (Carslaw and Jaeger, 1959). For a stepwise change ΔT in surface temperature at time t before present, the temperature perturbation at depth z is given by (Carslaw and Jaeger, 1959):

$$T_t(z) = \Delta T \text{erfc}\left(\frac{z}{2\sqrt{\kappa t}}\right) \tag{1.5}$$

where erfc is the complementary error function.

If the ground surface temperature variation is approximated by a series of constant values ΔT_k during K time intervals (t_{k-1}, t_k), the temperature perturbation can be written as follows:

$$T_t(z) = \sum_{k=1}^{K} \Delta T_k \left(\text{erfc}\frac{z}{2\sqrt{\kappa t_k}} - \text{erfc}\frac{z}{2\sqrt{\kappa t_{k-1}}}\right) \tag{1.6}$$

The ΔT_k represent the departure of the average GST during each time interval from T_o.

1.2.1 First order estimate of the GST History

We have directly used variations in the long-term surface temperature with depth to obtain a first order estimate of time variations in surface temperature. To interpret subsurface anomalies as records of GST history variations, we must separate the climate signal from the quasi steady-state temperature profile. The quasi steady-state thermal regime is estimated by a least squares linear fit to the

lowermost 100 m section of the temperature-depth profile. The slope and the surface intercept of the fitted line are interpreted as the "steady-state" temperature gradient Γ_o and the long-term surface temperature T_o respectively. The bottom part of the profile is the section least affected by the recent changes in surface temperature and dominated by the steady-state heat flow from Earth's interior. When we are using a shallower section of the profile, the estimated long-term temperature and gradient are more affected by recent perturbations in the surface temperature. The shallower the section, the more recent the perturbation. Thus we determine how the estimated long-term surface temperature varies with time by iterating through different sections of the temperature-depth profile. Using the scaling of equation 1.5, the time it takes for the surface temperature variation to propagate into the ground and the depth of the perturbations are related by:

$$t \approx z^2/4\kappa \tag{1.7}$$

with κ thermal diffusivity, z is the depth, and t is time.

This approach yields only a first order estimate because the temperature perturbations are attenuated as they are diffused downward. However, the temporal variation of the long-term surface temperature is obtained by extrapolating the semi-equilibrium profile to the surface. The effect of a small change in gradient on the long-term surface temperature is proportional to the average depth where the gradient is estimated. Variations in the calculated long-term surface temperature are thus less attenuated than the perturbations in the profile and may well provide a gross approximation of the GST history, but independent of the model assumptions in an inversion procedure.

1.2.2 Inversion

In order to obtain a more robust estimate of the GST histories, we have inverted the temperature-depth profiles for each site and, whenever profiles from

nearby sites are available, we have inverted them jointly. The inversion consists of determining T_o, Q_o, and the ΔT_k from the temperature-depth profile (equation 1.6). For each depth where temperature is measured, equation 1.6 yields a linear equation in ΔT_k. For N temperature measurements, we obtain a system of N linear equations with $K+2$ unknowns, T_o, Q_o, and K values of ΔT_k. Even when $N \geq K+2$, the system seldom yields a meaningful solution because it is ill-conditioned. This means that the solution is unstable and a small error in the data results in a very large error in the solution (Lanczos, 1961). Different authors have proposed different inversion techniques to obtain the GST history from the data (e.g., Vasseur *et al.*, 1983; Shen and Beck, 1983; Nielsen and Beck, 1989; Wang, 1992; Shen and Beck, 1991; Mareschal and Beltrami, 1992; Clauser and Mareschal, 1995; Mareschal *et al.*, 1999b). Here, to obtain a "solution" regardless of the number of equations and unknowns and to reduce the impact of noise and errors on this solution, singular value decomposition is used (Lanczos, 1961; Jackson, 1972; Menke, 1989). This technique is well documented and further details can be found in Mareschal and Beltrami (1992), Clauser and Mareschal (1995), Beltrami and Mareschal (1995), and Beltrami *et al.* (1997).

1.2.3 Simultaneous inversion

As meteorological trends remain correlated over a distance on the order of 500 km (Beltrami *et al.*, 1997), boreholes within the same region are assumed to have been affected by the same surface temperature variations and their subsurface temperature anomalies are expected to be consistent. This holds only if the surface conditions are identical for all boreholes. If these conditions are met, jointly inverting different temperature-depth profiles from the same region will increase the signal to noise ratio. Singular value decomposition was used to jointly invert the sites with multiple boreholes. A detailed description and discussion of the methodology can be found in papers by Beltrami and Mareschal (1995) and

Beltrami *et al.* (1997).

1.3 Data Description

We have used thirteen deep boreholes ($\geq$1500 m) across eastern and central Canada to determine the temperature throughout and after the LGC. All the sites are located in the southern portion of the Canadian Shield, which was covered by the Laurentide Ice Sheet that extended over most of Canada during the LGC (Figure 1.1). Borehole locations and depths are summarized in Table 1.1. All the holes that we logged were drilled for mining exploration. The only exception is Flin Flon that was drilled to be instrumented with low noise seismometers for monitoring nuclear tests. Detailed description of the measurement techniques as well as the relevant geological information can be obtained from the heat flow publications (Sass *et al.*, 1971; Mareschal *et al.*, 1999b,a; Rolandone *et al.*, 2003a,b; Perry *et al.*, 2006, 2009; Jaupart *et al.*, 2014). We shall briefly summarize the main steps of the measurement technique has been described in several papers (e.g. Mareschal *et al.*, 1989; Perry *et al.*, 2006; Lévy *et al.*, 2010). Temperature is measured at 10 m intervals along the hole by lowering a calibrated probe with a thermistor. The precision of the measurements is better than 0.005K with an overall accuracy estimated to be of the order 0.02K Thermal conductivity is measured on core samples. Samples are collected in every lithology with an average of one sample per 80m. The thermal conductivity is measured with a divided bar apparatus on five cylinders of the core with thickness varying between 0.2 and 1.0cm. This method based on five measurements on relatively large core samples provides the best estimate of the thermal conductivity of the bulk rock and is unaffected by small heterogeneities. Samples of the core have also been analyzed for heat production following the method described by Mareschal *et al.* (1989).

A description of eight sites, Flin Flon, Pipe, Manitouwadge 0610, Manitouwadge

0611, Balmertown, Falconbridge, Lockerby, and Sept Iles, can be found in Rolandone *et al.* (2003b) and Chouinard and Mareschal (2009). Five additional profiles (Owl, near Thompson, Manitoba, Victor and Craig Mines both near Sudbury, Ontario, Matagami and Val d'Or, Québec) were analyzed. The Val d'Or borehole was logged in 2010 to a depth of ~1750 m. It is situated 15 km east of the mining camp of Val d'Or, Québec in a flat forested area. The Matagami borehole is located near the mining camp of Matagami, some 300 km north of Val d'Or. The Owl borehole, which was logged in 1999 and 2001, is located ~5 km from the Birchtree Mine and ~8 km south of the city of Thompson, Manitoba. The two other new boreholes, Craig Mine and Victor Mine, are located within the Sudbury structure, north-east of Lake Huron, in Ontario. The Craig Mine borehole, near the town of Levack, north-west of Sudbury, was logged in 2004. The deep mine was in operation when measurements were made and pumping activity was continuous to keep the deep mine galleries from flooding. The Victor Mine site was sampled in 2013, close to the community of Skead, north-east of Sudbury, Ontario. Victor Mine operated in 1959 and 1960 but exploration and engineering work is presently underway to prepare for reopening the mine at greater depth.

We found systematic variations of thermal conductivity at Flin Flon, Thompson (Owl), and Matagami, and we corrected accordingly (Bullard, 1939). We calculated the thermal resistance and obtained a temperature *vs* thermal resistance profile that is almost linear. We calculated the heat flux as the slope of the temperature-resistance and found no discontinuity in heat flux along the profile (Table 1.1). For all the other sites that show no systematic variations in conductivity, we have used the mean thermal conductivity to calculate heat flux. Heat production was measured and found to only be significant at two sites, Lockerby (3μW m^{-3}) and Victor Mine (0.9μW m^{-3}), and therefore only taken into account at these sites. Variations in heat production with depth may affect the tempera-

ture profiles and the GST (Majorowicz and Šafanda, 2015). Because systematic variations of heat production with depth were not present at these sites, they were not included in the inversion. In absence of heat production and in steady-state, the heat flux does not vary with thermal resistance. Variations in heat flux with thermal resistance (or depth) is thus a diagnostic of departure from 1-D steady-state thermal regime. A decrease in heat flux toward the surface is associated with surface warming and enhanced heat flux is due to cooling. The heat flux profiles that we have calculated for all the sites (Figure 1.2) exhibit clear departures from 1-D steady-state condition. The heat flux was calculated as the product of the temperature gradient and the thermal conductivity within each interval. No smoothing was applied. As expected the gradient profile contains high frequency variations as the gradient always amplifies noise and errors in the temperature measurements. Some holes appear to be noisier at depth near the exploration targets because of small scale conductivity variations due to the presence of mineralization. Furthermore, the inclination of some of the holes decreases markedly at depth resulting in larger errors in the gradient. For example, the inclination Val d'Or, 85 degrees at the collar, was only 20 degrees near the end of the hole. Most of the profiles show a very pronounced increase of heat flux with depth at shallow depth (<200 m) and a clear trend of increasing heat flux between 500 and 1500 m. The increase at shallow depth is related to very recent (<300 years) climate warming. The trend between 500 and 1500 m is the result of the surface warming that followed the glacial retreat at *ca* 10 ka.

1.4 Analysis and Results

1.4.1 Long-term Surface Temperatures

Estimated long-term surface temperatures as a function of time and depth (i.e. proportional to depth squared) were determined for each borehole (Figure 1.3).

The time in these plots represents the time it took the signal to propagate and not the time that the surface temperature perturbation occurred. The range of long-term surface temperatures for each borehole was estimated over its sampled depth and reveal the persistent long-term climate trends. These trends are the mirror image of the heat flow trends.

A decreasing temperature trend with time and depth is apparent in all the boreholes in Manitoba except Pipe that does not show a clear trend. Variations of surface temperature are not consistent, with almost no trend at Pipe and a weak signal at Owl. The Flin Flon borehole is the deepest available for this study and provides a history four times longer than that of the two shallower boreholes at Owl and Pipe. It is consistent with a colder period coinciding with the LGM. In western Ontario, Manitouwadge 0611 exhibits very strong oscillations at depth. The source of noise is difficult to ascertain because of the complicated geological structure and the absence of thermal conductivity data. Borehole 0610 at Manitouwadge is consistent with colder temperatures during the LGM but the Balmertown hole does not show any variation in long-term surface temperature. Four profiles at Sudbury, are consistent with colder temperature during the LGM, but the amplitude of the trend varies between sites. Similar trends are observed for the three easternmost holes in Québec with long-term temperatures on average 5 K lower near the bottom of the holes than near the surface.

These first order estimates suggest colder surface temperatures during the LGM at most of the sites. In order to better quantify the surface temperature changes, we must turn to inversion and obtain the GST histories.

1.4.2 Individual inversions

The GST histories at all the studied sites for the time period of 100 to 100,000 years BP was inverted from the temperature-depth profiles. The time span of the

GST history model consists of 16 intervals whose distribution varies logarithmically because the resolution decreases with time. A singular value cutoff of 0.08 was used for all the individual profile inversions (Figures 1.4-1.7). The singular value cutoff eliminates the part of the solution that is affected by noise and effectively introduces a smoothing constraint on the solution (Mareschal and Beltrami, 1992). A summary of the inversion results can be found in Table 1.2. Two main episodes can be recognized in the GST histories: One is associated with a minimum temperature that occurred around the LGM at *ca* 20ka. The second is a warming observed at *ca* 2-6 ka coinciding with the Holocene Climatic Optimum (HCO), a warm period that followed the deglaciation (Lamb, 1995).

For the purpose of the discussion, we have grouped the sites sites that are from the same geographical region. We shall thus distinguish between Manitoba, western Ontario, the Sudbury area, and Québec.

The sites from Manitoba, Flin Flon, Owl and Pipe, have not recorded a very strong signal and do not exhibit common regional trends are observed (Figure 1.4). The lack of regional trends is expected as Thompson (Owl and Pipe) and Flin Flon sites are ~300 km apart and the present day ground surface temperatures differ by 3K. The weak signal recorded may be in part because the present ground surface temperature is very low; it is close to 0°C in Thompson where intermittent permafrost is found. At Flin Flon, where the present ground temperature is near 3°C, we found that ground surface temperature variations were small, confirming previous studies by Sass *et al.* (1971). The surface temperature was minimum around the LGM and was near the melting point of ice (-0.3° C). For Pipe, little to no signal was recorded. We found that there was minimal change in the ground surface temperature (~2.5 K in amplitude) over the past 100,000 years. For Owl, the amplitude of the temperature changes has doubled (~5 K), with the minimum temperature (-2.4° C) around the LGM and a warming around the HCO.

Although this result is plausible, some uncertainty remains as Guillou-Frottier *et al.* (1996) noted high heat flux correlated with high thermal conductivity in the Thompson Belt. The elevated thermal conductivity is due to the presence of vertical slices of quartzites, which increase thermal conductivity by a factor of 1.7. Furthermore, the site is affected by a poorly resolved conductivity structure as thermal conductivity measurements vary in the deepest part of the borehole, between 2.21 and 5.14 W m^{-1} K^{-1}. The lateral heat refraction effects due to the thermal conductivity contrast affect the temperature profiles and alter the GST history. For these reasons, we have little confidence in the robustness of the Owl GST history reconstruction. In western Ontario (Balmertown, Manitouwadge 0610, and 0611), results at all sites show minimum temperatures around the LGM, with a very weak minimum at Balmertown (Figure 1.5). However, the amplitude of the temperature change is much larger at Manitouwadge 0611 (~10 K) than Balmertown (~2 K) and Manitouwadge 0610 (~3 K). As the two Manitouwadge sites are only ~40 km apart, this difference is surprising. While Manitouwadge 0611 yields a plausible GST history, it appears to have an amplified signal. The site is located in a complex geological structure and lacks thermal conductivity data. There is also a change in the temperature gradient at 500 m, which cannot be accounted for. In the absence of thermal conductivity data, we cannot consider the GST history for Manitouwadge 0611 as reliable.

All four sites in the Sudbury region, Craig Mine, Falconbridge, Lockerby, and Victor Mine, have recorded minimal temperatures around the LGM (Fig 1.6). However, the minimum past temperatures for the region do vary between sites. The coldest minimum temperature was found at Craig Mine. The amplitude of the temperature changes for the site (~12 K) is much larger than those of the other sites, which vary between ~5-7 K. This difference is unexpected as these sites are all within the Sudbury craton and should have recorded similar histories.

The Craig Mine signal appears amplified, which could be the result of water flows induced by pumping at levels below 2000 m in the mine. We thus believe that the GST history for Craig Mine is not reliable. The minimum temperatures at Lockerby and Victor Mine, $2.8°C$ and $3.0°C$, are also the highest of the study. These are also the only two sites with non-negligible heat production, 3μW m^{-3} and 0.9μW m^{-3} respectively. The corrections for heat production produce an increase of the temperature gradient proportional to depth and result in an amplification of the warming signal in the profile. Consequently, the minimum and maximum temperatures would be higher at these sites, Lockerby and Victor Mine, than those with negligible heat production.

The GST histories from the three boreholes in Québec, Matagami, Val d'Or and Sept Iles, display regional differences (Figure 1.7). However, for all three sites, the minimum temperatures are synchronous and occurred around the LGM. For all the sites used in this study, the lowest minimum temperature occurred in this region, $-1.4°C$ at Sept Iles.

At all sites, excluding Pipe mine, we found that the ice retreat was followed by a warm episode, that can be associated with the HCO, a warm period whose maximal temperatures have been dated at 4.4-6.8 ka with palynological reconstructions from northern Ontario and northern Michigan (Boudreau *et al.*, 2005; Davis *et al.*, 2000).

We have compared the ranges of temperature in the inverted GST histories with those of the long-term surface temperature variations for all the sites (Table 1.4). Although the total range varies between sites from $\sim$2 K to $\sim$8 K, the two methods yield consistent values that differ by less than 1 K at most of the sites. The warming trend in the long-term surface temperature variations is consistent with the inverted GST histories. This correlation between the long-term surface tem-

perature ranges and the persistent long-term GST history trends suggests that our results are robust. The inversion of borehole profiles has a very limited resolving power and short period oscillations can seldom be recovered. In practice, the duration of an episode must be proportional (1/3 to 1/2) to the time when it occurred. The last glacial period is easily identified, but shorter period events such as the HCO that lasted 1-2 kyr around 5 ka are just beyond the threshold of resolution. It is thus possible, that constraining the GST to include the HCO would result in colder GST during the LGM, as suggested by Will Gosnold in his comment. This would require obtaining proxy data from sites close to Flin Flon and Thompson. This also requires documenting the temperature conditions at the bottom of Lake Agassiz which covered most of Manitoba after the glacial retreat.

1.4.3 Simultaneous Inversion

We have inverted simultaneously the boreholes of Thompson (Owl and Pipe), Manitouwadge (0610 and 0611) and Sudbury (Craig Mine, Falconbridge, Lockerby, and Victor Mine) to observe regional trends and to improve the signal to noise ratio (Figure 1.8). The simultaneous inversion results are summarized in Table 1.3. For simultaneous inversion, the temperature-depth profiles were truncated to ensure a common depth for all the boreholes. This insures consistency and facilitates comparison because we are examining the subsurface temperature anomalies for the same time period. For all inversions, the minimum temperature occurs around the LGM and the deglaciation is followed by a warming associated with the HCO. Altough Owl and Manitouwadge 0611 have questionable individual inversions, we have still performed simultaneaous inversions for the regions of Thompson and Manitouwadge in an attempt to decrease the signal to noise ratio. For Thompson, the width of the GST history temperature range is $\sim$4 K. As Pipe did not appear to record a signal, the simultaneous inversion appears to have damped

slightly the questionable signal recorded at Owl. The amplitude difference for the Manitouwadge GST history is ~8 K, between that of 0610 (~3 K) and 0611 (~10 K).

The Sudbury simultaneous inversion was performed with and without Craig Mine. This was done to check whether the inclusion of Craig Mine, a site which we suspect to have been affected by water flow, affects the reconstructions. Both inversions display similar trends; however, there is a difference in the range of temperature variations. The inversion excluding Craig Mine yielded a ΔT of 7 K, similar to those of the individual inversions of Falconbridge (~7 K), Lockerby (~7 K) and Victor Mine (~5 K). Upon inclusion of Craig Mine, ΔT was increased to 11K, demonstrating that the presence of a signal due to water flow in the temperature profile at this site has a strong effect on the results of the simultaneous inversion.

1.5 Discussion

The minimum temperatures of the GST histories occur around the LGM, representing the basal temperatures of the Laurentide Ice Sheet. These temperatures vary spatially and range from -1.4 to $3.0^{o}C$, near or above the pressure melting point of ice. Such spatial variation is expected as numerous studies have demonstrated present-day spatial basal temperature variability beneath the Antarctic and Greenland Ice Sheets (e.g., Dahl-Jensen *et al.*, 1998; Pattyn, 2010; Schneider *et al.*, 2006). The highest basal temperatures occur within the Sudbury basin at Lockerby and Victor Mine. The Sudbury region has the highest average heat flux of the Canadian Shield, ~54mW m^{-2}, because crustal heat production is higher than average (Perry *et al.*, 2009). The lowest basal temperature is recorded at Sept Iles, where the heat flux is the lowest of the studied regions, ~34mW m^{-2}. These correlations suggest a link between heat flux and basal temperatures. This

is further supported by modelling work showing that heat flux influences the thermal structure and properties of ice sheets, including basal temperatures and ice flow (Greve, 2005; Pollard *et al.*, 2005; Llubes *et al.*, 2006). However, the Sept Iles basal temperature has also been linked to its proximity to the edge of the ice sheet and area of thinner ice (Rolandone *et al.*, 2003b). Our study is consistent with a possible link between basal temperature and heat flux along with ice dynamics in the Laurentide Ice Sheet during the LGC but further modelling work is necessary to confirm such a relationship. Variations in these parameters (heat flux and ice dynamics) could account for the differences observed in the basal temperatures beneath the Fennoscandian and Laurentide ice sheets.

The basal temperatures recorded, near the pressure melting point of ice, indicate the possibility of basal flow and ice streams, two important factors affecting ice sheet evolution. These processes have been suggested by geomorphological evidence presented by Dyke *et al.* (2002) and predicted by the ICE-5G model (Peltier, 2004). Basal flow has the ability to transport large amounts of water from the interior of the ice sheet, leading to thinning of the ice sheet and climatically-vulnerable ice. It is postulated to be a key factor in glacial terminations (Marshall and Clark, 2002). Furthermore, these temperatures demonstrate that the southern portion of the Laurentide Ice Sheet was not frozen to the bed, suggesting basal sliding. These conditions can lead to instability. Widespread basal sliding and increase surface meltwater could have been a factor resulting in the rapid collapse of the Laurentide Ice Sheet (Zwally *et al.*, 2002). However, these basal temperatures and associated melt persisted prior to and throughout the LGM over more than 30,000 years with deglaciation only occurring rapidly during the early Holocene (Carlson *et al.*, 2008). While this indicates that basal temperatures near the pressure melting point of ice cannot be solely responsible for ice sheet instability and collapse, it demonstrates that they are a key parameter in ice sheet evolution,

one that ice sheet evolution models must take into account. Elevated basal temperatures, near or above the pressure melting point of ice, have been recorded in the present-day ice sheets (Fahnestock *et al.*, 2001; Pritchard *et al.*, 2012). Our results indicate that alone this cannot be considered as an indication of ice sheet collapse. However, combined with other processes it could lead to instability and collapse.

1.6 Conclusions

Thirteen deep boreholes from eastern and central Canada were analyzed to determine the GST histories for the last 100 kyr. The long term trends are consistent between sites. A warm period following the retreat of the ice sheet is inferred at ~2-6 ka in the inverted GST histories, correlated to the Holocene Climatic Optimum.

The surface temperatures reached their minima during the LGM and post glacial warming started *ca* 10ka. The corresponding temperatures at the base of of the Laurentide Ice Sheet range from -1.4 to $3.0°C$, and are all near or above the pressure melting point of ice. Such temperatures allow for basal flow and fast flowing ice streams, two important factors affecting ice sheet evolution, illustrating the need for models of ice sheet evolution to account for such a key parameters as basal temperature. Despite the suggestion that melting took place at its base, the Laurentide ice sheet persisted throughout the LGM over more than 30,000 years. This demonstrates that basal temperatures near the melting point of ice do not indicate that an ice sheet is on the verge of collapse. However, combined with other processes it could lead to instability and collapse.

The differences between GST histories at different sites raise other questions concerning the controls on temperatures at the base of ice sheets. Equilibrium between heat flow from the Earth's interior and heat advection by glacial flow de-

termines the temperature at the boundary between the ice and the bedrock. The correlation between higher heat flux and higher basal temperatures in the Sudbury region suggests that variations in crustal heat flux may account for some of the regional differences in basal temperatures along with the dynamics of ice thickness controlled by the accumulation rate and the distance to the edge of the ice sheet.

It is also noteworthy that similar deep borehole studies in Europe suggest that basal temperatures beneath the Fennoscandian Ice Sheet and in the Urals during the LGC were much colder (Kukkonen and Jõeleht, 2003; Demezhko *et al.*, 2013) than those observed in Canada (Chouinard and Mareschal, 2009). Because of the geological similarities between the two regions, this contrast is likely to be due to differences in climate and ice dynamics between Europe and North America during the LGC.

Acknowledgements

We appreciate the constructive review from Dmitry Demezhko and comments by reviewer V.M.Hamza. Thanks to W.Gosnold and J.Majorowicz for their interest and useful comments.This work was supported by grants from the Natural Sciences and Engineering Research Council of Canada Discovery Grant (NSERC-DG, 140576948), a NSERC-CREATE award *Training Program in Climate Sciences*, the Atlantic Computational Excellence Network (ACEnet), and the Atlantic Canada Opportunities Agency (AIF-ACOA) to HB. H. Beltrami holds a Canada Research Chair. C.Pickler is funded by a NSERC-CREATE *Training Program in Climate Sciences* based at St.Francis Xavier University.

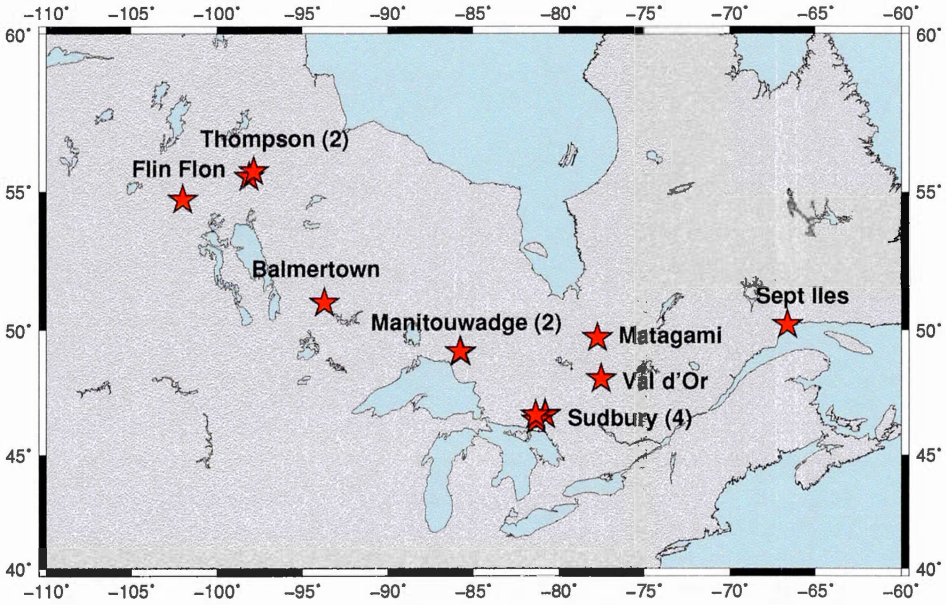

Figure 1.1 Map of central and eastern Canada and adjoining US showing the location of sampled boreholes. Thompson (Owl and Pipe), Manitouwadge (0610 and 0611) and Sudbury (Falconbridge, Lockerby, Craig Mine, and Victor Mine) have several boreholes present within a small region. The number of profiles available at locations with multiple holes is enclosed in parenthesis.

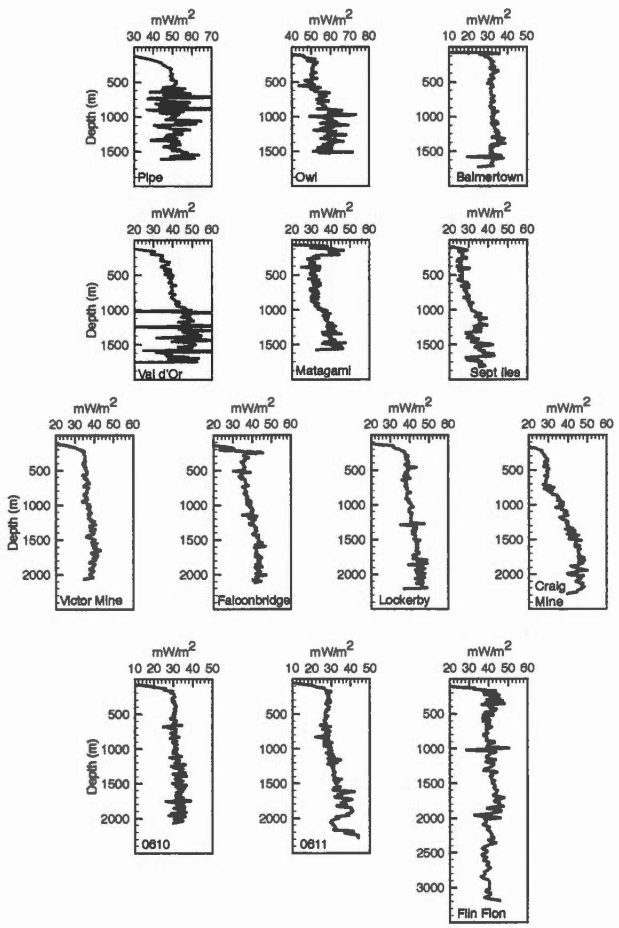

Figure 1.2 Heat flux variation as a function of depth. Heat flux is calculated as the product of thermal conductivity by the temperature gradient calculated over 3 points. The Flin Flon, Owl and Matagami profiles have been corrected to account for thermal conductivity variations with depth as shown in Table 1.1.

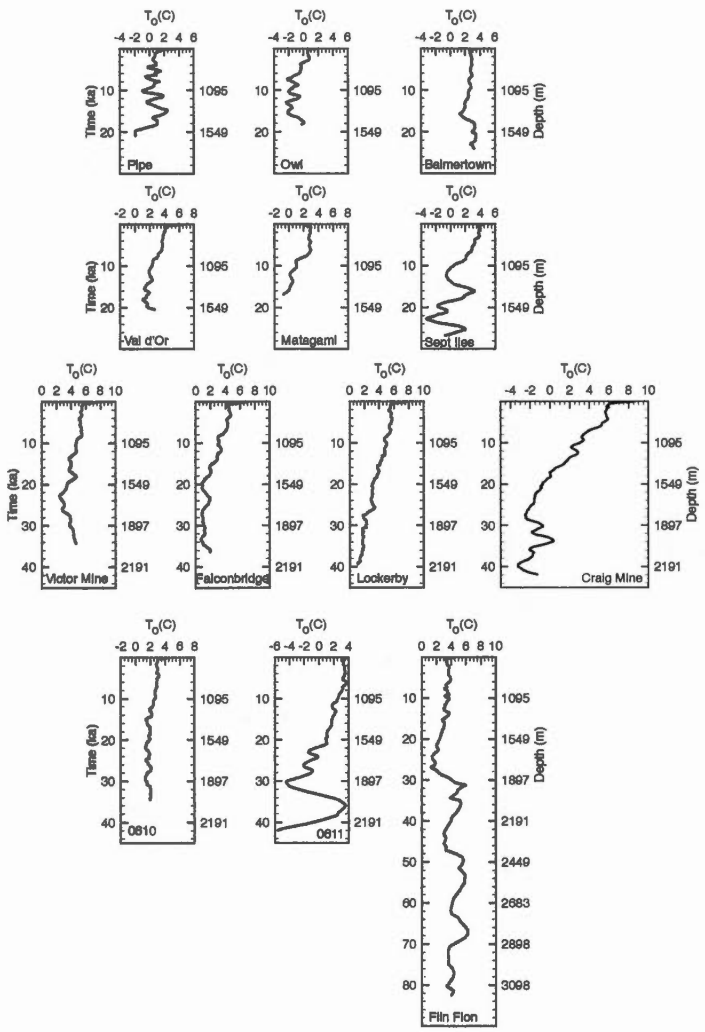

Figure 1.3 Long-term surface temperature variations over time (left y-axis) and depth (right y-axis) for all the boreholes. Time is determined from depth by equation 1.7.

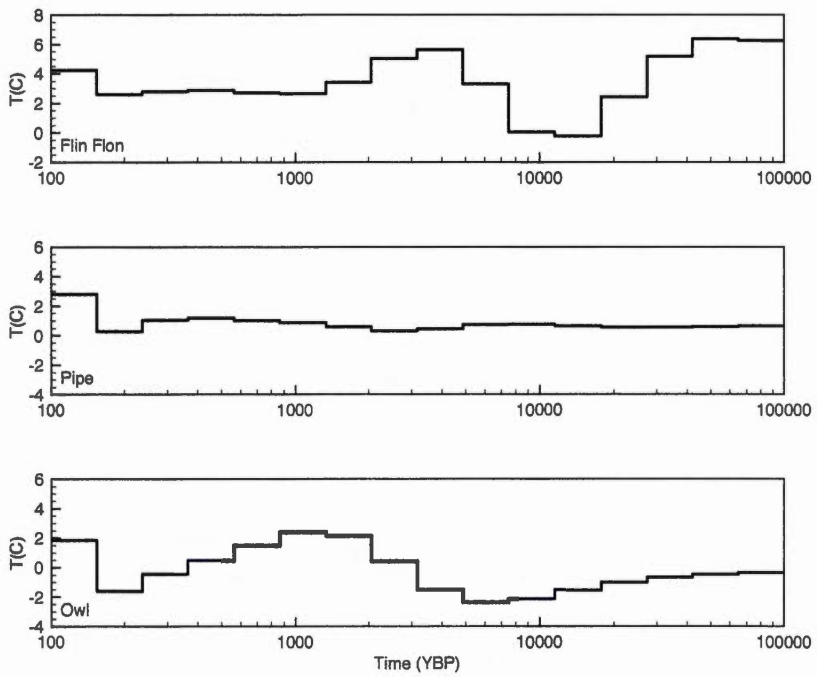

Figure 1.4 Ground Surface Temperature History from the Manitoba boreholes, at Flin Flon and Thompson (Pipe and Owl). The temperatures have been shifted with respect to the reference surface temperature of the site, T_o, as shown in Table 1.2.

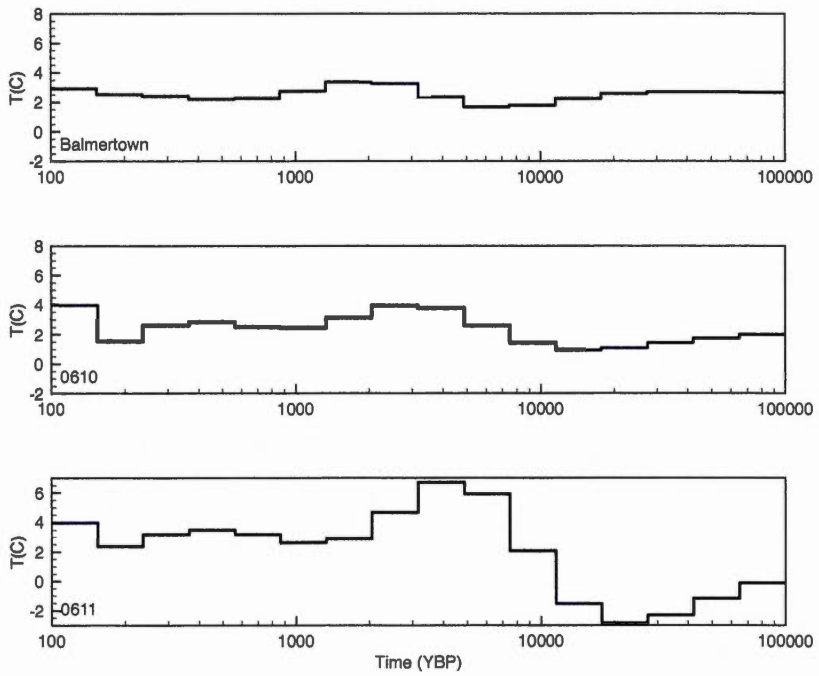

Figure 1.5 Ground Surface Temperature History for the western Ontario boreholes: Balmertown and Manitouwadge 0610 and 0611. The temperatures have been shifted with respect to the reference surface temperature of the site, T_o, as shown in Table 1.2.

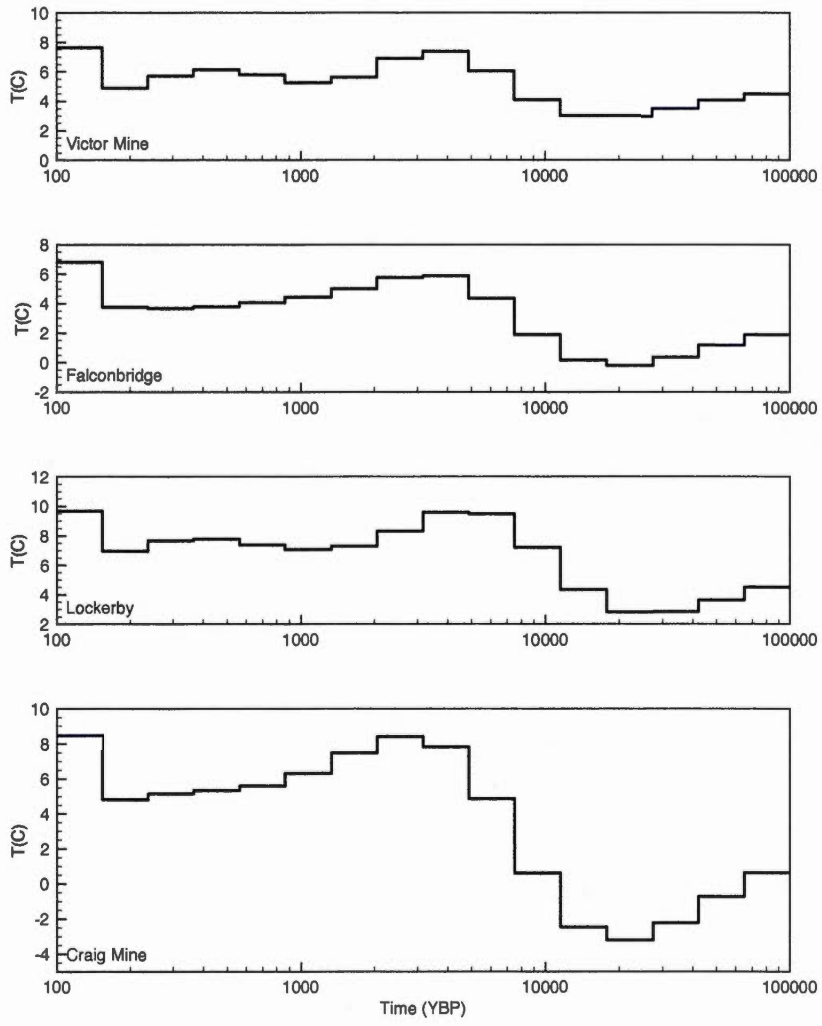

Figure 1.6 Ground Surface Temperature History for all the boreholes around Sudbury, Ontario (Victor Mine, Falconbridge, Lockerby, and Craig Mine).The temperatures have been shifted with respect to the reference surface temperature of the site, T_o, as shown in Table 1.2.

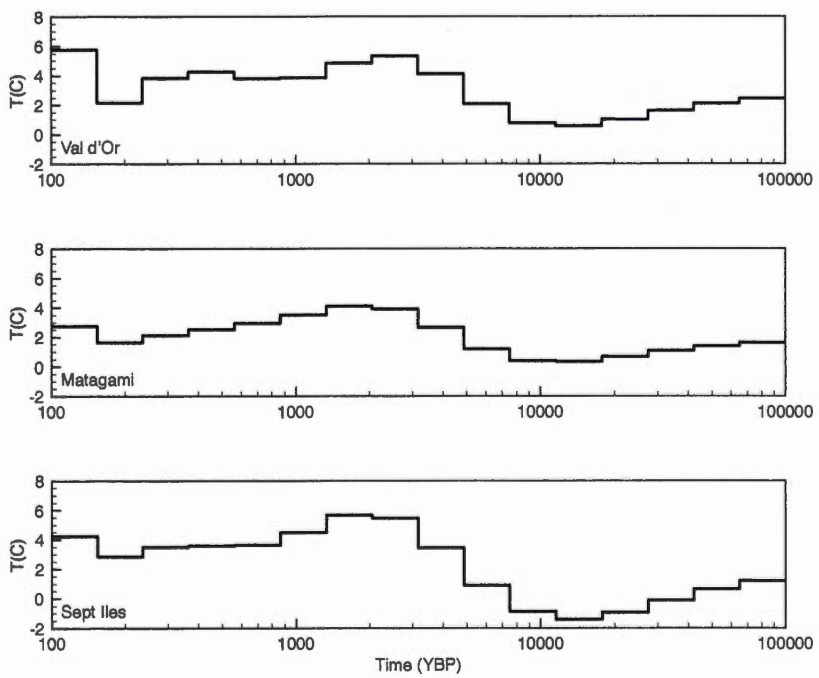

Figure 1.7 Ground Surface Temperature History for the boreholes in Quebec, Matagami, Val d'Or and Sept-Iles. The temperatures have been shifted with respect to the reference surface temperature of the site, T_o, as shown in Table 1.2.

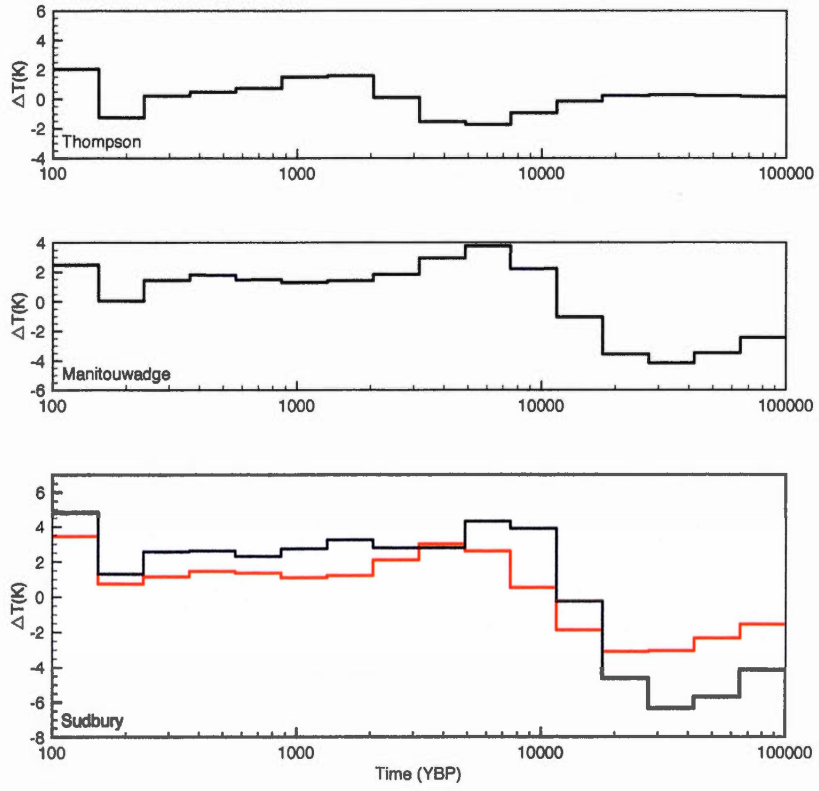

Figure 1.8 GST changes from simultaneous inversion with respect to the long-term temperature at 100 ka. The Sudbury GST changes include (black) and exclude (red) Craig Mine.

Table 1.1 Technical information concerning the boreholes used in this study, where λ is thermal conductivity and Q is heat flux.

Site	Log ID	Latitude	Longitude	Depth (m)	λ (W m^{-1} K^{-1})	Q (mW m^{-2})	Reference
FlinFlon	n/a	54°43′	102°00′	3196	3.51 (≤1920m) 2.83 (1920-2300m) 2.51 (≥2300) m	42	(Sass *et al.*, 1971)
Thompson - Pipe	01-14	55°29′10″	98°07′42″	1610	3.24	49	(Mareschal *et al.*, 1999a; Rolandone *et al.*, 2002; Chouinard and Mareschal, 2009)
Thompson - Owl	00-17, 01-16	55°40′17″	97°51′35″	1568	3.0 (<1200m) 3.6 (>1200m)	52	(Mareschal *et al.*, 1999a; Rolandone *et al.*, 2002)
Balmertown	00-02	51°01′59″	93°42′56″	1724	3.3	35	(Rolandone *et al.*, 2003a)
Manitouwadge - 0610	06-10	49°09′07″	85°43′46″	2064	2.74	40	(Rolandone *et al.*, 2003b; Chouinard and Mareschal, 2009)
Manitouwadge - 0611	06-11	49°10′16″	85°46′31″	2279	-	-	(Rolandone *et al.*, 2003b; Chouinard and Mareschal, 2009)
Sudbury - Victor Mine	13-01	46°40′17″	80°48′34″	2060	2.7	44	
Sudbury - Falconbrige	03-16	46°39′05″	80°47′30″	2122	2.74	47	(Perry *et al.*, 2009)
Sudbury - Lockerby	04-01	46°26′00″	81°18′55″	2207	3.29	58	(Perry *et al.*, 2009)
Sudbury - Craig Mine	04-02	46°38′34″	81°21′03″	2279	2.65	-	(Chouinard and Mareschal, 2009)
Val d'Or	10-08	48°06′02″	77°31′26″	1754	3.81	47	(Jaupart *et al.*, 2014)
Matagami	04-09	49°42′29″	77°44′28″	1579	3.27 (≤1000m) 4.02 (>1000m)	42	
Sept Iles	98-20	50°12′46″	66°38′19″	1820	2.04	32	(Mareschal *et al.*, 1999b; Chouinard and Mareschal, 2009)

Table 1.2 Summary of GST history results where T_o is the long-term surface temperature, Q_o is the quasi-equilibrium heat flow, T_{min} is the minimal temperature, T_{pgw} is the maximum temperature attained during the postglacial warming, t_{min} and t_{pgw} is the occurrence of the minimal temperature and maximum postglacial warming temperature. Parentheses indicate sites where the GST history is not reliable.

Site	T_o ($°C$)	Q_o (mW m^{-2})	T_{min} ($°C$)	t_{min} (ka)	T_{pgw} ($°C$)	t_{pgw} (ka)
FlinFlon	3.8	38.7	-0.25	10-20	5.64	3-5
Pipe	0.7	51.8	0.27	0.15-0.2	-	-
(Owl)[a]	-0.3	54.9	-2.36	5-7.5	2.40	0.9-1
Balmertown	2.6	33.0	1.65	5-7.5	3.36	1-2
Manitouwadge 0610	2.3	35.6	0.95	10-20	3.95	2-3
(Manitouwadge 0611)[b]	1.7	-	-2.83	20-30	6.71	3-5
Victor Mine	4.5	42.1	3.00	10-30	7.34	3-5
Falconbridge	3.1	45.7	-0.20	20-30	5.88	5-7.5
Lockerby	4.1	57.7	2.84	10-30	9.58	3-5
(Craig Mine)[c]	3.0	45.2	-3.20	20-30	8.41	2-3
Val d'Or	2.9	41.9	0.58	10-20	5.33	2-3
Matagami	1.9	47.5	0.34	10-20	4.10	1-2
Sept Iles	2.1	34.7	-1.42	10-20	5.66	1-2

[a]The temperature profile at this site may be distorted by horizontal contrasts in thermal conductivity, [b]The temperature profile in the lowermost part of the hole may be affected by subvertical layering and thermal conductivity contrasts, [c]The temperature profile may be affected by waterflow caused by pumping in the nearby mine.

Table 1.3 Summary of GST history results for simultaneous inversions where t_{min} and t_{pgw} is the occurrence of the minimal temperature and maximal temperature associated with postglacial warming, and ΔT is the temperature range

Site	$\Delta T(GSTH)$ (K)	t_{min} (ka)	t_{pgw} (ka)
Thompson	3.8	5-7.5	1-2
Manitouwadge	7.9	30-40	5-7.5
Sudbury	11.2	30-40	5-7.5
Sudbury (exc. Craig)	6.6	20-30	3-5

Table 1.4 Ranges in surface temperature variations estimated from: the iteration of the long-term surface temperature as a function of depth (column 1) and from inversion of the GST history (column 2), along with the difference between the two (column 3).

Site	ΔT_o (°C)	ΔT(GSTH) (°C)	Difference
Flin Flon	5.1	6.6	1.5
Thompson, Pipe Mine	5.6	2.5	3.1
Thompson, Owl[a]	5.3	4.8	0.5
Balmertown	2.3	1.7	0.6
Manitouwadge, 0610	3.3	3.0	0.3
Manitouwadge, 0611[b]	9.6	9.5	0.1
Sudbury, Victor Mine	4.9	4.6	0.3
Sudbury, Falconbridge	6.2	7.0	0.8
Sudbury, Lockerby	6.6	6.8	0.2
Sudbury Craig Mine[c]	11.9	11.7	0.2
Val d'Or	5.5	5.2	0.3
Matagami	4.1	3.8	0.3
Sept Iles	7.8	7.1	0.7

[a]The temperature profile at this site may be distorted by horizontal contrasts in thermal conductivity, [b]The temperature profile in the lowermost part of the hole may be affected by subvertical layering and thermal conductivity contrasts, [c]The temperature profile may be affected by waterflow caused by pumping in the nearby mine.

CHAPTER II

CLIMATE TRENDS IN NORTHERN ONTARIO AND QUÉBEC FROM BOREHOLE TEMPERATURE PROFILES

Manuscript published in Climate of the Past[1]

---

[1]Pickler, C., Beltrami, H., and Mareschal, J.C., 2016. Climate trends in northern Ontario and Québec from borehole temperature profiles, Climate of the Past, 12, 2215-2227, doi:10.5194/cp-12-2215-2016

Abstract

The ground surface temperature histories of the past 500 years were reconstructed at 10 sites containing 18 boreholes in northeastern Canada. The boreholes, between 400 and 800 m deep, are located north of 51°N, and west and east of James Bay in northern Ontario and Québec. We find that both sides of James Bay have experienced similar ground surface temperature histories with a warming of 1.51±0.76 K during the period of 1850 to 2000, similar to borehole reconstructions for the southern portion of the Superior Province and in agreement with available proxy data. A cooling period corresponding to the Little Ice Age was found at only one site. Despite permafrost maps locating the sites in a region of discontinuous permafrost, the ground surface temperature histories suggest that the potential for permafrost was minimal to absent over the past 500 years. This could be the result of air surface temperature interpolation used in permafrost models being unsuitable to account for the spatial variability of ground temperatures along with an offset between ground and air surface temperatures due to the snow cover.

2.1 Introduction

Earth's subsurface thermal regime is governed by the outflow of heat from the interior and by temporal variations in ground surface temperature (GST). The heat flux from the interior of the Earth varies on time scales of the order of a few million of years in active tectonic regions and several 100 Myr in stable continents. It can be considered as steady state relative to the timescale of climatic surface temperature variations. To determine the heat flow from the Earth's interior, temperature-depth profiles are measured in boreholes. In homogeneous rocks with no heat production, the steady-state temperature profile linearly increases with depth. Persistent temporal changes in the ground surface energy balance cause variations of the ground temperature that diffuse downwards and are recorded as temperature anomalies superimposed on the linear steady-state geotherm (e.g., Hotchkiss and Ingersoll, 1934; Birch, 1948; Beck, 1977). The extent to which the ground surface temperature changes are recorded is proportional to their duration and amplitude and inversely proportional to the time when they occurred. For periodic oscillations of the surface temperature, the temperature is propagated downward as a damped wave. The amplitude of the wave decreases exponentially with depth over a length scale δ (skin depth) proportional to the square root of the period ($\delta = \sqrt{\kappa T/\pi}$), where κ is the thermal diffusivity of the rock, $\approx 10^{-6}$ $m^2\ s^{-1}$ or $\approx 31.5\ m^2\ yr^{-1}$. This damping removes the high-frequency variability that is present in meteorological records and allows for the preservation of the long-term climatic trends in the ground temperature signal (e.g., Beltrami and Mareschal, 1995).

From the interpretation of temperature-depth profiles, it is possible to infer centennial trends in Earth's surface temperature variations. The first attempt to infer climate history from temperature-depth profiles was the study by Hotchkiss and

Ingersoll (1934) who estimated the timing of the ice retreat at the end of the last glaciation. It was, however, not until the 1970s that systematic studies were undertaken to infer past climate from such profiles (e.g., Cermak, 1971; Sass *et al.*, 1971; Vasseur *et al.*, 1983). In the 1980s, with increasing concern over global warming, use of borehole temperature-depth profiles to estimate recent (<300 years) climate change became widespread following the study of Lachenbruch and Marshall (1986). This has lead to many local, regional, and global studies (e.g., Huang *et al.*, 2000; Harris and Chapman, 2001; Gosselin and Mareschal, 2003; Beltrami and Bourlon, 2004; Pollack and Smerdon, 2004; Chouinard *et al.*, 2007; Pickler *et al.*, 2016b).

Because of the availability of suitable temperature-depth profiles in the Canadian Shield, many studies have been undertaken in central and eastern Canada. The majority of these studies have used temperature-depth profiles from the southern portion of the Superior Province of the Canadian Shield (~45°-50°N), where many mining exploration holes are readily available and the crystalline rocks are less likely to be affected by groundwater flow than sedimentary rocks. These studies have shown a warming signal of ~1-2 K over the last ~150-200 years following a period of cooling about 200-500 yr BP associated with the Little Ice Age (LIA) (e.g., Beltrami and Mareschal, 1992; Wang *et al.*, 1992; Guillou-Frottier *et al.*, 1998; Gosselin and Mareschal, 2003; Chouinard and Mareschal, 2007) .

For logistical reasons, mining exploration has been restricted to the southernmost part of the Shield and the few holes that have been drilled in northern regions cannot be measured because they are blocked by permafrost. Nevertheless, a few studies were conducted at higher latitudes. Majorowicz *et al.* (2004) reconstructed the GST history for 61 temperature-depth profiles between 60°N and 82°N in northern Canada. They found strong evidence that GST warming started

in the late 18th century and continued until present. Simultaneous inversion of their data yielded a warming of ~2K for the last 500 years. Studies in Ellesmere Island (above 60°N) have shown varying trends, confirming that temperatures do not increase uniformly over Arctic regions. Taylor *et al.* (2006) reconstructed the 500-year GST history from three boreholes and found a 3 K warming since the LIA minimum, ~200 yr BP, which is consistent with Beltrami and Taylor (1995) results and the oxygen isotopes studies on ice cores from the region (Fisher and Koerner, 1994). Chouinard *et al.* (2007) used three temperature-depth profiles in a region with continuous permafrost at the northernmost tip of Québec to infer the GST history. They found a very strong and recent warming of ~2.5 K, with the largest part of this warming occurring in the preceding 15 years, i.e. much later than in Ellesmere Island. Because of lack of adequate borehole temperature depth profiles in eastern Canada between 51°N and 60°N, the large region between the Canadian Arctic and the southern part of the Canadian Shield has not been studied and the climate trends of the last 500 years for this region remain unclear except for boreholes at Voisey Bay, at 56°N on the east coast of Labrador, which show almost no climate signal (Mareschal *et al.*, 2000).

The first motivation of this study is to reduce the gap in data between the Arctic and southeastern Canada. We shall examine 18 temperature-depth profiles measured at 10 sites from eastern Canada to reconstruct the GST histories for the last 500 years. The sites are located in the poorly sampled region north of 51°N, west and east of James Bay in northern Ontario and Québec. They are to the north of the previous eastern Canada studies and south of the Arctic ones, in a part of the Superior Province where heat flux is extremely low ($< 30 \text{mW m}^{-2}$) (Jaupart *et al.*, 2014).

The second motivation of the study is to assess whether borehole temperature

profiles can be used to retrace the evolution of permafrost in northern Ontario and Québec. Permafrost maps locate the boreholes in a region of discontinuous permafrost (Brown *et al.*, 2002). All sites, excluding Noront, lie in discontinuous isolated patches of permafrost, i.e. where less than %10 of the ground is frozen. Noront lies near the southern boundary of extensive discontinuous permafrost, i.e. where permafrost affects between 50-90% of the ground. In regions with an absence of ground temperature measurements, such as northern Ontario and Québec, permafrost maps are estimated from surface air temperature and their contour lines (Heginbottom, 2002). The -2.5°C mean annual surface air temperature (SAT) contour line for the period 1950-1980 crosses the southern part of our study region in Ontario, and most of the Québec sites are located between -2.5 and -5°C SAT contour lines (Phillips, 2002). However, permafrost was not encountered during sampling of the Québec or Ontario boreholes. It is also worth pointing out that the ground is covered by thick snow cover during several months (from mid-December to late April) in the regions above 50°N. Studies demonstrated that the ground surface temperatures are strongly affected by the duration of the snow cover and are offset from SAT (Bartlett *et al.*, 2005; Zhang, 2005; González-Rouco *et al.*, 2006, 2009; García-García *et al.*, 2016). In these regions with extensive snow cover, the borehole temperature profiles are affected by changes in both SAT and snow cover. Meteorological and proxy data indicate that there is more snowfall and longer snow cover on the ground in the Québec region than in Ontario (Bégin, 2000; Brown and Mote, 2009; Brown, 2010; Environment Canada, 2010; Nicault *et al.*, 2014). This points to possibly warmer present ground surface temperatures and smaller permafrost extent in northern Québec than in Ontario, and the prospect for different ground surface temperature histories between the regions.

2.2 Theory

Assuming Earth is a half-space where physical properties only vary with depth, the temperature at depth z, $T(z)$, can be written as (Jaupart and Mareschal, 2011):

$$T(z) = T_o + Q_o R(z) - \int_0^z \frac{dz'}{\lambda(z')} \int_0^{z'} H(z'')dz'' + T_t(z) \tag{2.1}$$

where T_o is the reference surface temperature, Q_o the reference surface heat flux, the integral accounts for the vertical distribution of heat producing elements $H(z)$, and $T_t(z)$ is the temperature perturbation at depth z due to time-varying changes to the surface boundary condition. The thermal depth $R(z)$ is defined as:

$$R(z) = \int_0^z \frac{dz'}{\lambda(z')} \tag{2.2}$$

where λ is the thermal conductivity.

The temperature perturbation can be calculated by the following equation (Carslaw and Jaeger, 1959):

$$T_t(z) = \int_0^\infty \frac{z}{2\sqrt{\pi\kappa t^3}} \exp\left(\frac{-z^2}{4\kappa t}\right) T_o(t)dt \tag{2.3}$$

where κ is thermal diffusivity and $T_o(t)$ is the surface temperature at time t before present. For a step change in surface temperature, ΔT, at time t before present, the temperature perturbation $T_t(z)$ is given by Carslaw and Jaeger (1959):

$$T_t(z) = \Delta T \mathrm{erfc}\left(\frac{z}{2\sqrt{\kappa t}}\right) \tag{2.4}$$

where $erfc$ is the complementary error function. If the GST perturbations are

approximated by their mean values ΔT_k during K intervals (t_{k-1}, t_k), the temperature perturbation is written as follows:

$$T_t(z) = \sum_{k=1}^{K} \Delta T_k (\text{erfc}\frac{z}{2\sqrt{\kappa t_k}} - \text{erfc}\frac{z}{2\sqrt{\kappa t_{k-1}}}) \tag{2.5}$$

ΔT_k is the average difference between the ground surface temperature during the time interval (t_{k-1}, t_k) and the reference surface temperature T_o.

2.2.1 Inversion

To reconstruct the GST history for each temperature-depth profile, we must invert equation 2.5. The inversion involves solving for the parameters T_o, Q_o, and ΔT_k of the temperature-depth profile. Equation 2.5 yields a system of linear equations in the unknown parameters for each depth where temperature has been measured. If N temperature measurements were made in the borehole, a system of N linear equations with $K + 2$ unknowns, T_o, Q_o, and the K values of ΔT_k is obtained. However this system of equations is ill-conditioned and its solution is unstable to small perturbations in the temperature data, i.e. a small error in the data results in a very large error in the solution (Lanczos, 1961). Different inversion methods are available to stabilize (regularize) the solution of ill-posed problems (Backus-Gilbert method, Tikhonov regularization algorithm, Bayesian methods, singular value decomposition, Monte Carlo methods). All these inversion techniques have been applied to reconstruct the GST history (e.g., Vasseur *et al.*, 1983; Nielsen and Beck, 1989; Shen and Beck, 1991; Mareschal and Beltrami, 1992; Clauser and Mareschal, 1995; Mareschal *et al.*, 1999b). In this paper, we have used the singular value decomposition because it is a very simple method to reduce the impact of noise and errors on the solution (Lanczos, 1961). This technique is well documented for geophysical studies (Jackson, 1972; Menke, 1989) and its application

for inversion of the ground temperature history is straightforward (Mareschal and Beltrami, 1992).

For sites including several boreholes with similar surface conditions, the data are inverted simultaneously because it is assumed that they have experienced the same surface temperature variations and therefore consistent subsurface temperature anomalies. It was expected that consistent trends in the temperature profiles would reinforce each other while errors and random noise would cancel each other. However, the resulting improvement in the signal to noise ratio remains marginal unless a sufficiently large number of profiles with the same GST history are available, which is almost never the case. Simultaneous inversion is described in detail and discussed by Beltrami and Mareschal (1992), Clauser and Mareschal (1995), and Beltrami *et al.* (1997), among others.

2.3 Description of data

Figure 2.1 shows the locations of the thirteen sites including twenty-five boreholes across northern Ontario and Québec. The heat flow of these sites has previously been studied and a detailed description of the measurement techniques and sites can be found in the heat flow publications (Jessop, 1968; Jessop and Lewis, 1978; Lévy *et al.*, 2010; Jaupart *et al.*, 2014). Their temperature-depth profiles can be found in Jaume-Santero *et al.* (2016). All the sites are located north of 51°N, west and east of James Bay, and the boreholes range in depth between 400 and 800 m. All the holes were cased in the upper ~10-15 m and, excluding Otoskwin and Nielsen Island, were drilled for mining exploration purposes. The temperature was measured at 10 m intervals using a calibrated thermistor. The sampling rate is higher at Otoskwin with temperature measurements every 1 m, while Nielsen Island was measured every 30 m. The overall accuracy is estimated on the or-

der of 0.02 K with a precision of greater than 0.005 K. Thermal conductivity was measured on core samples by the method of divided bars (Misener and Beck, 1960). Radiogenic heat production measurements were also made on core samples but are not needed for corrections because the holes are not deep and the heat production rate is low.

Only 18 holes proved suitable for inversion of the ground surface temperature. Their location and depth can be found in Table 2.1. Three northern Ontario sites are located in a region of discontinuous isolated patches of permafrost: Musselwhite, Thierry Mine, and Otoskwin. One site, Noront, lies near the southern edge of a region with extensive discontinuous permafrost. Thierry Mine (0605, 0606, 0608) and Noront (1012, 1013, 1014, 1015) include several boreholes. Six sites are located in northern Québec in a region of discontinuous isolated patches of permafrost (Nielsen Island,LaGrande, Eastmain, Eleonore, Corvet, Camp Coulon), with Eastmain (0803, 0804) and Camp Coulon (0712, 0713, 0714) having multiple boreholes. Systematic variations in thermal conductivity observed at Nielsen Island were corrected by using the thermal depth (Bullard, 1939). Some measurements were not used for this study for different reasons (Table 2.2). Boreholes less than 300 m deep were rejected for being too shallow. When the mean distance to a lake was less than the depth of the hole, or less than 300 m, they were rejected. Furthermore, boreholes were deemed too steep and were rejected if they had a slope of 5% or more over a distance comparable to the depth. The profile at Miminiska Lake (Ontario) is too shallow to be inverted; the boreholes at Clearwater (Québec) are plunging under a lake that affects the temperature profiles; the borehole at Poste Lemoyne is on the side of a very steep hill and the profile is seriously perturbed by the topography. We also discarded one of the temperature profiles at the Eleonore site because the borehole was plunging under a recently

filled water reservoir and one of the profiles at the LaGrande site because it was a few metres away from the edge of a 30 m cliff. The borehole temperature-depth profiles at sites with multiple boreholes were truncated at the depth of the shallowest borehole to ensure that the same period of time was being studied (Thierry Mine at 530 m, Noront at 400 m, Eastmain at 400 m, and Camp Coulon at 400 m) (Beltrami *et al.*, 2011). The temperature anomaly for each site was calculated by subtracting from the data the estimated steady-state temperature obtained by least-square fitting of a linear function to the bottom 100 m of the profile (Figures 2.2-2.3). Tests were made to show that, below 300 m, the heat flux does not vary with the selected depth interval (Lévy *et al.*, 2010; Jaupart *et al.*, 2014) and that the reference temperature profile is stable.

2.4 Results

The temperature-depth profiles from the 10 sites were inverted to reconstruct the GST histories for the last 500 years divided in intervals of 20 years (Figures 2.4-2.6). Simultaneous inversion was used at sites with multiple boreholes: Thierry Mine, Noront, Eastmain, and Camp Coulon. The cutoff value or number of eigenvalues determines which part of the solution is eliminated to reduce the impact of noise. A lower cutoff value results in higher resolution in the reconstruction of the GST but at the expense of stability (Mareschal and Beltrami, 1992). Three eigenvalues (0.2 cutoff) were retained for all the sites except Otoskwin and Corvet, where four eigenvalues (0.08 cutoff) were retained. The results of the inversions are summarized in Table 2.3. Although the ground surface temperature histories differ in their details, they consistently show a trend of warming relative to the reference temperature (i.e. temperature 500 years before logging). Only one site shows indications that the GST was affected by the LIA, a cold period that occurred between 200-500 yr BP.

In northern Ontario, the trends of the inferred GST differ between sites. Otoskwin is the only site to show a LIA signal, with a cooling of ~0.5 K with respect to the reference temperature (500 yr BP). Evidence for this cooling can be found in the temperature anomaly at ~200 m but is also observed at Musselwhite and TM0608, where no LIA is reconstructed (Figure 2.2). Moreover, there is a noticeable change in the Otoskwin temperature gradient at ~200 m, which cannot be correlated to variations in thermal conductivity measured on 80 samples from the borehole. The recent warming at Musselwhite and Otoskwin occurred around the same time but it is observed earlier (~250-300 yr BP) at Thierry Mine and Noront (Figure 2.4). The total amplitude of warming differs greatly between the sites: 0.50 K with respect to reference temperature at Otoskwin, 0.88 K at Musselwhite, 1.85 K at Noront, and 2.85 K at Thierry Mine. It is likely that the Thierry Mine signal was amplified by the clearing of vegetation that took place during the operation of the mine between 1934 and 1950.

Unlike for northern Ontario, a LIA signal was not found for any of the northern Québec sites (Figures 2.5-2.6). A LIA signal was expected because pollen data have suggested that the cooling during the LIA (up to -0.3°C for North America) was strongest in northern Québec (Gajewski, 1988; Viau and Gajewski, 2009; Viau *et al.*, 2012). However, a cooling signal at ~200 m, which could be associated with the LIA, is observed in the temperature anomaly of CC0713 (Figure 2.3). Discontinuities are observed in the temperature anomaly of CC0712 between 100 and 300 m. These are also observed in the temperature gradient and could be due to small water flows. The onset of the recent climate warming is the same for all the sites (~100-150 yr BP), except Eleonore, where it began ~200-300 yr BP. The amplitude of the warming varies between 0.5 and 2 K (Figures 2.5-2.6) with the largest warming occuring at Corvet (2.18 K).

2.5 Discussion and Conclusions

Borehole temperature profiles in northern Ontario and Québec consistently show a ground surface temperature increase of 1.51±0.76 K above the reference temperature. Most of this increase took place for the period of 1850 to 2000. Thierry Mine shows larger than average warming signals: 2.85 K. The area around the Thierry Mine boreholes (0605, 0606, 0608) was cleared in the 1940s after the first opening of the mine and a satellite image locates all three boreholes ~300 m from a lake. Lakes disturb a profile if they are at a distance less than the depth of the boreholes (Lewis and Wang, 1992). The proximity to the lake along with the change in vegetation cover could explain the enhanced warming signal (Lewis and Wang, 1998; Lewis, 1998). This illustrates the significant influence of non-climatic effects on ground surface temperature reconstructions from borehole temperature-depth profiles.

A cooling period corresponding to the LIA was found for only one site, Otoskwin (Ontario), which exhibits marked perturbations of the temperature profile. While spatial and temporal variation in the LIA have been noted (Matthews and Briffa, 2005), the absence of a consistent LIA signal in northern Ontario and Québec deserves some discussion. The LIA cooling period has been inferred from different proxies and selected borehole temperature-depth profiles in eastern Canada (e.g., Archambault and Bergeron, 1992; Beltrami and Mareschal, 1992; Wang and Lewis, 1992; Chouinard *et al.*, 2007; Bunbury *et al.*, 2012). For example, pollen data indicate a pronounced LIA cooling in Québec (Viau and Gajewski, 2009; Gajewski, 1988). The lack of LIA signal in the majority of the borehole inversions could be related to a combination of several factors. One is the limited resolution of the inversion of borehole temperature profiles. In the presence of noise, a period of weak cooling between 500 and 200 yr BP followed by strong warming is diffi-

cult to resolve. Resolution at Otoskwin is better because the singular value cutoff was lowest at this site. Furthermore, Mareschal and Beltrami (1992) showed that resolution decreases when noise and errors must be filtered and a higher singular value cutoff required to reduce the impact of noise but retain the gross features of the solution. Profiles and anomalies of Musselwhite and TM0608 are noisy, this could explain the absence of LIA signal in the reconstructions. However, the CC0713 temperature anomaly is less noisy and shows a mild cooling of $\leq$0.2 K. A test run with 1 K cooling between 1600 and 1800 and varying singular value cutoff showed that, in noise-free synthetic data, a 1 K cooling cannot be resolved with less than five singular values. This explains why a mild cooling, such as that observed at CC0713 ($\leq$0.2 K) and in pollen data ($\leq$0.3 K) (Gajewski, 1988; Viau and Gajewski, 2009; Viau *et al.*, 2012), could not resolved. Also, Chouinard and Mareschal (2007) suggested that the LIA could have started $\sim$100 years earlier in northern Québec than in southern Canada. Resolving the LIA would require a borehole deeper than $\sim$400 m, which is not the case of all the holes. Let us also point out that the sampling resolution at Nielsen Island is low, with measurements only every 30 m, which is not sufficient to resolve a LIA signal. While the absence of LIA signal in Québec was unexpected, its absence in northern Ontario confirms the findings of Gosselin and Mareschal (2003), who found only two sites with a LIA signal among 33 temperature-depth profiles from northwestern Ontario. They hypothesized that the lack of LIA signal could be due to the influence of Lake Superior because the two sites with LIA signals were above 50°N and the furthest from Lake Superior. This is not supported by the present study because the four Ontario sites are several hundreds of kilometres away from Lake Superior. It is also possible that the LIA signal is masked by other physical effects, such as an advance and retreat of permafrost or a change in the precipitation regime and the duration of the ground snow cover during the LIA.

No geographic trends in the GST histories were observed, despite different SAT conditions. Meteorological data from the NOAA weekly dataset and eight general circulation models (GCMs) for the period of 1970-1999 display a longer snow cover duration in northern Québec than in northern Ontario (Brown and Mote, 2009). The higher precipitation is confirmed by proxy reconstructions of lake levels and tree forms (Bégin, 2000; Lavoie and Payette, 1992). Because of the greater snowfall and longer snow cover, the present ground surface relative to air surface temperatures in Québec are warmer than in Ontario. However, these dissimilar conditions have not resulted in noticeable discordance between the GST histories between northern Ontario and Québec, suggesting that the same differences in precipitation persisted throughout the period reconstructed.

The magnitude of the recent warming is about the same as the ~1-2 K warming for the period of 1850 to 2000 inferred from several studies in the southern portion of the Superior Province (Beltrami and Mareschal, 1992; Shen and Beck, 1992; Chouinard and Mareschal, 2007) and less than the very pronounced warming in the eastern Canadian Arctic (Beltrami and Taylor, 1995; Taylor *et al.*, 2006; Chouinard *et al.*, 2007).

The sites are located in a region described as discontinuous permafrost, where ground temperatures are slightly below freezing, at least according to the Canadian and world permafrost maps. No sign of permafrost was found at any of the measured sites nor at the sites that were excluded (see Table 2.2); however, permafrost has been reported in the James Bay lowlands near Eleonore, Eastmain, and Lagrande (Thibault and Payette, 2009). Not only are the present average ground surface temperatures well above the freezing point of water, but, except for Nielsen Island, the ground surface temperature histories retrieved from inversion reveal that the temperature has remained well above the freezing point for

the last 500 years, indicating that the potential for permafrost was minimal to absent. We have also noted that during logging of more than 100 holes in the regions of Manitoba, Saskatchewan, and northern Ontario classified as discontinuous permafrost, permafrost has been encountered at only one hole, north of the town of Lynn Lake in northern Manitoba (Guillou-Frottier *et al.*, 1998). Clearly, the spatial distribution of permafrost outlined in the available permafrost maps is questionable, possibly because they are not based on sufficiently deep ground temperature measurements but estimated from interpolated sparse records of SAT (Heginbottom, 2002; Gruber, 2012). The discrepancy between permafrost maps and direct field observations reveal that SAT interpolations are unsuitable to estimate the spatial variations of ground temperatures. This is likely because the maximum thickness of snow exceeds 1 m at the end of the winter remaining on the ground from mid-December to mid-April, resulting in a large offset between the GST and SAT (Zhang, 2005; Grosse *et al.*, 2016). Our study suggests that borehole temperature profiles could be used in the future to assess the reality of the permafrost retreat assumed to have occurred after the LIA (Halsey *et al.*, 1995; Schuur *et al.*, 2008). Furthermore, borehole temperature profiles might be a better means for determining the southern extent of areas of past and present permafrost than current permafrost maps and a useful tool for validation of climate models.

Appendix - Detailed Site Description

Ten sites, including 18 boreholes, were utilized to reconstruct the ground surface temperature history of northern Ontario and Québec for the past 500 years. A detailed description of the rock type and geological unit of each site can be found in Table 2.4 and heat flow studies of the region (Jessop, 1968; Jessop and Lewis, 1978; Lévy *et al.*, 2010; Jaupart *et al.*, 2014).

Four sites (Musselwhite, Thierry Mine, Otoskwin, Noront) comprising nine boreholes are located in northern Ontario. The Musselwhite (0601) site is located in a clearing of ~60 m in diameter with a lake ~330 m to the west and ~180 m to the east. Three boreholes (0605, 0606, 0608) are located at Thierry Mine, ~500 m away from a large clearing. This clearing is associated with the development of the nearby mine in 1934-1950. Furthermore, all three sites are ~300 m from a lake. 0605 and 0608 are found in a clearing due to drilling of ~80 m in diameter. The Otoskwin borehole was measured in 1985 and is located ~180 m from the Otoskwin River. The final four Ontario boreholes (1012, 1013, 1014, 1015) are found in Noront. The sites are fairly flat, swampy and muddy. They are in the McFaulds Lake project, ~300 km north of the town of Geraldton and within a region referred to as the Ring of Fire of the James Bay Lowlands. N1012 and N1013 are ~40 m apart, ~500 from N1015 and ~400 m from N1014. The complex lithological column has led to noisy temperature-depth profiles (Jaupart *et al.*, 2014).

Northern Québec is home to the remaining nine boreholes, found in six distinct sites. Nielsen Island is the northern most site of this study. It was logged in 1977 and is located on an island in the Hudson Bay. The La Grande borehole (0405) is in a large clearing for drilling, in fairly flat and swampy region. It is located

~400 m from a main Hydro Québec power line and power line clearing. Eleonore (0502) is ~200 m from the Opinaco reservoir and is dipping towards the reservoir. Two boreholes (0803, 0804) are in Eastmain, ~220 km from the mining camp of Matagami. 0803 is ~50 m south of a road but is dipping away from the road. Corvet (0716) is located in a fairly flat area. The final three boreholes (0712, 0713, 0714) are in Camp Coulon. 0713 is ~20 km north of the hydroelectric station of Laforge-Deux. 0712 and 0714 are ~450 m apart and located on top of a small relief, with 0712 found in a clearing of ~30 m diameter.

Acknowledgements

The authors are grateful to Christian Chouinard, Claude Jaupart and our colleagues at the Institut de Physique du Globe de Paris who helped with field measurements and core sample analysis. We appreicate the useful and constructive comments from two reviewers, an anonymous reviewer and A.E.Taylor, R.Way and Editor A.Winguth. This work was supported by grants from the Natural Sciences and Engineering Research Council of Canada Discovery Grant (NSERC DG 140576948) and the Canada Research Program (CRC 230687) to H. Beltrami. Computational facilities provided by the Atlantic Computational Excellence Network (ACENnet-Compute Canada) with support from the Canadian Foundation for Innovation. H. Beltrami holds a Canada Research Chair in Climate Dynamics. C.Pickler is funded by graduate fellowships from a NSERC CREATE Training Program in Climate Sciences based at St.Francis Xavier University.

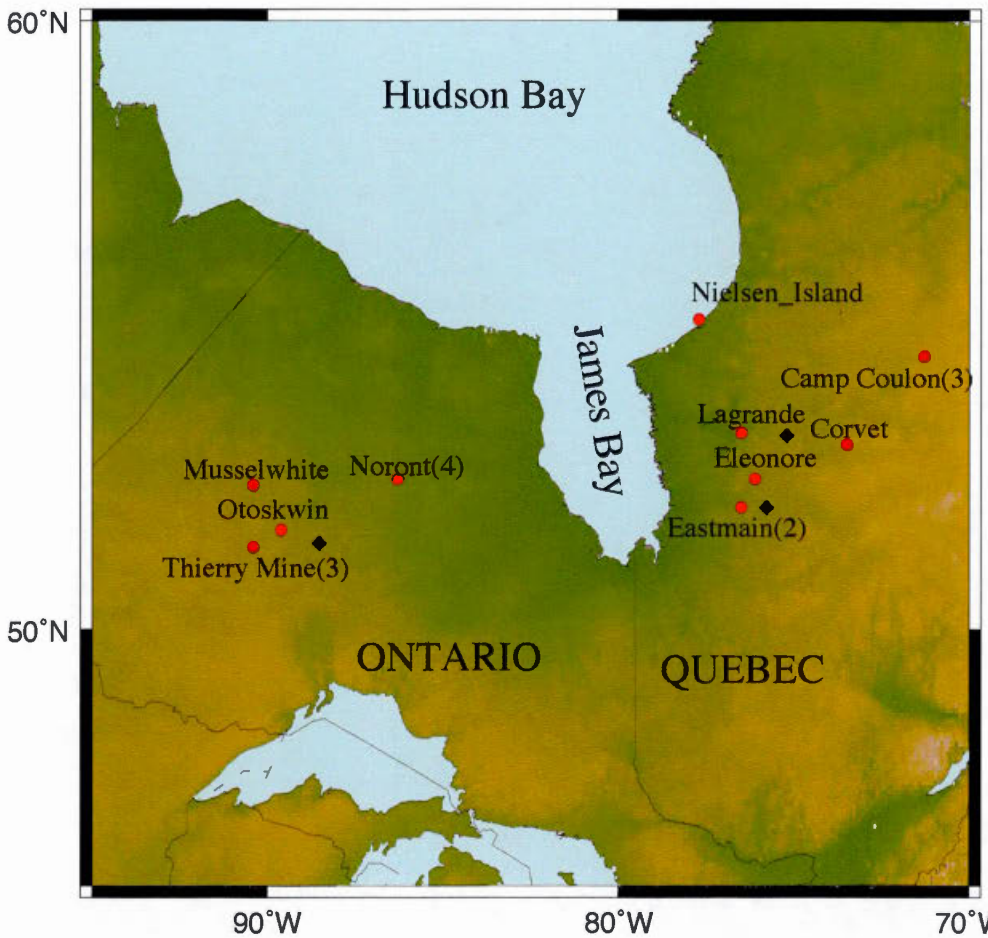

Figure 2.1 Map of Ontario and western Québec showing the location of sites (red dots). For sites with several boreholes (Camp Coulon , Eastmain, Thierry Mine, and Noront), the number of profiles available is enclosed in parenthesis. Black diamonds show the locations of sites that were discarded.

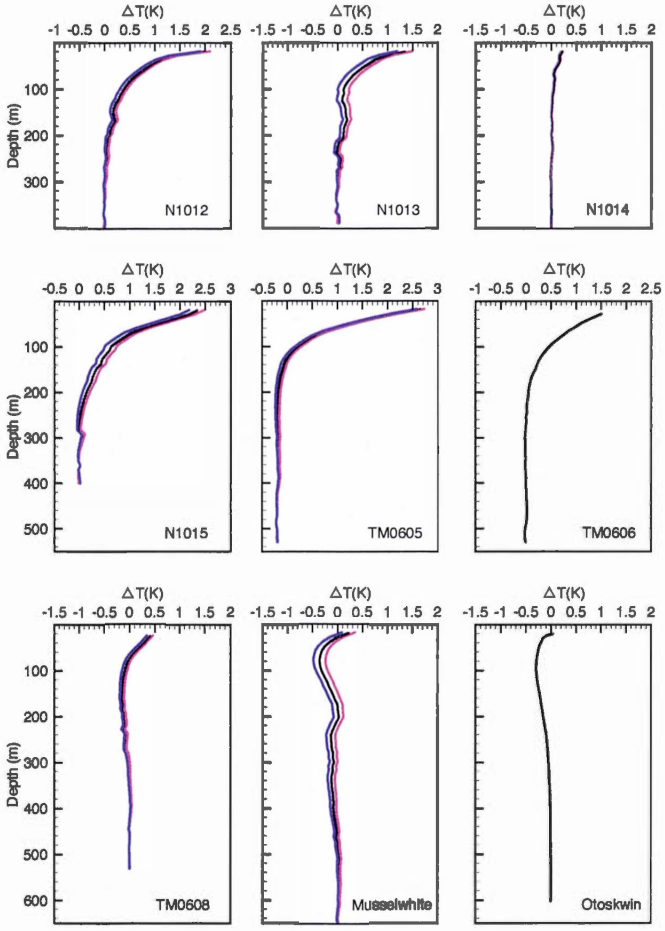

Figure 2.2 Temperature anomalies for the northern Ontario boreholes. Holes TM0605, TM0606, and TM0608 are from the Thierry Mine site; holes N1012, N1013, N1014, and N1015 belong to the Noront site. The anomaly is obtained by subtracting the estimated steady-state geotherm obtained by the least-square fit of a straight line to the bottom 100 m of the borehole temperature-depth profile. The black line represents the best linear fit, while the pink and blue lines are the upper and lower bounds, respectively, of the 2σ confidence intervals. For N1014, TM0606, and Otoskwin, the upper and lower bounds of the confidence interval are not visible due to the temperature scale. The temperature anomaly at Musselwhite was cut at 650 m.

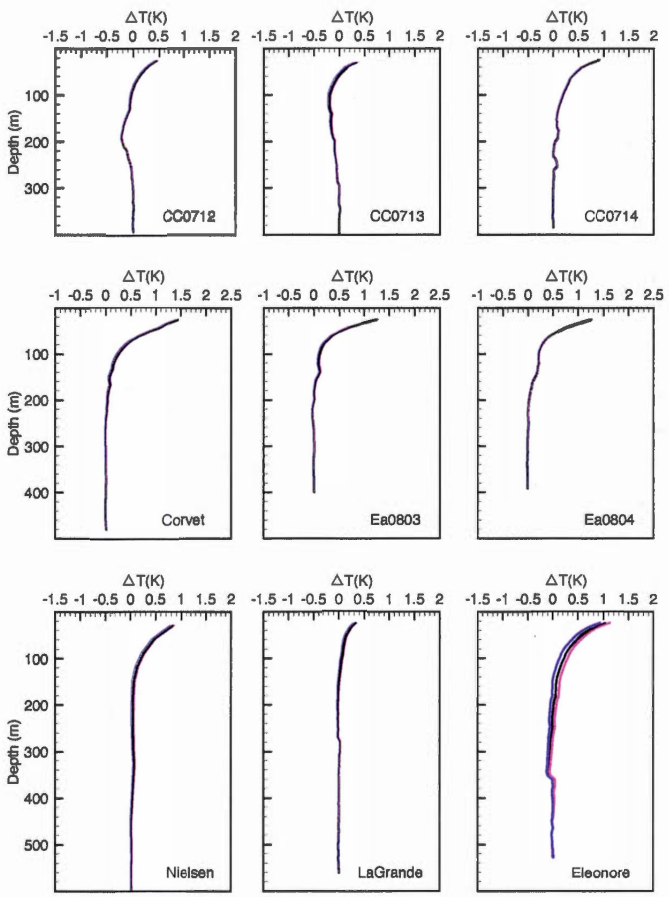

Figure 2.3 Temperature anomalies for the northern Québec boreholes. CC0712, CC0713, CC0714 are the boreholes from Camp Coulon; Ea0803 and Ea0804 are the boreholes from Eastmain . The anomaly is obtained by subtracting the estimated steady-state geotherm obtained by the least-square fit of a straight line to the bottom 100 m of the borehole temperature-depth profile. The black line represents the best linear fit, while the pink and blue lines represent the upper and lower bounds, respectively, of the 2σ confidence intervals. The temperature anomaly at Nielsen Island was cut at 600m.

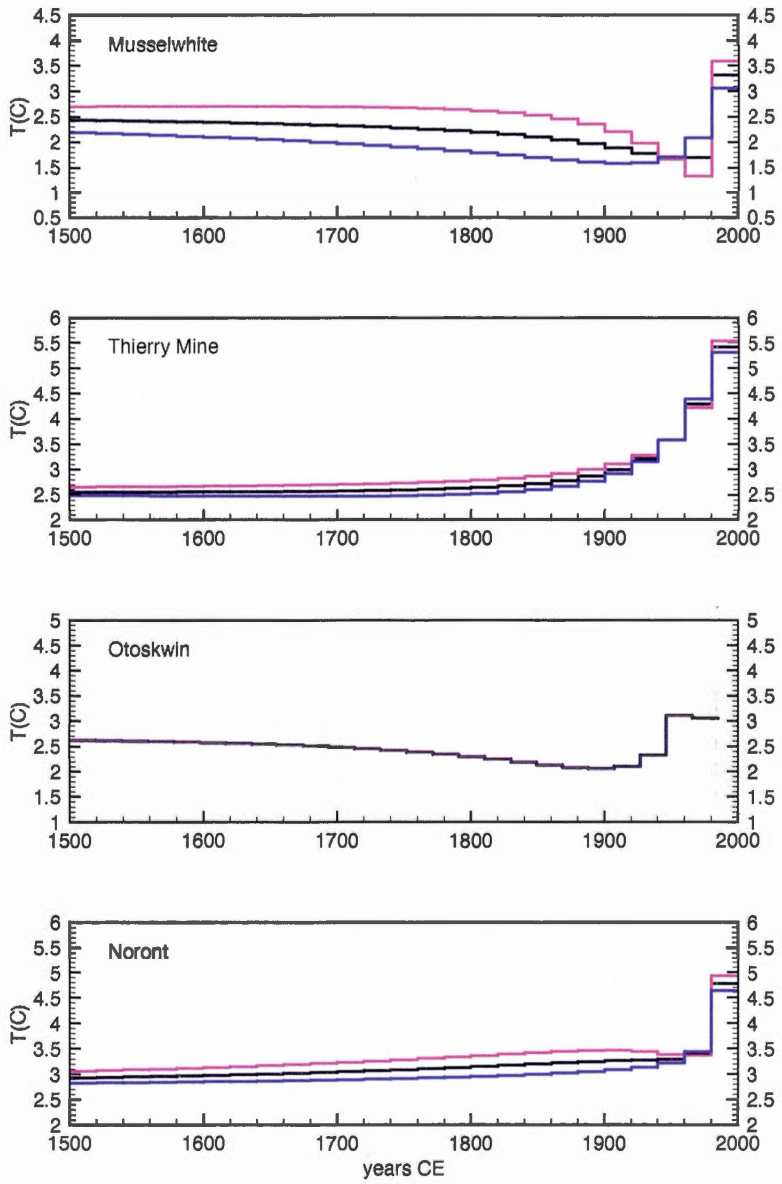

Figure 2.4 GST histories for the northern Ontario sites determined by inversion of the anomalies. For multiple holes at a given site (Thierry Mine and Noront), simultaneous inversion was used. The pink and blue lines represent the inversions of the upper and lower bounds of the anomaly. For Otoskwin, the three lines are superposed.

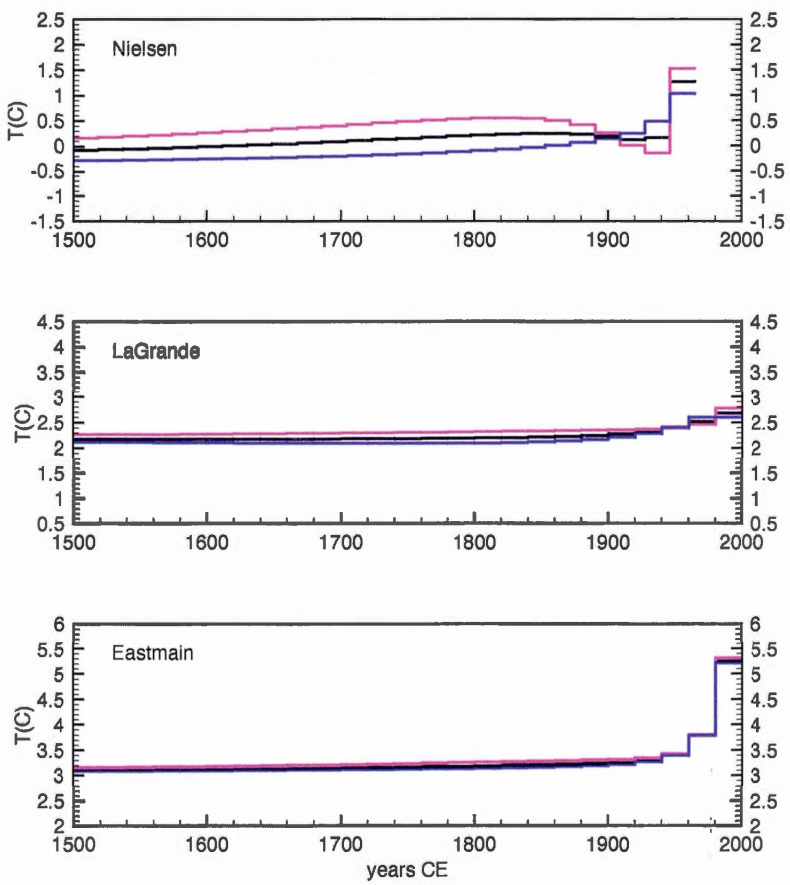

Figure 2.5 GST histories for the northern Québec sites. Simultaneous inversion was used for Eastmain, which includes two holes. The pink and blue lines represent the inversions of the upper and lower bounds of the anomaly.

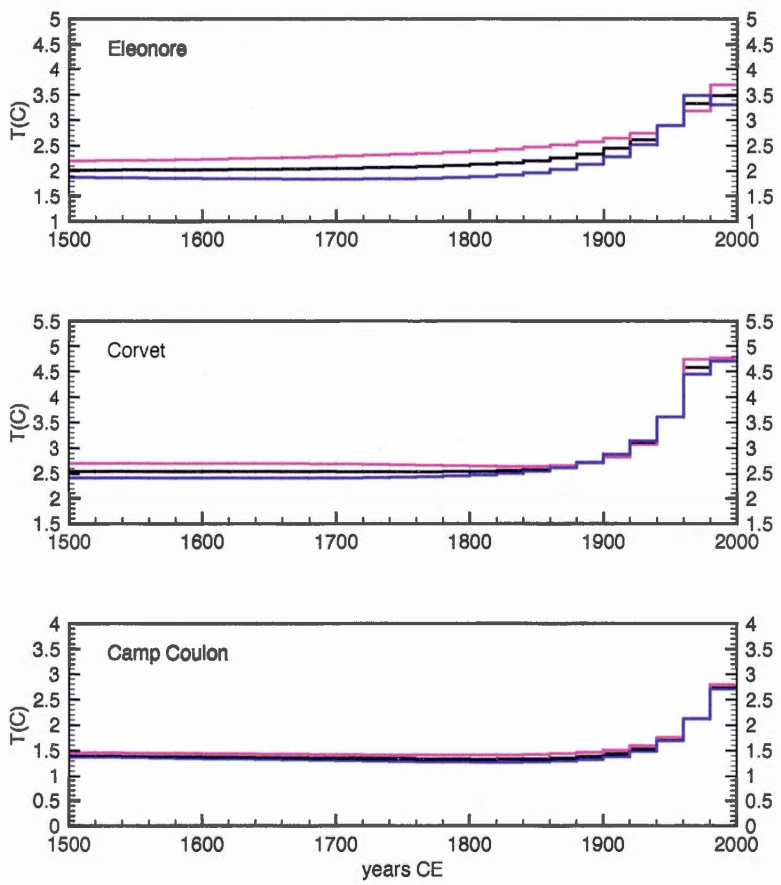

Figure 2.6 GST histories for the northern Québec sites. Simultaneous inversion was used for Camp Coulon, which includes more than one hole. The pink and blue lines represent the inversions of the upper and lower bounds of the anomaly.

Table 2.1 Location and technical information concerning the boreholes used in this study, where true depth is the depth corrected for the dip of the borehole, λ is the thermal conductivity, Q is the heat flux, and Q_{corr} is the heat flux corrected for post glacial warming

Site	Log ID	Latitude	Longitude	Dip (°)	True depth (m)	λ (W m^{-1} K^{-1})	Q (mW m^{-2})	Q_{corr} (mW m^{-2})	Reference
Musselwhite	0601	52°37′28.3″	90°23′32.7″	76	740	2.73	30.7	33	Lévy *et al.* (2010)
Thierry Mine							**28**		
	0605	51°30′24″	90°21′11″	74	802	2.91	26.8	29.7	Lévy *et al.* (2010)
	0606	51°30′22″	90°21′11″	70	530	2.61	24.4	27.0	Lévy *et al.* (2010)
	0608	51°30′24.3″	90°21′10.7″	62	737	2.60	24.6	27.1	Lévy *et al.* (2010)
Otoskwin							**25**		
	n/a	51°49.5′	89°35.9′	90	602	2.79	20	25	Jessop and Lewis (1978)
Noront							**35**		
	1012	52°44′23.9″	86°17′42.1″	68	761	3.2	34.1	37.6	Jaupart *et al.* (2014)
	1013	52°44′25″	86°17′42.1″	55	389	3.1	28.3	34.1	Jaupart *et al.* (2014)
	1014	52°44′29.9″	86°17′59.9″	77	762	3.1	31.7	35.6	Jaupart *et al.* (2014)
	1015	52°44′25.5″N	86°18′11.9″W	75	806	3.1	29.5	33.4	Jaupart *et al.* (2014)
Nielsen Island							**26**		
	0-77	55°23.7′	77°41.0′	90	1408	5.5 ($\leq$ 400m) 2.4 (> 400 m)	-	26.8	Jessop (1968)
LaGrande							**22**		
	0405	53°31′45″	76°33′15″	60	600	2.89	19.2	21.9	Lévy *et al.* (2010)
Eastmain							**34**		
	0803	52°10′16″	76°27′66″	60	398	2.9	28.8	34.1	Jaupart *et al.* (2014)
	0804	52°10′16″	76°27′66″	60	390	2.9	26.7	32.9	Jaupart *et al.* (2014)
Eleonore							**31**		
	0502	52°42′05″	76°04′46″	56	527	2.47	30.7	32.8	Lévy *et al.* (2010)
Corvet							**27**		
	0716	53°19.072′N	73°55.760′W	67	479	2.80	24.0	26.8	Lévy *et al.* (2010)
Camp Coulon							**28**		
	0712	54°47′43″	71°17′09″	54	561	3.69	26.4	29.0	Lévy *et al.* (2010)
	0713	54°47′95″	71°17′20″	40	460	3.73	24.5	27.5	Lévy *et al.* (2010)
	0714	54°47′43″	71°17′34″	56	384	-	-	-	Lévy *et al.* (2010)

Table 2.2 Location and technical information concering boreholes not suitable for this study, where T_o is the reference surface temperature and Q_o is the reference heat flux

Site	Log ID	Latitude	Longitude	T_o (°C)	Q_o (mW m^{-2})	Remark	Reference
Miminiska	0603	51°34′51″	88°31′09″	3.33±0.02	25.8±1.5	Too shallow	(Lévy *et al.*, 2010)
LaGrande	0406	53°31′42″	76°33′49″	2.67±0.005	14.1±0.3	Topography	(Lévy *et al.*, 2010)
Eleonore	0503	52°42′00″	76°04′45″	2.56±0.01	27.7±0.6	Reservoir	(Lévy *et al.*, 2010)
Clearwater	0505	52°12′33″	75°48′38″	2.33±0.02	30.6±0.4	Lake	(Lévy *et al.*, 2010)
	0506	52°12′31″	75°48′23″	2.23±0.01	31.3±0.2	Lake	(Lévy *et al.*, 2010)
	0507	52°12′39″	75°48′23″	2.73±0.004	30.5±0.3	Lake	(Lévy *et al.*, 2010)
Poste Lemoyne	0715	53°27′37″	75°12′21″	1.83±0.004	24.5±0.2	Topography	(Lévy *et al.*, 2010)

Table 2.3 Summary GST History Results where T_o is the reference surface temperature, Q_o is the reference heat flux, ΔT is the difference between the maximal temperature and the reference temperature 500 years before logging.

Site	Log ID	year	T_o (°C)	Q_o (mW m^{-2})	ΔT (K)	LIA
Musselwhite	0601	2006	2.56±0.01	30.0±0.5	0.88	no
Thierry Mine					2.85	no
	0605	2006	2.63±0.01	25.9±0.5		
	0606	2006	2.55±0.01	23.5±0.7		
	0608	2006	2.62±0.01	23.9±0.3		
Otoskwin	n/a	1985	2.81±0.001	19.5±0.05	0.50	yes
Noront					1.85	no
	1012	2010	1.16±0.01	35.5±0.9		
	1013	2010	1.51±0.02	31.3±1.5		
	1014	2010	1.78±0.004	32.2±0.3		
	1015	2010	2.35±0.02	27.6±1.4		
Nielsen Island	0-77	1977	-0.43±0.02	23.7±0.4	1.35	no
LaGrande	0405	2004	2.18±0.004	19.4±0.2	0.50	no
Eastmain					2.15	no
	0803	2008	2.98±0.01	27.3±0.4		
	0804	2008	3.01±0.003	27.0±0.2		
Eleonore	0502	2005	2.04±0.01	30.9±0.5	1.46	no
Corvet	0716	2007	2.45±0.01	24.9±0.3	2.18	no
Camp Coulon					1.34	no
	0712	2007	1.46±0.01	26.6±0.4		
	0713	2007	1.83±0.01	24.2±0.6		
	0714	2007	1.33±0.004	-		

Table 2.4 Geological unit and rock type concerning the boreholes used in this study

Site	Log ID	Rock Type	Geological Unit	Reference
Musselwhite	0601	gneiss	Sachigo subprovince	Lévy *et al.* (2010)
Thierry Mine	0605	granite	Uchi belt	Lévy *et al.* (2010)
	0606			Lévy *et al.* (2010)
	0608			Lévy *et al.* (2010)
Otoskwin	n/a	-	-	Jessop and Lewis (1978)
Noront	1012	-	North Caribou terrane	Jaupart *et al.* (2014)
	1013			Jaupart *et al.* (2014)
	1014			Jaupart *et al.* (2014)
	1015			Jaupart *et al.* (2014)
Nielsen Island	0-77	-	-	Jessop (1968)
LaGrande	0405	granodiorite	LaGrande volcano-plutonic belt	Lévy *et al.* (2010)
Eastmain	0803	metasedimentary and volcanics	LaGrande volcano-plutonic belt	Jaupart *et al.* (2014)
	0804			Jaupart *et al.* (2014)
Eleonore	0502	wacke	LaGrande volcano-plutonic belt	Lévy *et al.* (2010)
Corvet	0716	intermediate volcanics	LaGrande volcano-plutonic belt	Lévy *et al.* (2010)
Camp Coulon	0712	rhyolite	LaGrande volcano-plutonic belt	Lévy *et al.* (2010)
	0713			Lévy *et al.* (2010)
	0714			Lévy *et al.* (2010)

CHAPTER III

CLIMATE TRENDS FOR THE PAST 500 YEARS IN NORTHERN CHILE FROM BOREHOLE TEMPERATURE DATA

Carolyne Pickler[1], Hugo Beltrami[2], Jean-Claude Mareschal[1]

[1]Centre de Recherche en Géochimie et en Géodynamique (GEOTOP), Université du Québec à Montréal, Montréal, Québec, Canada

[2]Climate & Atmospheric Sciences Institute and Department of Earth Sciences, St. Francis Xavier University, Antigonish, Nova Scotia, Canada

Abstract

The ground surface temperature histories for the last 500 years were reconstructed from nine temperature-depth profiles in northern Chile. Differing trends have been observed in the region. In the northern coastal region of Chile, there is no perceptible climate signal, while the northern central Chilean region, between 26°S and 28°S, the data suggest a cooling from ~1850 to ~1980 followed by a 1.9 K warming starting ~20-40 years BP. A warming of similar amplitude is inferred in the ground surface temperature histories for Peru and the semiarid regions of South America. Such warming is greater than that inferred by the CRUTEM4 data, climate reconstructions for central Chile and southern South America, and the PMIP3/CMIP5 surface temperature simulation for the north-central Chile gridpoint. Neither the simulations nor the proxy data climate reconstructions show a cooling period. These differences are associated with a local trend not resolved in the gridpoints of the CRUTEM4 or PMIP3/CMIP5. More data and reconstructions are required to determine the long-term climate trends in northern Chile.

3.1 Introduction

To assess and predict the long-term effects of the modern climate warming, understanding and simulating Earth's complex climate and its variability is crucial. All the inferences on the future climate system come from general circulation models (GCMs). Experiments with GCMs allow for the study of future climate scenarios. Due to the limited resolution of GCMs, climatic relevant processes that operate at less than GCM grid size scale have been parametrized differently between different models. This yields simulations with a wide range of variability. Therefore, these models must be tested against paleoclimate data and reconstructions to assess the robustness of their climate projections.

As the meteorological record only extends back as far as 150 years, proxy based climate reconstructions are required to evaluate climate projections and provide insight to the long-term trends of climate variables. There has been significant work on paleoclimatic reconstructions for the Northern Hemisphere (e.g., Mann *et al.*, 1999; Moberg *et al.*, 2005; Rutherford *et al.*, 2005). However, there are few climate reconstructions for the Southern Hemisphere and the majority of them rely on a small number of data sets (Huang *et al.*, 2000; Mann and Jones, 2003; IPCC, 2013). This absence of paleoclimatic data leads to uncertainty in the forcings of the Southern Hemisphere's climate system. Studies have been initiated to fill in this gap (e.g., Villalba *et al.*, 2009; Neukom and Gergis, 2012). As of 2012, 174 monthly to annually resolved climate proxy records covering the last 2000 years have been collected (Neukom and Gergis, 2012). Using this expanded data set of terrestrial and oceanic paleoclimate records, Neukom *et al.* (2014) obtained a millennial ensemble reconstruction of annually resolved temperature variations for the Southern Hemisphere. They compared this with an independent Northern Hemisphere temperature reconstruction ensemble and found that the post-1974

warming period was the only period of the last millennium when both hemispheres experienced warm extremes. Their results imply that the global climate system cannot be solely represented by external forcings and Northern Hemisphere variations and highlight the need for more paleoclimate records from the Southern Hemisphere.

South America is a key region in understanding the climate system of the Southern Hemisphere as it is the largest landmass in the Southern Hemisphere and extends from 10°N to 55°S. The continent separates the Atlantic and Pacific Oceans, influencing ocean circulation and global climate. Because of the limited amount of paleoclimate data, the majority of studies have been restricted to the southern portion of the continent. This is an important region lies in the center of the modern westerly wind field and therefore allows for the examination of past westerly wind variability (Boninsegna *et al.*, 2009; Villalba *et al.*, 2009; PAGES-2K Network, 2013; Flantua *et al.*, 2016). Moy *et al.* (2009) analyzed multiple paleoclimate records, including meteorological, palynological, and dendrochronological data, and observed a temperature decrease and increase in westerly wind intensity during the Little Ice Age, along with arid conditions during the Medieval Climate Anomaly. Neukom *et al.* (2010) examined the hydroclimate of southern South America for the past 500 years using a multiproxy approach and inferred a multicentennial increase in summer precipitation and a decrease in winter precipitation into the 20th century. However, these studies have neglected the northern two-thirds of the South American continent, including the Atacama desert in northern Chile (PAGES-2K Network, 2013).

Studying the climate of northern Chile is key to understanding how extremely sensitive arid environments respond to climatic variations. Furthermore, the natural resources and ecosystem of northern Chile have been put under ever increasing

pressure as the economic development of the region grows (Messerli *et al.*, 1997). It is, therefore, paramount to understand the long-term climatic variations of the region. There have been regional paleoclimatic studies in northern Chile with the majority focusing on reconciling the mid-Holocene paradox, a period ~4-9 ka BP where it is uncertain whether the climate of the Atacama desert and the Central Andes was dry or humid (Bobst *et al.*, 2001; Grosjean *et al.*, 2003). Paleosoils, groundwater, abiotic proxy data, and aquatic plant pollen from lake sediments imply a very humid early Holocene and an extremely dry mid-Holocene (Bobst *et al.*, 2001; Grosjean *et al.*, 2001), while terrestrial plant pollen from lake sediments does not (Betancourt *et al.*, 2000; Latorre *et al.*, 2002). On the other hand, the recent climate and its variations have not been the focal point of these studies. The objective of this study is to provide insight to the climate of northern Chile and South America for the past 500 years by adding new data and ground surface temperature (GST) reconstructions and comparing with other proxy climate reconstructions and climate model simulations.

Earth's subsurface thermal regime is governed by the outflow of heat from Earth's interior and long-term changes in GST. If there are no GST changes, subsurface temperature increases linearly with depth. When persistent temporal GST variations occur, they diffuse downward and are recorded as perturbations to Earth's steady-state geotherm (see, e.g., Hotchkiss and Ingersoll, 1934; Birch, 1948; Beck, 1977). The duration, amplitude and time when GST changes occur govern the extent to which they are recorded. Attempts to infer past climate from these borehole temperature-depth profiles began in the 1930s (Hotchkiss and Ingersoll, 1934). It was, however, only in the 1970s that systematic studies to infer past climate were undertaken (Cermak, 1971; Sass *et al.*, 1971; Beck, 1977). As of the 1980s, the technique became more widespread due to concerns about increasing global temperatures (Lachenbruch and Marshall, 1986; Lachenbruch, 1988).

Over the years, many global, regional, and local reconstructions have been undertaken (Huang *et al.*, 2000; Harris and Chapman, 2001; Pollack and Smerdon, 2004; Jaume-Santero *et al.*, 2016; Pickler *et al.*, 2016a). However, the majority of these studies have focused on the Northern Hemisphere with little attention to the Southern Hemisphere and South America due to a lack of data. There are numerous high-resolution borehole temperature-depth measurements in South America, primarily made for heat flow studies (Figure 3.1) (Watanabe *et al.*, 1980; Uyeda and Watanabe, 1982; Hamza and Muñoz, 1996; Springer and Förster, 1998). The first heat flow measurements date back to the mid sixties before the marked warming observed in the Northern Hemisphere. Uyeda and Watanabe (1970) conducted a preliminary study of heat flow in South America. The majority of thermal gradients are normal or subnormal over the continent with high values in the Andes and low values on the Pacific coast and along the Amazon River. Additional measurements have been made in Brazil but the data are in publications of limited access (e.g., Vitorello *et al.*, 1980; Hamza *et al.*, 1987). Uyeda and Watanabe (1982) examined 25 heat flow measurements from western South America to investigate heat flow in the subduction plate boundary area of the region. They found low heat flux near the trench and high heat flux on the volcanic arc, similar to the trends observed in other arc-trench systems. Springer and Förster (1998) collected 74 heat flow measurements across the central Andes subduction zone in Chile and Bolivia to study large scale heat flux variations. They concluded that the heat flux pattern of the Central Andean subduction zone is similar to that of the active margin of the North American continent. But, they noted that differences in subduction parameters results in different lithospheric thermal conditions. Only a few of these borehole temperature profiles are useful for climate studies because of depth range and inadequate sampling. Furthermore, the only accessible archive of the temperature profiles are the publications. The uneven distribution of available and suitable borehole temperature measurements leaves several areas void of mea-

surements. Huang *et al.* (2000) undertook a global reconstruction of temperatures for the past five centuries and inferred a five century cumulative temperature increase of 1.4 K over South America. Because this study relies only on 16 borehole temperature-depth profiles, additional data are needed to confirm its conclusions. Hamza and Vieira (2011) analyzed over 30 borehole temperature-depth profiles from the Amazon region, the Cordilleran region of Colombia, eastern Brazil and the Cordilleran region of Peru. They inferred a warming of 2-3.5°C from the early 20th century to present with similar trends observed in tropical and subtropical zones. On the other hand, semi-arid zones had a warming of 1.4-2.2°C from the late 19th century to present.

As part of an attempt to enlarge the South American borehole temperature data set, we have collected 31 borehole temperature-depth profiles measured in 1994, 2012, and 2015 in northern Chile, a region that was void of data, and reconstructed the GST history for the past 500 years. We shall compare these reconstructions with model outputs and meteorological data for the region, along with proxy climate reconstructions for central Chile and southern South America to assess their robustness and determine climate trends for northern Chile.

3.2 Methodology

To utilize temperature-depth profiles to reconstruct GST histories, we assume that Earth is a half-space where physical properties vary solely with depth, heat is transported only by vertical conduction, and that changes in the surface temperature boundary condition propagate into the subsurface and are recorded as temperature perturbations, $T_t(z)$, of the quasi-steady state temperature profile. The temperature at depth, $T(z)$, can then be written as (Jaupart and Mareschal, 2011):

$$T(z) = T_o + q_o R(z) - \int_0^z \frac{dz'}{\lambda(z')} \int_0^{z'} H(z'')dz'' + T_t(z) \tag{3.1}$$

where T_o is the long-term ground surface temperature, q_o is the quasi-steady state heat flux, $\lambda(z)$ is the thermal conductivity, z is the depth, $H(z)$ is the radioactive heat production, and $T_t(z)$ is the temperature perturbation at depth z. $R(z)$ is the thermal depth, which is defined as:

$$R(z) = \int_0^z \frac{dz'}{\lambda(z')} \tag{3.2}$$

The temperature perturbation, $T_t(z)$, can be written as (Carslaw and Jaeger, 1959):

$$T_t(z) = \int_0^\infty \frac{z}{2\sqrt{\pi\kappa t^3}} \exp\left(\frac{-z^2}{4\kappa t}\right) T_o(t)dt \tag{3.3}$$

where κ is the thermal diffusivity, t is time before present, and $T_o(t)$ is the surface temperature at time t. For a stepwise change in ΔT in surface temperature at time t before present, the temperature perturbation, $T_t(z)$, is given as (Carslaw and Jaeger, 1959):

$$T_t(z) = \Delta T \text{erfc}\left(\frac{z}{2\sqrt{\kappa t}}\right) \tag{3.4}$$

where erfc is the complementary error function. The surface temperture, $T_o(t)$, can then be approximated by a series of constant values, ΔT_k, over K time intervals (t_{k-1}, t_k), and the perturbation, $T_t(z)$, is as follows:

$$T_t(z) = \sum_{k=1}^{K} \Delta T_k (\mathrm{erfc}\frac{z}{2\sqrt{\kappa t_k}} - \mathrm{erfc}\frac{z}{2\sqrt{\kappa t_{k-1}}}) \tag{3.5}$$

The ΔT_k values represent the difference between the average GST during the time interval (t_{k-1}, t_k) and T_o.

3.2.1 Inversion

In order to reconstruct the GST history, equation 3.3 (where heat production is neglected) and 3.5 are combined to obtain one linear equation for each measured depth (z) with $K + 2$ unknowns, T_o, q_o, and ΔT_k. The inversion involves solving the system of equations for the unknown parameters. This can be done by: (1) solving for the $K + 2$ unknown parameters simultaneously or (2) determining independently T_o and Γ_o, the long-term ground surface temperature and quasi-steady state temperature gradient. Here, we use the second technique. T_o and Γ_o are calculated by the linear regression of the bottommost 100 m of the temperature-depth profile. The bottommost 100 m of the temperature-depth profile is used since it is assumed to be sufficiently deep to be free of short period surface temperature perturbations and represent the geothermal quasi-steady state. An estimate of the maximum error at a 95% confidence interval of T_o and Γ_o is also provided by the linear regression and are the upper and lower bounds of the geothermal quasi-steady state, referred to as the extremal steady states. The anomaly or temperature perturbation, T_t, is then obtained by the subtraction of this linear fit from the data. If N temperature measurements were made, we are now left with a system of N linear equations with K unknowns, the K values of ΔT_k. This system of equations is ill-conditioned and its solution is unstable (Lanczos, 1961). To stabilize the solution, various inversion techniques have been used (Bayesian methods, singular value decomposition, Monte-Carlo methods) and applied to GST history reconstructions (e.g., Vasseur *et al.*, 1983; Shen and

Beck, 1983; Nielsen and Beck, 1989; Mareschal and Beltrami, 1992; Wang *et al.*, 1992; Clauser and Mareschal, 1995). We are using singular value decomposition (SVD) because its application to GST reconstructions is straightforward. More details can be found in Mareschal and Beltrami (1992) and Clauser and Mareschal (1995).

3.2.2 Simultaneous inversion

Simultaneous inversion is used at sites with multiple boreholes. These sites are expected to have experienced the same surface temperature variations and have consistent subsurface temperature anomalies. Inverting these sites simultaneously for a common GST history model results in increasing the signal to noise ratio and reinforcing trends in the temperature anomalies. This technique has been widely used and is discussed further in Beltrami and Mareschal (1992), Clauser and Mareschal (1995) and Beltrami *et al.* (1997).

3.3 Data description and selection

Thirty-one borehole temperature-depth profiles varying in depth from 118 m to 557 m were logged at 11 sites in northern Chile (Figure 3.2). All boreholes are located in the Atacama desert, an arid region with little to no vegetation. The profiles were measured during three different campaigns in 1994, 2012, and 2015 (Springer, 1997; Springer and Förster, 1998; Gurza Fausto, 2014). Locations, depths, elevations, and campaign details are summarized in Tables 3.1, 3.2, and 3.3. All boreholes logged were drilled for mining exploration purposes. The data were obtained using different measurement techniques. Digital optic-fibre temperature sensing (DTS) was used in 1994 and 2015. It is based on the measurement of a backscattered laser light pulse through a fibre-optic cable (Förster *et al.*, 1997; Förster and Schrötter, 1997). This results in the instantaneous measurement of

the entire profile once the cable has been completely lowered into the borehole. A detailed description of this methodology can be found in Förster *et al.* (1997), Förster and Schrötter (1997), Hausner *et al.* (2011) and Suárez *et al.* (2011). The remaining profiles were measured using the conventional method of lowering a calibrated thermistor into the borehole and measuring temperature with depth. In 2012, temperature was measured continually by lowering the thermistor into the borehole at an average speed of ~10-15 m/min. In 1994 and 2015, temperatures were measured at 2 m and 10 m intervals, respectively. All sites were resampled at 10 m intervals to ensure they were weighted evenly. Förster *et al.* (1997) and Wisian *et al.* (1997) ran tests to ensure the compatibility of the two methods (DTS and conventional). An offset in the temperature-depth profiles was found and attributed to the calibration of the measurement tools. This effect is considered unimportant when examining temperature changes but must be taken into consideration when calculating the long-term GST.

To determine the suitability of the borehole temperature-depth profiles for climate studies, several selection criteria were used and lead to the rejection of 20 temperature-depth profiles (Table 3.4). Firstly, the tectonic setting of the 31 borehole temperature-depth profiles was considered. They were measured in the tectonically active central Andean orogeny. Uplift and erosion occur within an orogeny and can alter the temperature gradient (Jeffreys, 1938; Benfield, 1949; Jaupart and Mareschal, 2011). However, these tectonic effects operate on a much larger timescale than the 500 year period studied here and are therefore considered to be negligible. Secondly, to reconstruct 500 years, boreholes must be at least 300 m deep and have measurements in the top 100 m. Any sites less than 300 m deep and/or with no measurements in the top 100 m were deemed too shallow and rejected. Furthermore, profiles were visually inspected to ensure no discontinuities, signs of water flow, or other perturbations that would make them

unsuitable for climate reconstructions. As topography is known to distort the temperature isotherms, sites in regions of significant topography were rejected (Jeffreys, 1938). This left eleven profiles suitable for climate studies. However, two of the retained profiles are repeat measurements and do not provide additional information. The measurement and repeat measurement of the borehole temperature data at the Vallenar site (ala1110/ala1110-2) were done using the same technique (conventional method with continuous sampling) and yield identical profiles. The retained profile (ala1110-2) was chosen arbitrarily. The second site with repeat measurements was borehole 1501/DDH2489A at Inca de Oro. The borehole temperature data were measured using the two different techniques, conventional and DTS. Because DTS has a lower resolution than the conventional method, the DTS profile (DDH2489A) was discarded.

After data selection, nine independent profiles were retained for climate reconstructions (Figure 3.3-3.4). They were truncated at 300 m to ensure we were studying the same time period (Beltrami *et al.*, 2011). These profiles are distributed between four sites in northern coastal Chile (Michilla) and north-central Chile (Inca de Oro, Totoral, Vallenar) (Figure 3.2). The two regions, northern coastal Chile and north-central Chile, are separated by over 500 km. The three Michilla boreholes, in northern coastal Chile, are ~10 km from the coast. They were measured in a relatively flat area near the Michilla open pit mine. The remaining three sites (Inca de Oro, Totoral, Vallenar) are found in north-central Chile between 26°S and 28°S. Four boreholes were logged at Inca de Oro in a flat region, ~1 km from the Inca de Oro mine and less than 100 km from the coast. The Totoral borehole was ~75 km south-west of the city of Copiapó and located in a relatively flat area, ~50 km from the coast. The remaining borehole of Vallenar is located between two hills, ~20 km south-west of the city of Vallenar and ~40 km from the coast.

3.4 Results

The GST changes for the past 500 years relative to the measurement date were reconstructed for the four retained sites (Michilla, Inca de Oro, Totoral, Vallenar) using a model consisting of 25 time-steps of 20 years (Figures 3.5-3.8). Sites with multiple boreholes (Michilla and Inca de Oro) were inverted simultaneously to increase the signal to noise ratio (Beltrami *et al.*, 1997). Furthermore, as we expect meteorological trends to be correlated over <500 km, the six borehole temperature-depth profiles in north-central Chile (Inca de Oro, Totoral, Vallenar) were also inverted simultaneously (Figure 3.9). Three eigenvalues were retained for all the inversions. The number of eigenvalues retained acts as a smoothing constraint by removing part of the solution that is most affected by noise (Mareschal and Beltrami, 1992). The inversion results are summarized in Table 3.5.

The GST history of northern coastal Chile (Michilla) shows no warming or cooling for the past 500 years (Figure 3.5). However, the temperature anomalies of the three Michilla profiles show very weak climate signals that are not consistent between profiles (Figure 3.4). Two of the temperature anomalies indicate a cooling (~0.2 K), while the other suggests a warming (~0.5 K). The small amplitude and inconsistencies point to the absence of a signal above the level of noise. This differs from the trends observed in north-central Chile, which is plausible as the two regions are over 500 km apart.

A climate signal has been recorded in the GST history of the three north-central Chile sites (Inca de Oro, Totoral, Vallenar) (Figures 3.6-3.8). Two main periods appear: (1) no warming or cooling between 1500 and ~1800 and (2) a recent climate warming. There are differences between sites with respect to the amplitude and timing of this warming. The warming at Inca de Oro and Vallenar is very

recent, beginning in 1960, while that of Totoral starts much earlier, ~1800. This warming ranges in amplitude from 0.4 K at Vallenar to 2.2 K at Inca de Oro. It continues until present (2000) at Inca de Oro and Vallenar. However, at Totoral, the maximum temperature, a warming of 1.7 K, is reached in 1960 and followed by a cooling of ~1 K until present. The robustness of this cooling is questionable as it is not marked in the temperature anomaly and may be outside the resolution of our reconstructions. Between ~1800 and 1960, cooling of 0.9 K and 1.1 K are found at Inca de Oro and Vallenar, respectively. It is also apparent in the temperature anomalies for the Vallenar and Inca de Oro, excluding borehole 1505 (Figure 3.4). This cooling is not present in the GST history or temperature anomaly of Totoral.

The simultaneous inversion of the six northern-central Chile borehole temperature-depth profiles yields a GST history similar to those of Inca de Oro and Vallenar (Figure 3.9). There is no warming or cooling between 1500 and ~1800. A cooling of 0.6 K is inferred between ~1800 to 1960, followed by a warming of 1.9 K until present.

3.5 Discussion

3.5.1 Comparison between GST histories

A recent climate warming of ~0.5-2 K with respect to the long-term GST is reconstructed at all sites in north-central Chile. The amplitude of this warming agrees with that suggested by Huang *et al.* (2000) for the South American continent (1.4 K). Furthermore, its amplitude agrees with the warming of ~1.4-2.2°C inferred for semi-arid regions of South America, starting in the late 19th century (Hamza and Vieira, 2011). The timing of this warming coincides with that of the Totoral site but is much earlier than at Inca de Oro, Vallenar, and north-central Chile, which occurred ~20-40 years BP. There is also no evidence of cooling in the GST

for semi-arid South America, suggesting that this cooling is a regional feature of north-central Chile.

The global reconstruction of Huang *et al.* (2000) did not analyze any borehole temperature-depth profiles from northern Chile, but analyzed four borehole temperature depth profiles from the semi-arid region of Peru. Only two of these profiles meet our selection criteria (LM18 and LOB525), the others (LOB527 and PEN742) are too shallow. Figure 3.10 compares the Peruvian GST history with that for north-central Chile. The GST history for the Peruvian boreholes was determined by the simultaneous inversion of the temperature anomalies (obtained using the technique outlined in section 3.2.1) cut at 300 m and retaining 3 eigenvalues. Since these boreholes were measured in 1979, the GST history was reconstructed with respect to the year of measurement. The Peruvian and the north-central Chile GSTs agree for the period between 1500 and ~1800, where no cooling or warming is observed. Following this period, the Peruvian GST shows a warming signal of 1.6 K until 1979. The amplitude of this warming signal agrees with that of north-central Chile (1.9 K) but it starts much earlier and no cooling period is inferred. However, examining the GST of LM18, the Peruvian site closest to the border with Chile and at the northern edge of the Atacama desert, a cooling of ~0.5 K is present from ~1800 to 1950, agreeing with that observed in north-central Chile. This leads us to hypothesize that this cooling is a local trend.

3.5.2 Comparison with meteorological data

Meteorological data from the CRUTEM4 for the northern coastal and north-central Chile gridpoints are available but only extend back ~100 years (Jones *et al.*, 2012). The CRUTEM4 data for northern coastal Chile and north-central Chile show a warming trend over the past 100 years, highlighting the absence of

climate signal in the northern coastal Chile GST history. This warming agrees with the recent warming in the GST history for the north-central Chile, but its amplitude is ~4 times less than that of the GST history. The north-central Chile CRUTEM4 gridpoint extends across several climatic zones from the coast to the Andes. The climate of the Andes and the coast are cooler than that of the Atacama desert. Their influence could explain the smaller warming signal. Furthermore, it could explain the absence of a cooling signal, which cannot be resolved on the gridpoint scale.

Examination of meteorological data from Copiapó, a city less than 100 km from Inca de Oro in north-central Chile, shows a temperature decrease of ~2.5 K between 1950 and 1960. To determine whether this cooling could be resolved by in the GST reconstruction, a test was run for a synthetic profile with a cooling of 2.5 K between 1950 and 1960. The profile was inverted for a history of the last 500 years in intervals of 20 years, retaining 3 eigenvalues. The inversion yielded a cooling of 0.5 K between 1800 and 1960, showing that a strong local cooling between 1950 and 1960 could be interpreted as the cooling trend in the north-central GST history.

3.5.3 Comparison with other climate proxies

The north-central Chile GST history was also compared with the linear regression 5-year smoothed austral summer surface air temperature reconstruction from sedimentary pigments at Laguna Aculeo, central Chile (von Gunten *et al.*, 2009) and the southern South America austral summer surface air temperatures inferred from 22 annually resolved predictors from natural and anthropogenic archives (Neukom *et al.*, 2010) (Figure 3.11). While there have been paleoclimatic studies in northern Chile, they do not focus on the recent climate, i.e. the last 1000 years (e.g., Bobst *et al.*, 2001; Grosjean *et al.*, 2003), leading to the comparison with

the von Gunten *et al.* (2009) and Neukom *et al.* (2010) data. This also provides insight to whether the trends in northern Chile are regional or extend through central Chile and southern South America. From 1500 to 1700, there is no warming or cooling observed in any of the proxy climate reconstructions. Decadal variations, which cannot be resolved in the GST, are observed from 1700 to 1900 in the climate reconstruction for central Chile and southern South America. The climate reconstructions for the three regions show a recent climate warming but differences are noted with respect to the timing of its onset and its amplitude. In southern South America and central Chile, a recent warming of ~0.5 K starting ~150 years BP is inferred. In northern Chile, the warming begins significantly later, ~20-40 years BP, and reaches a maximum of 1.9 K with respect to the long-term GST. No cooling trend is observed in the central Chile or southern South America climate reconstructions. These differences suggest that the cooling and greater amplitude recent warming are regional features of north-central Chile but the absence of warming or cooling from 1500 to 1700 is a climate trend for southern South America.

3.5.4 Comparison with models

The simulations of the last millennium for the Paleoclimate Modelling Intercomparison Project Phase III (PMIP3) of the Coupled Model Intercomparison Project Phase 5 (CMIP5) provide insight to the climate of the last millennium (Braconnot *et al.*, 2012; Taylor *et al.*, 2012). The six models used to determine the multi-model mean surface temperature anomaly are outlined in Table 3.6. The multi-model mean surface temperature anomaly from the last millennium PMIP3/CMIP5 simulations for the gridpoints of northern coastal and north-central Chile show similar trends. Between 1500 and 1900, there is no warming or cooling. From 1900 to present, there is a warming of ~1 K. This supports the absence of climate signal

in the GST history of northern coastal Chile. Similarities are observed between the multi-model mean surface temperature anomaly for the north-central Chile gridpoint and the GST history for the region (Figure 3.12). Both infer no warming or cooling between 1500 and ~1800 and a recent warming. The warming of the PMIP3/CMIP5 surface temperature simulation is half and starts earlier than that reconstructed by the GST history. No cooling is observed in the PMIP3/CMIP5 surface temperature simulation for the north-central Chile gridpoint. This further suggests that this cooling trend and greater amplitude recent warming are local trends for north-central Chile and cannot be resolved on the PMIP3/CMIP5 gridpoint scale.

3.6 Conclusions

Thirty-one temperature-depth profiles from northern Chile were collected to reconstruct the GST history for the past 500 years. No climate signal was recorded in the northern coastal Chile profiles. The GST history for north-central Chile shows a period of no warming or cooling between 200-500 years BP, a cooling of 0.6 K from ~60-200 years BP followed by a recent climate warming of 1.9 K for ~20-40 years BP. The absence of warming or cooling from ~200-500 years BP is also found in other GST histories for South America, climate reconstructions for central Chile and southern South America, and the PMIP3/CMIP5 surface temperature simulation for the northern coastal and north-central Chile gridpoints. A cooling signal from ~1850 to ~1960 coinciding with that inferred in the GST history for north-central Chile is only observed in the GST reconstruction for the Peruvian borehole (LM18) at the northern edge of the Atacama desert. The amplitude of the recent warming agrees with GST reconstructions for Peru and semiarid regions of South America but is greater than that inferred by the CRUTEM4 data, climate reconstructions for central Chile and southern South America and the PMIP3/CMIP5 surface temperature simulation for the north-

central Chile gridpoint. Differences are also observed with respect to the timing of the recent warming. While it begins ~20-40 years BP in the north-central Chile GST, it starts ~100 years BP in the other South American GST histories, climate reconstruction for central Chile and southern South America, CRUTEM4 data for the north-central Chile gridpoint, and the PMIP3/CMIP5 surface temperature simulation for north-central Chile.

Differences are hypothesized to be due to regional trends in the Atacama desert, which cannot be resolved on the PMIP3/CMIP5 or CRUTEM4 gridpoint scale, and do not occur in central Chile or southern South America. The period of no warming or cooling from 200-500 years BP appears be a regional trend for all of South America. However, more data and reconstructions are required to confirm these conclusions and determine the long-term climate trends for northern Chile.

Appendix-Boreholes not suitable for climate

The borehole temperature-depth profiles that did not meet the selection criteria for climate studies can be found in Figure 3.13. The majority of borehole temperature-depth profiles were rejected because they were deemed too shallow, i.e. they were less than 300 m deep or had no measurements in the top 100 m. Some were also eliminated due to discontinuities, signs of water flow, or other perturbations through visual inspection of the profiles. Furthermore, sites were excluded due to topography since it is known to distort the temperature isotherms (Jeffreys, 1938).

3.6.1 El Loa

The site is mountainous and includes two boreholes. This is the furthest east and has the highest elevation (3950 m) among all the sites in this report. The temperature-depth profiles were too shallow for climate studies. They indicated high heat flux in the region (Figure 3.13), which could be attributed to the proximity of two volcanoes, the Miño Volcano ($\sim$6 km) and the Cerro Aucanquilcha ($\sim$20 km).

3.6.2 Mansa Mina

The Mansa Mina borehole is located in a relatively flat region. It is $<$10 km from Chuquicamata mine, which is by extracted volume the largest open pit mine in the world, and $\sim$10 km from the city of Calama. It is too shallow for climate studies.

3.6.3 Sierra Limon Verde

Six borehole temperature-depth profiles were measured in Sierra Limon Verde. They are shallower than 300 m and found within 25 km. Boreholes MODD37 MODD38, and MODD45 lie on top of a ~400 m high hill. SLV-A and SLV-B are situated on the southern flank of this hill and MODD34 on the northern slope. The site is ~25 km from the city of Calama and ~35 km from the Mansa Mina borehole.

3.6.4 Sierra Gorda

The two boreholes are located in a relatively flat region, ~30 km south-east of the village of Sierra Gorda and were too shallow to be retained for climate studies. They are separated by ~9 km and are close to the Sierra Gorda open pit mine.

3.6.5 Vallenar

This site, ~ 20 km from Vallenar and ~40 km from the coast, has two boreholes that have been measured twice using the same measurement technique. The repeat measurements were not included in order to not bias the reconstructions and only borehole ala1110 was retained for climate studies. The temperature-depth measurement of borehole ala0901 was discarded for being too shallow. Borehole ala0901 is ~300 m from borehole ala1110 and is located between two hills, ~ 20 km from Vallenar and ~40 km from the coast.

3.6.6 Copiapó

Two boreholes, ~200 m apart, were measured at Copiapó. The temperature-depth profile of borehole 1507/DDH009 was measured twice using different techniques, conventional and DTS. The two boreholes are in an area of significant topogra-

phy, ~10 km east of the city of Copiapó. Since topography distorts temperature isotherms, the temperature-depth profiles were rejected. Furthermore, discontinuities were noted in the profiles of boreholes 1506 and 1507.

3.6.7 Totoral

The site is in a relatively flat area, ~75 km south-west of Copiapó, and ~50 km from the coast. Two temperature-depth profiles for borehole 1509/RC370 were obtained using the conventional method and DTS. The profile obtained using DTS was retained, while that measured using the conventional method showed discontinuities probably caused by instrumental problems and was rejected.

3.6.8 Punta Diaz

The site is on top of a ~100 m hill and ~3 km from the town of Punta Diaz. Signs of water flow are present in the temperature-depth profile, which lead to its exclusion.

3.6.9 San José de Coquimbana

The site is on the side of a small hill, ~40 km from Vallenar and ~30 km from the coast. Using DTS and the conventional method, two temperature-depth profiles were measured for borehole 1511/RC363. Both profiles show signs of water flow and were discarded.

Acknowledgements

The authors are grateful to CODELCO for access to the boreholes during the 2015 campaign and to Andrea Förster for the borehole temperature-depth profiles from her 1994 campaign. A special thanks to Arlette Chacon-Oecklers for organizing the 2015 campaign and her invaluable help sampling the boreholes. We appreciated the help during sampling from Marie-Theresa, Nicole and Lizette. This work was supported by grants from the National Sciences and Engineering Research Council of Canada Discovery Grant (NSERC DG 140576948) and the Canada Research Program (CRC 230687) to H.Beltrami. H.Beltrami holds a Canada Research Chair in Climate Dynamics. C.Pickler was funded by graduate fellowships from UQAM and a NSERC CREATE Training Program in Climate Sciences based at St.Francis Xavier University.

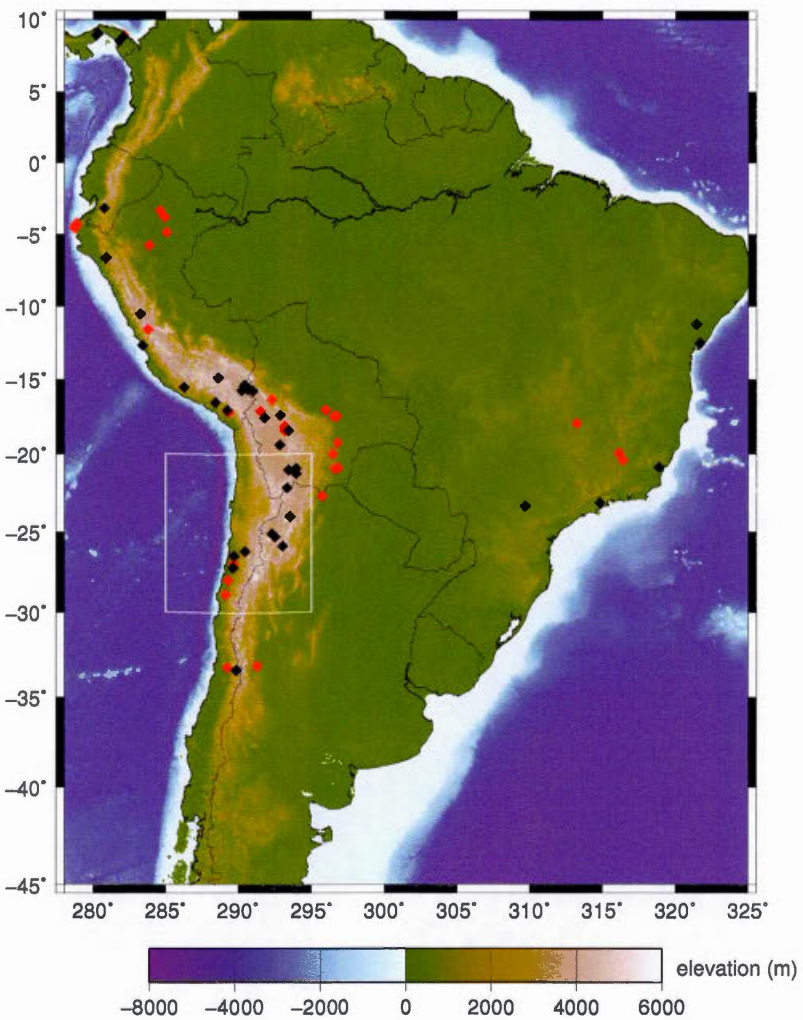

Figure 3.1 Map of South America including locations of borehole temperature measurements for heat flow studies (Lucazeau, personal communication). Red diamonds represents boreholes deeper than 200 m, while black are boreholes shallower than 200 m. More than 100 bottom-hole temperature measurements, mainly in Brazil, are not included as they are not useful for climate studies. The rectangle indicates the study region of northern Chile.

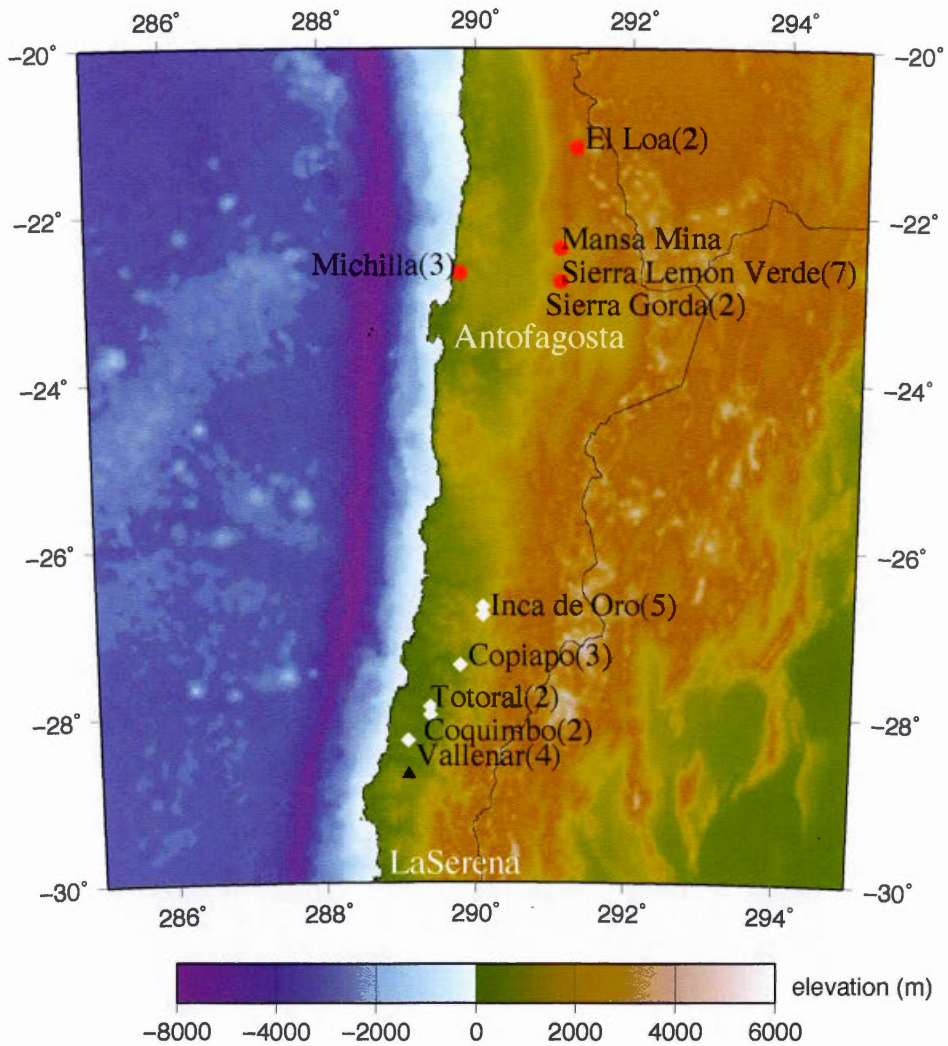

Figure 3.2 Map of northern Chile with locations of boreholes used in this study. The number of boreholes at each site is indicated in parenthesis. Red circles indicate borehole temperature-depth profiles measured in 1994, black triangles are measured in 2012, and white diamonds are measured in 2015. Sites with borehole temperature-depth profiles deemed suitable for climate are Michilla, Totoral, Inca de Oro, and Vallenar.

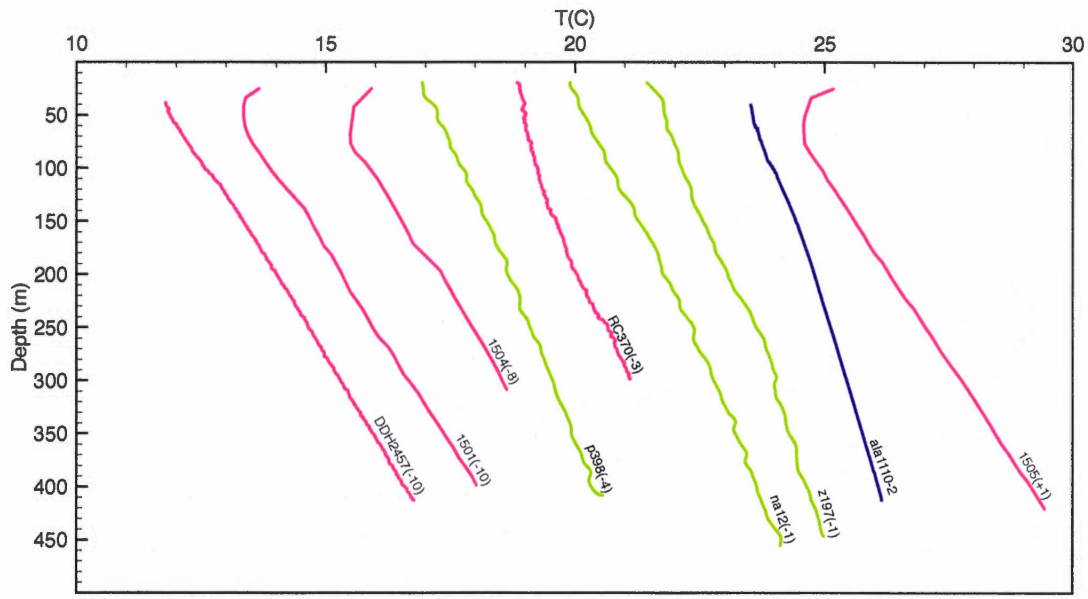

Figure 3.3 Retained temperature-depth profiles measured in 1994 (green), 2012 (blue), and 2015 (pink). Temperature scale is shifted as indicated in parenthesis.

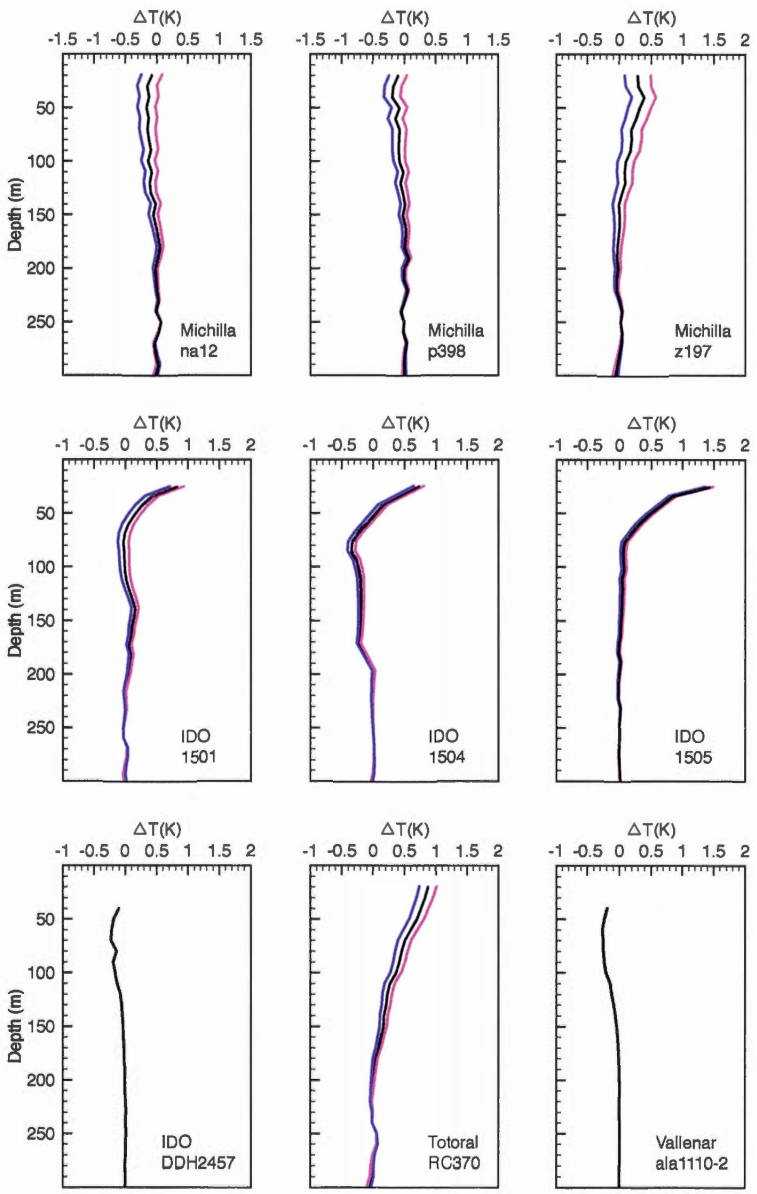

Figure 3.4 Temperature anomalies for the retained temperature-depth profiles, where IDO is Inca de Oro. The pink and blue lines represent the upper and lower bounds of the temperature anomaly. These are not visible at IDO-DDH2457 and Vallenar ala1110-2 because they are superimposed.

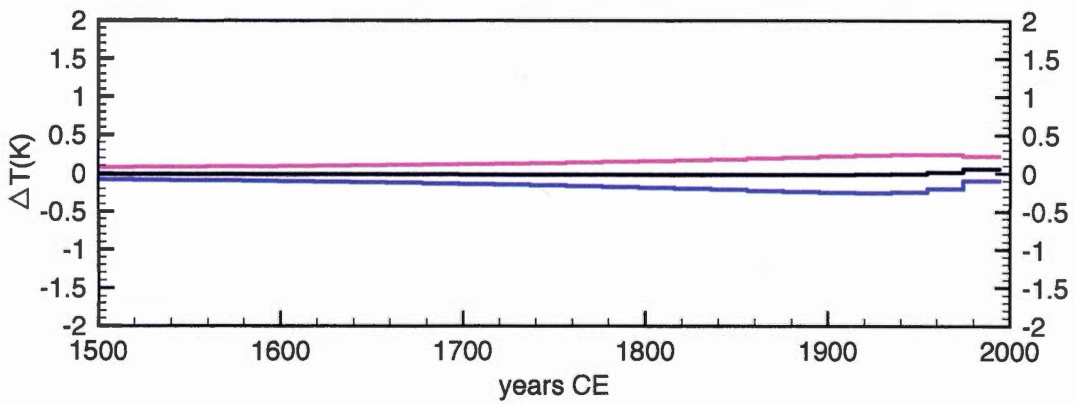

Figure 3.5 GST history for northern coastal Chile (Michilla) determined for its period of measurement (1994) from the simultaneous inversion of na12, p398, and z197, where 3 eigenvalues are retained. The pink and blue lines represent the inversion of the upper and lower bounds of the temperature anomaly or the extremal steady states.

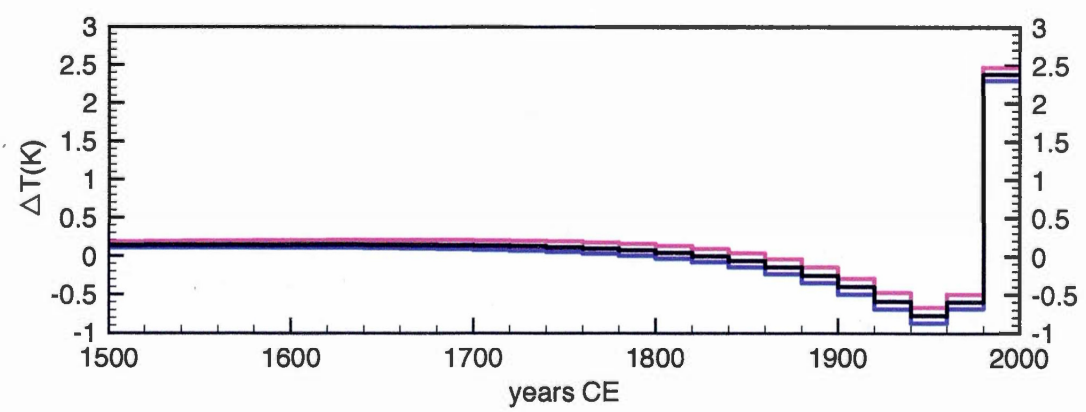

Figure 3.6 GST history for Inca de Oro determined from the simultaneous inversion of DDH2457, 1501, 1504, and 1505, with 3 eigenvalues retained. The pink and blue lines represent the inversion of the upper and lower bounds of the temperature anomaly or the extremal steady states.

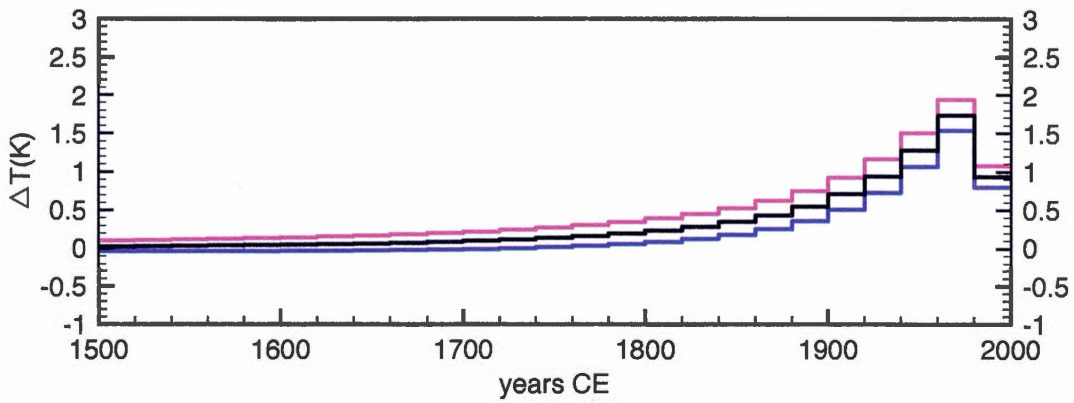

Figure 3.7 GST history for Totoral (RC370), with 3 eigenvalues retained. The pink and blue lines represent the inversion of the upper and lower bounds of the temperature anomaly or the extremal steady states.

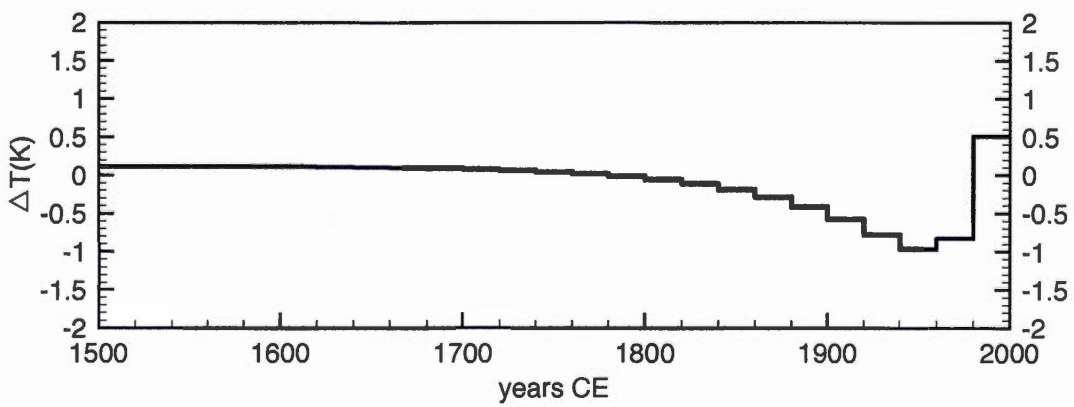

Figure 3.8 GST history for Vallenar (ala1110-2), with 3 eigenvalues retained. The inversion of the upper and lower bounds of the temperature anomaly or the extremal steady states are not visible because the three lines are superimposed.

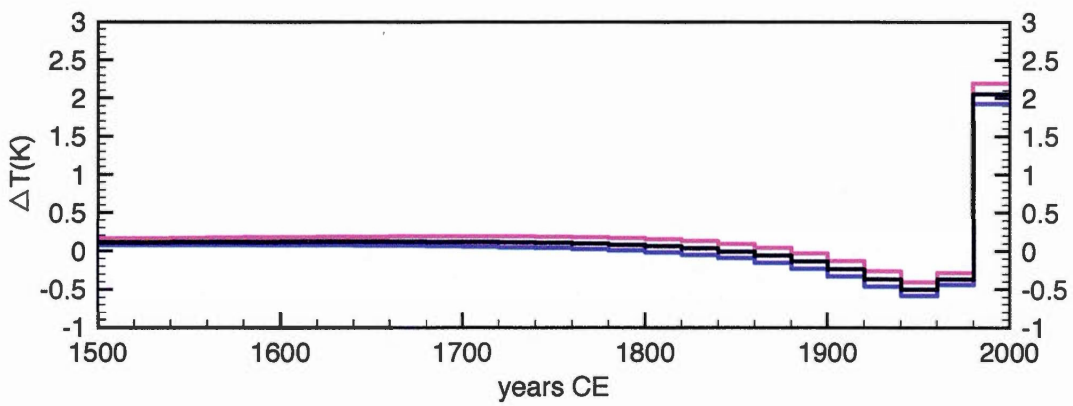

Figure 3.9 GST history for north-central Chile determined by the simultaneous inversion of DDH2457, 1501, 1504, 1505, RC370, and ala1110-2, with 3 eigenvalues retained. The pink and blue lines represent the inversion of the upper and lower bounds of the temperature anomaly or the extremal steady states.

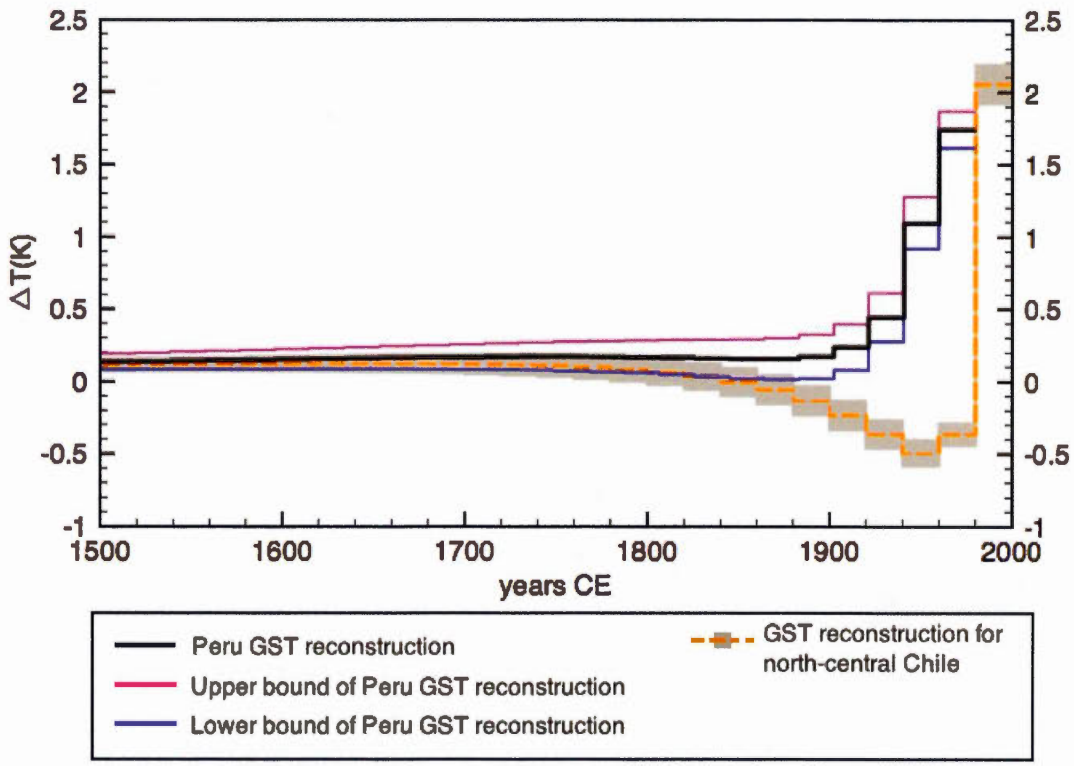

Figure 3.10 Comparison of GST histories for Peruvian boreholes (black) and north-central Chile (orange) with its upper and lower bounds (grey shaded area). The GST for the Peruvian boreholes is reconstructed with respect to its measurement time (1979) and obtained by the simultaneous inversion of LM18 and LOB525. The inversion of the upper and lower bounds of the temperature anomaly for the Peruvian boreholes are represented by the pink and blue lines, respectively.

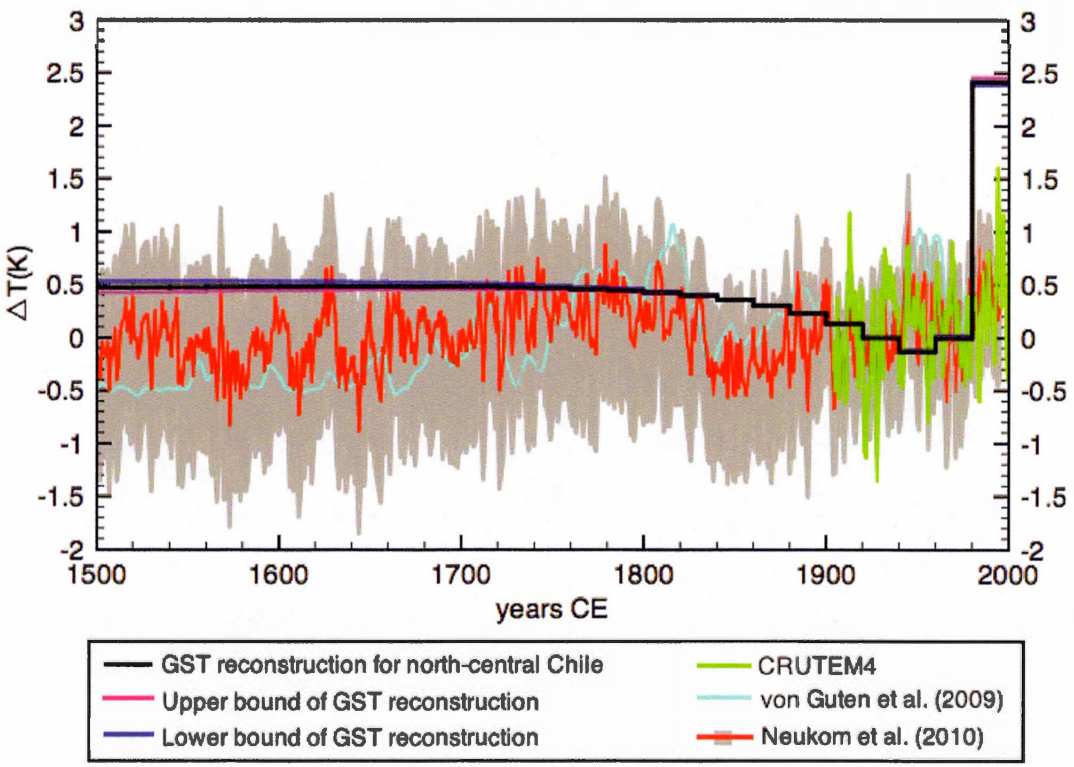

Figure 3.11 Comparison of GST history for north-central Chile (black) along with the upper and lower bounds of the inversion (pink and blue lines, respectively), the CRUTEM4 data for the north-central Chile gridpoint (green) (Jones *et al.*, 2012), the austral summer surface air temperature reconstruction from sedimentary pigments for the past 500 years (aqua) at Laguna Aculeo, central Chile (von Gunten *et al.*, 2009), and the austral summer surface air temperature reconstruction for southern South America (red) with its 2σ standard deviation (grey shaded area) (Neukom *et al.*, 2010). They are all presented as temperature departures from the 1920-1940 mean.

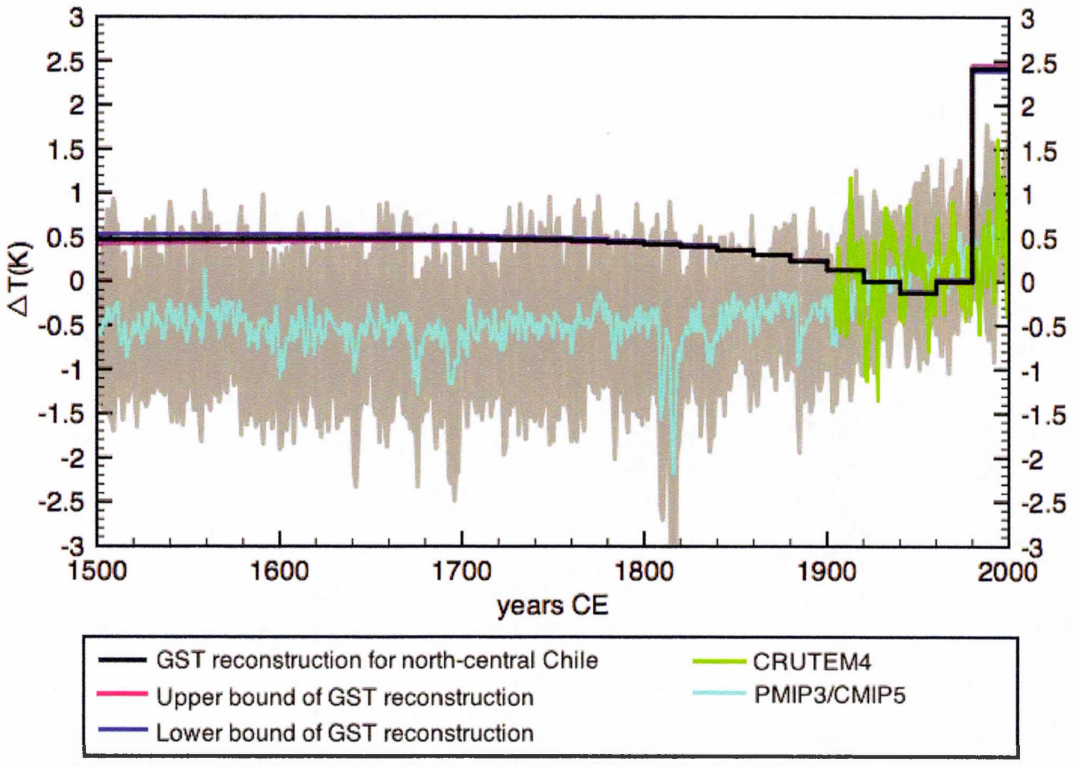

Figure 3.12 Comparison of GST history for north-central Chile (black) along with the upper and lower bounds of the inversion (pink and blue lines, respectively), the CRUTEM4 data for the north-central Chile gridpoint (Jones *et al.*, 2012), and the multi-model mean surface temperature anomaly reconstruction for the PMIP3/CMIP5 (aqua) with its 2σ standard deviation (grey shaded area). They are all presented as temperature departures from the 1920-1940 mean.

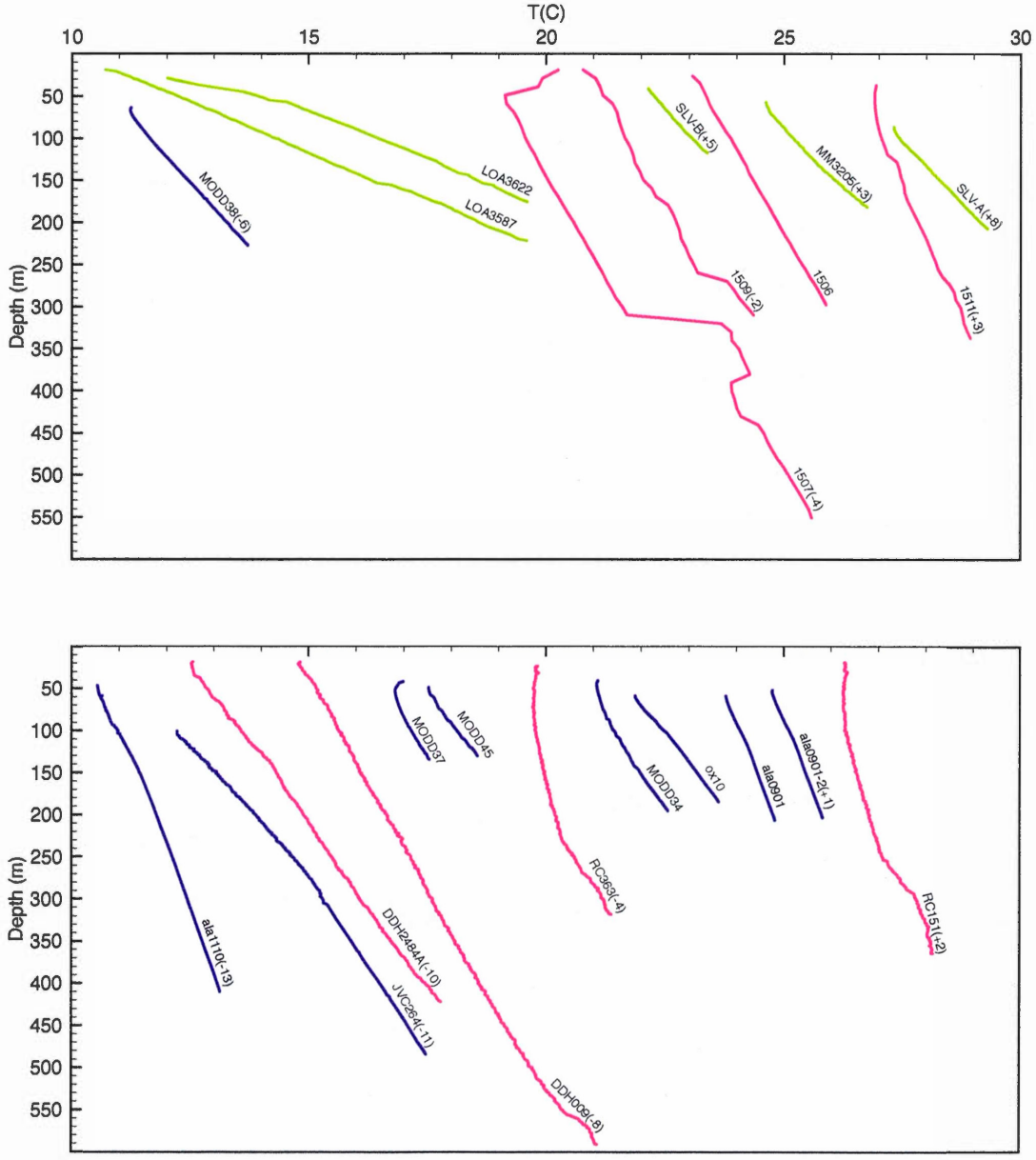

Figure 3.13 Rejected temperature-depth profiles measured in 1994 (green), 2012 (blue), and 2015 (pink). Temperature scale is shifted as indicated in parenthesis.

Table 3.1 Location and technical information concerning the borehole temperature-depth profiles measured in 1994 by Springer (1997) and Springer and Förster (1998)

Site	Log ID	Measurement Technique	Latitude (S)	Longitude (W)	Depth Range (m)	Elevation (m)	Suitable climate?
El Loa			21°09.1′	68°39.1′		3950	
	LOA3587	Thermistor (2 m)*			20-222		no
	LOA3622	Thermistor (2 m)*			30-176		no
Mansa Mina	MM3205	Thermistor (2 m)*	22°22.3′	68°54.9′	58-182	2423	no
Sierra Limon Verde	SLV-A	Thermistor (2 m)*	22°49.1′	68°54.8′	86-206	2516	no
	SLV-B	Thermistor (2 m)*	22°49.1′	68°54.8′	42-118	2516	no
Michilla			22°40.7′	70°10.9′		849	
	na12	DTS†			20-455		yes
	p398	DTS†			20-408		yes
	z197	DTS†			20-446		yes

*Value in parenthesis indicates sampling interval and yields temperature measurements with a precision of 0.01°C.

† Temperature measurements with a precision of 0.3°C.

Table 3.2 Location and technical information concerning the borehole temperature-depth profiles measured in 2012 by Gurza Fausto (2014)

Site	Log ID	Measurement Technique	Latitude (S)	Longitude (W)	Depth Range (m)	Elevation (m)	Suitable climate?
Sierra Limon Verde	MODD34	Thermistor (cont.)*	22°35.308′	68°54.865′	42-196	2704	no
	MODD37	Thermistor (cont.)*	22°41.059′	68°54.619′	43-135	2931	no
	MODD45	Thermistor (cont.)*	22°43.223′	68°55.441′	50-131	2910	no
	MODD38	Thermistor (cont.)*	22°43.660′	68°55.723′	65-228	2980	no
Sierra Gorda	ox10	Thermistor (cont.)*	23°0.454′	69°5.021′	60-185	2368	no
	JCV264	Thermistor (cont.)*	23°4.765′	69°5.666′	102-485	2379	no
Vallenar	ala901	Thermistor (cont.)*	28°39.855′	70°54.505′	60-207	490	no
	ala901-2	Thermistor (cont.)*	28°39.855′	70°54.505′	53-204	490	no
	ala1110	Thermistor (cont.)*	28°39.979′	70°54.624′	48-411	521	yes
	ala1110-2	Thermistor (cont.)*	28°39.979′	70°54.624′	41-412	521	yes

* Value in parenthesis indicates continuous sampling and yields temperature measurements with an accuracy of 0.05°C.

Table 3.3 Location and technical information concerning the borehole temperature-depth profiles measured in 2015

Site	Log ID	Measurement Technique	Latitude (S)	Longitude (W)	Depth Range (m)	Elevation (m)	Suitable climate?
Inca de Oro	DDH2457	DTS†	26°45′10.8″	69°53′38.4″	39-413	1628	yes
	1501	Thermistor (10 m)*	26°45′14″	69°53′42″	26-398	1621	yes
	DDH2489A/1501	DTS†	26°45′14″	69°53′42″	20-422	1621	yes
	1504	Thermistor (10 m)*	26°45′20″	69°53′42″	26-309	1626	yes
	1505	Thermistor (10 m)*	26°45′20″	69°53′38″	26-420	1630	yes
Copiapó	1506	Thermistor (10 m)*	27°22′49″	70°13′25″	26-297	679	no
	1507	Thermistor (10 m)*	27°22′55″	70°13′27″	20-550	703	no
	DDH009/1507	DTS†	27°22′55″	70°13′27″	20-557	703	no
Totoral	1509	Thermistor (10 m)*	27°58′51″	70°36′60″	20-310	400	no
	RC370/1509	DTS†	27°58′51″	70°36′60″	20-298	400	yes
Punta Diaz	RC151	DTS†	28°01′56.3″	70°38′44.2″	20-365	480	no
San José de Coquimbana	1511	Thermistor (10 m)*	28°15′35″	70°51′27″	36-335	354	no
	RC363/1511	DTS†	28°15′35″	70°51′27″	20-314	354	no

*Value in parenthesis indicates sampling interval and yields measurements with a precision better than 0.005 K and an accuracy on the order of 0.02 K.

† Temperature measurements with a precision of 0.3°C.

Table 3.4 Technical information concerning boreholes not suitable for this study

Site	Log ID	Year Measured	Remark	Reference
El Loa	LOA3587	1994	Too shallow	(Springer, 1997; Springer and Förster, 1998)
El Loa	LOA3622	1994	Too shallow	(Springer, 1997; Springer and Förster, 1998)
Mansa Mina	MM3205	1994	Too shallow	(Springer, 1997; Springer and Förster, 1998)
Sierra Limon Verde	MODD34	2012	Too shallow	(Gurza Fausto, 2014)
	MODD37	2012	Too shallow	(Gurza Fausto, 2014)
	MODD45	2012	Too shallow	(Gurza Fausto, 2014)
	MODD38	2012	Too shallow	(Gurza Fausto, 2014)
	SLV-A	1994	Too shallow	(Springer, 1997; Springer and Förster, 1998)
	SLV-B	1994	Too shallow	(Springer, 1997; Springer and Förster, 1998)
Sierra Gorda	ox10	2012	Too shallow	(Gurza Fausto, 2014)
	JCV264	2012	Top 100 m absent	(Gurza Fausto, 2014)
Inca de Oro	DDH2489A	2015	Remeasurement of 1501 by DTS	-
Copiapó	1506	2015	Topography, Discontinuity	-
	1507	2015	Topography, Discontinuity	-
	DDH009	2015	Topography	-
Totoral	1509	2015	Discontinuity	-
Punta Diaz	RC151	2015	Water Flow	-
San José de Coquimbana	1511	2015	Water Flow	-
	RC363	2015	Water Flow	-
Vallenar	ala901	2012	Too shallow	(Gurza Fausto, 2014)
	ala901-2	2012	Too shallow, Duplicate of ala0901	(Gurza Fausto, 2014)
	ala1110	2012	Duplicate of ala1110-2	(Gurza Fausto, 2014)

Table 3.5 Summary of inversion results where T_o is the long-term surface temperature, Γ_o is the quasi-steady state temperature gradient and ΔT is the difference between the maximal temperature and the temperature at 1500 years CE.

Site	Log ID	T_o ($°C$)	Γ_o (km^{-1})	ΔT (K)
Michilla				0.1
	na12	20.86±0.01	9.9±0.1	
	p398	20.91±0.01	8.8±0.2	
	z197	22.01±0.01	10.4±0.3	
Inca de Oro				2.2
	DDH2457	22.44±0.01	12.9±0.1	
	1501	22.48±0.02	14.0±0.5	
	1504	22.88±0.02	12.3±0.3	
	1505	22.38±0.01	14.6±0.3	
Totoral	RC370	20.79±0.01	11.3±0.2	1.7
Vallenar	ala1110-2	23.48±0.00	6.6±0.01	0.4

Table 3.6 Summary of models used to calculate the multi-model mean surface temperature anomaly from the PMIP3/CMIP5 simulation

Model	Reference
BCC-CSM1.1	(Li *et al.*, 2014)
CCSM4.0	(Gent *et al.*, 2011)
GISS-E2-R	(Schmidt *et al.*, 2014)
IPSL-CM5A	(Mignot and Bony, 2013)
MPI-ESM	(Giorgetta *et al.*, 2013)
MRI-CGCM3	(Yukimoto *et al.*, 2012)

CONCLUSION

The results presented in this dissertation have expanded the spatial and temporal scale of climate studies based on borehole temperature data. The timescale was extended by inferring the long-term climatic trends for 100-100,000 years BP from thirteen deep boreholes ($\geq$1500 m) in eastern and central Canada. Boreholes temperature data and reconstructions were obtained in regions void of data, improving the spatial coverage. Twenty-five boreholes were sampled and the climate of the past 500 years in northern Ontario and Québec was reconstructed. This region on both sides of James Bay was previously void of data. The temperature-depth profiles of thirty-one boreholes in northern Chile were collected and used to infer the climate trends of the last 500 years. Prior to this work, no GST reconstructions had been undertaken in northern Chile, which lies in South America, a continent with very few paleoclimatic reconstructions. All of these works have also provided insight to the ground thermal regime, basal temperatures of ice sheets, various measurement techniques, and robustness of GCM outputs.

In the first chapter, entitled "Laurentide Ice Sheet basal temperatures at the last glacial cycle as inferred from borehole data", the GST histories of the past 100-100,000 yrs BP for the region covered by the southern portion of the Laurentide Ice Sheet in eastern and central Canada were determined. This yielded GST for the last glacial maximum near the pressure melting point of ice (-1.4-3.0°C). As the region was covered by the ice sheet during this period, they represent the basal temperatures of the ice sheet. They indicate the possibility of basal flow and ice streams, which could lead to instability. However, the ice sheet persisted

over more than ~30,000 years with deglaciation only occurring rapidly during the Holocene (Carlson *et al.*, 2008). Fahnestock *et al.* (2001) and Pritchard *et al.* (2012) have found basal temperatures near or above the pressure melting point of ice in the present-day ice sheets. Our study shows that this alone is not an indication that the ice sheets are unstable, but combined with other processes it could lead to instability and collapse.

The second chapter, "Climate trends in northern Ontario and Québec from borehole temperature profiles", involved the examination of twenty-five boreholes temperature depth profiles to determine the GST histories of 10 sites in northern Ontario and Québec for the past 500 years. The GST histories showed a warming of ~1-2 K for the past 150 years, agreeing with reconstructions for the southern portion of the Superior Province and proxy data (Beltrami and Mareschal, 1992; Shen and Beck, 1992; Chouinard and Mareschal, 2007). A little ice age signal was present at only one site, Otoskwin. This was surprising as pollen reconstructions infer their coldest little ice age signal in northern Québec (Gajewski, 1988; Viau and Gajewski, 2009). This could be the result of insufficient resolution since a less than 1 K cooling between 200 and 500 years BP is difficult to resolve in the presence of noise. It could also be associated with an early little ice age (Chouinard *et al.*, 2007) or be masked by physical effects, such as changes in snow cover or the advance and retreat of permafrost (Gosselin and Mareschal, 2003). Furthermore, permafrost maps locate all the boreholes, excluding Nielsen Island, in a region of discontinuous isolated patches of permafrost. Nielsen Island lies in a region of sporadic discontinuous permafrost. Permafrost was not encountered during sampling of any of the twenty-five boreholes and the GST histories of all sites, except Nielsen Island, remained above 0°C. This suggest that potential for permafrost was minimal to absent over the past 500 years. Moreover, researchers from the GEOTOP and the Institut de Physique du Globe de Paris sampled more than 60

boreholes in the sporadic discontinuous permafrost region of Manitoba and only encountered permafrost at one site. This points to possible discrepancies with permafrost maps, which could be the result of: (1) surface air temperature (SAT) interpolation used in permafrost maps being unsuitable to represent the spatial variability of ground temperatures and/or (2) an offset between ground and air surface temperatures due to snow cover in the region. Our study suggests that borehole temperature data and reconstructions could be used to assess the evolution of permafrost and be a useful tool for the validation of permafrost models and maps.

In the third chapter, the GST histories for the past 500 years in northern Chile were determined from 31 borehole temperature-depth profiles. The boreholes are located in two regions, northern coastal Chile and north-central Chile. Differing trends were observed between the regions, which is not surprising as they are over 500 km apart. Northern coastal Chile recorded no warming or cooling signal. On the other hand, the GST history of north-central Chile inferred no warming or cooling between ~200-500 years BP, a cooling of 0.6 K from ~40-200 years BP and recent warming trend of 1.9 K, ~20-40 years BP. The period of no warming or cooling between 200-500 years BP appears to be a regional trends for southern South America since it is observed in the climate reconstructions for central Chile and southern South America and in the surface temperature simulation of the PMIP3/CMIP5. The cooling signal was only observed in the GST for north-central Chile and for the Peruvian site at the northern edge of the Atacama desert. This suggests that it is a regional trend of the Atacama desert. The recent warming was also observed in the GST histories of Peru and the semiarid regions of South America, meteorological data for the north-central Chile gridpoint, climate reconstructions for central Chile and southern South America, and the climate simulation for the north-central Chile gridpoint of the PMIP3/CMIP5. Differ-

ences are noted with respect to the onset and amplitude of this warming. The amplitude of this recent warming only agrees with the GST histories for semiarid South America and Peru. The onset of the recent warming was ~20-40 years BP in the GST of north-central Chile. But, it started earlier, ~100-150 years BP in the GST histories for semiarid South America and Peru, the meteorological data, the climate reconstructions for central Chile and southern South America and the surface temperature simulation from the PMIP3/CMIP5. The differences in amplitude and timing are hypothesized to be related to a regional Atacama trend that cannot be resolved on the gridpoint scale. More data and reconstructions are required to confirm these conclusions and determine the long-term climate trends of northern Chile.

These results open the door for future works. Due to a lack of deep boreholes ($\geq$1500 m), we were constrained to examining the basal temperatures of the southern portion of the Laurentide Ice Sheet during the LGC. Mining exploration and operations have been moving further north, especially in Québec. This could increase the number of deep boreholes ($\geq$1500 m) available. Their measurement and analysis will expand the dataset and infer the basal conditions of a greater portion of the Laurentide Ice Sheet. The database of borehole temperature-profiles could be used to reconstruct the GST histories in permafrost regions and provide insight to the evolution of permafrost for the past 500 years.

In northern Chile, the database of borehole temperature-profiles must be increased to determine the long-term climatic trends. Due to an absence of climate signal, it is probably not worth targeting the northern coastal region. Efforts should be focus on the north-central region but care must be taken to ensure that suitable boreholes with available core samples are found. The majority of boreholes used in our study had collapsed resulting in them being too shallow

and core samples were not available. Our results also showed that the conventional method has greater resolution than DTS. Therefore, new measurements of borehole temperature-depth profiles for climate studies should be made using the conventional method. This will provide measurements with greater resolution to resolve the climate trends of northern Chile. Furthermore, due to the poor distribution of borehole temperature-depth profiles across South America, a systematic effort should be undertaken obtain profiles across the continent and infer their GST histories.

In conclusion, we have shown that borehole temperature data can provide insight to climate trends on varying spatial and temporal scales. In Canada, we have expanded the temporal and spatial scale of these studies by using data from deep boreholes to infer long-term climatic trends. We also collected data and determined reconstructions in regions not previously covered. Furthermore, we showed that borehole temperature data and reconstructions are useful tools to examine the ground thermal regime and for permafrost studies. In Chile, we have compiled new data. Our results should be viewed as preliminary but they open an avenue for future studies.

APPENDIX A

GST RECONSTRUCTIONS FROM INVERSION OF THE TEMPERATURE ANOMALY

In the first chapter, "Laurentide Ice Sheet basal temperatures at the Last Glacial Cycle as inferred from borehole data", the basal temperatures of the Laurentide Ice Sheet during the LGC were estimated from borehole temperature data. The methodology utilized varies from that presented in the other two chapters of this dissertation. In order to reconstruct GST from borehole temperature data, we must solve for the $K+2$ unknown parameters (T_o, q_o, and ΔT_k) from the system of linear equations for each measured depth (z). This can be done by: (1) solving for the $K+2$ unknown parameters simultaneous or (2) T_o and q_o can be determined independently of ΔT_k. The first technique was used in this chapter. Here, we demonstrate that the second technique leads to similar results and conclusions.

For each site, the linear regression of the bottommost 200 m of the temperature-depth profile was calculated to determine T_o and Γ_o, the long-term surface temperature and the quasi-steady state temperature gradient. This represents the geothermal quasi-steady state. An estimate of the maximum error at a 95% confidence interval of T_o and Γ_o were provided by this linear regression and are the upper and lower bounds of the geothermal quasi-steady state. The temperature anomaly (T_t) is then obtained by the subtraction of the quasi-steady state

geotherm from the temperature-depth profile.

The temperature anomalies of the thirteen sites were inverted to reconstruct the GST histories from 100 to 100,000 years using a model consisting of 16 time-steps whose distribution varies logarithmically (Figures A.2-A.13). A singular value cutoff of 0.08 was used, retaining 4 eigenvalues. The temperatures obtained during the last glacial maximum range between -1.14°C and 3°C and are near the pressure melting point of ice. These basal temperatures indicate the possibility of basal melt and fast flowing ice streams. Furthermore, the warmest basal temperatures and highest heat flux are recorded at Sudbury (Victor Mine and Lockerby), agreeing with the reconstructions from the full log and suggest a possible relationship between basal temperatures and heat flux. These are the same conclusions as drawn using the alternative method. The minimum temperatures obtained using the two methods are compared in Table A.1. Differences can be attributed to the depth interval used to obtain the temperature anomaly. These results show that both techniques (inversion from temperature anomaly and full log) yield similar results and lead to the same conclusions.

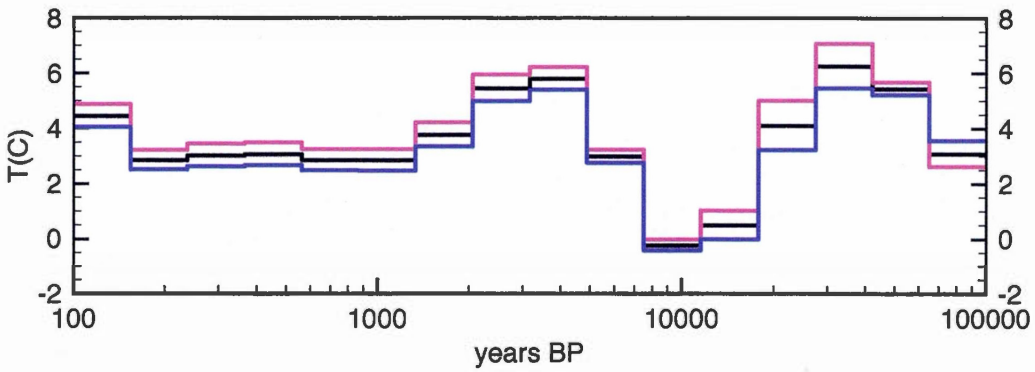

Figure A.1 GST history for Flin Flon, where 4 eigenvalues are retained. The pink and blue lines represent the inversion of the upper and lower bounds of the geothermal quasi-steady state or the extremal steady states.

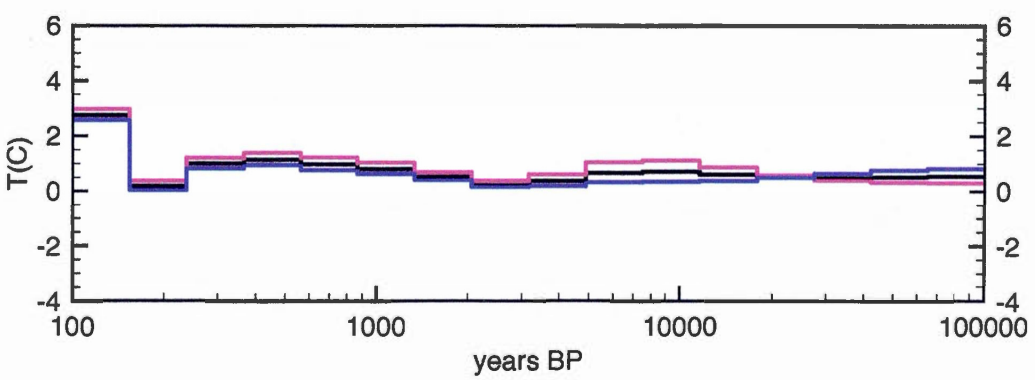

Figure A.2 GST history for Pipe Mine (Thompson), where 4 eigenvalues are retained. The pink and blue lines represent the inversion of the upper and lower bounds of the geothermal quasi-steady state or the extremal steady states.

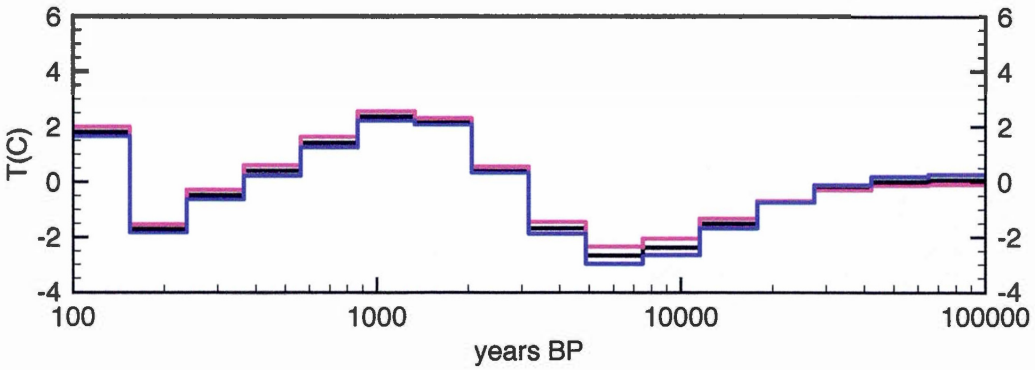

Figure A.3 GST history for Owl (Thompson), where 4 eigenvalues are retained. The pink and blue lines represent the inversion of the upper and lower bounds of the geothermal quasi-steady state or the extremal steady states.

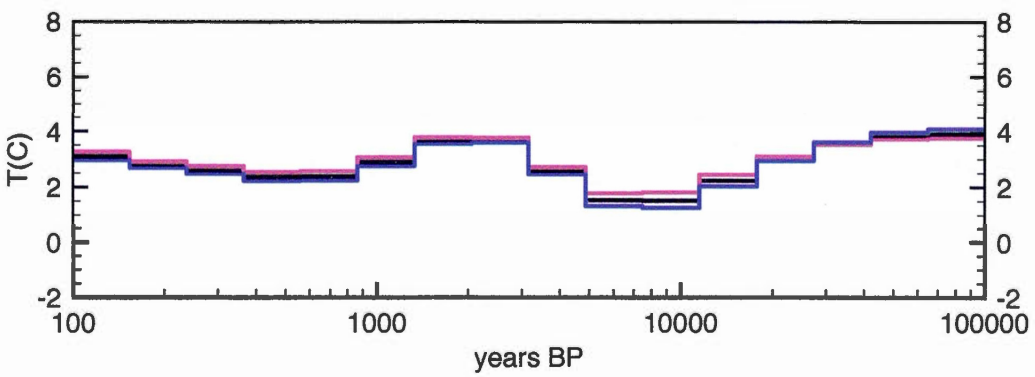

Figure A.4 GST history for Balmertown, where 4 eigenvalues are retained. The pink and blue lines represent the inversion of the upper and lower bounds of the geothermal quasi-steady state or the extremal steady states.

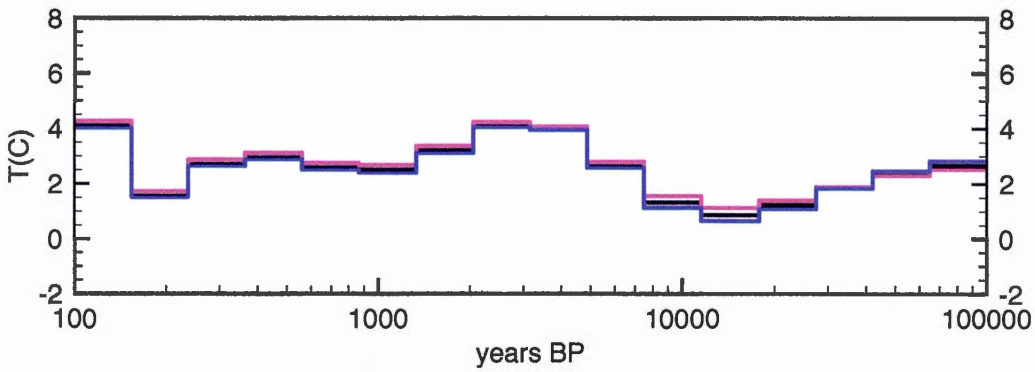

Figure A.5 GST history for Manitouwadge 0610 (Geco0610), where 4 eigenvalues are retained. The pink and blue lines represent the inversion of the upper and lower bounds of the geothermal quasi-steady state or the extremal steady states.

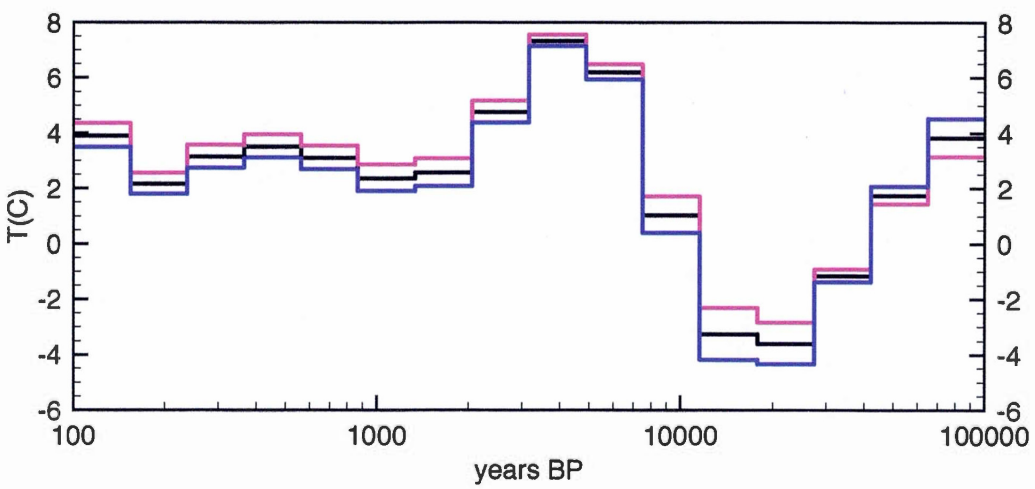

Figure A.6 GST history for Manitouwadge 0611 (Geco0611), where 4 eigenvalues are retained. The pink and blue lines represent the inversion of the upper and lower bounds of the geothermal quasi-steady state or the extremal steady states.

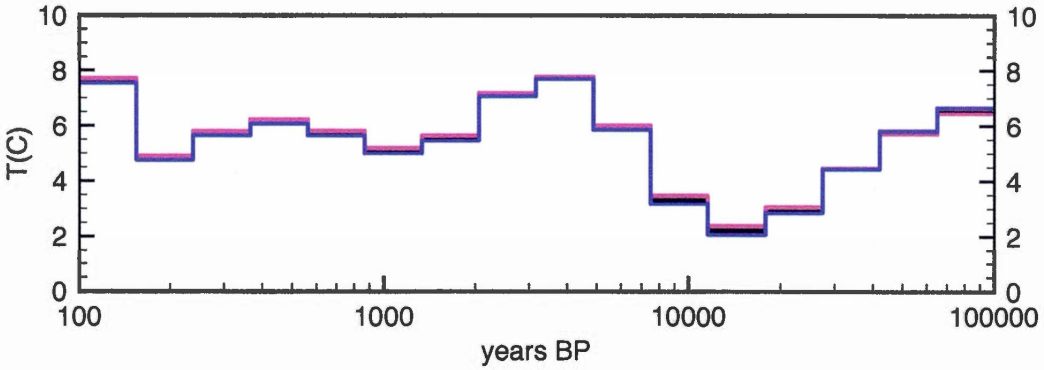

Figure A.7 GST history for Victor Mine (Sudbury), where 4 eigenvalues are retained. The pink and blue lines represent the inversion of the upper and lower bounds of the geothermal quasi-steady state or the extremal steady states.

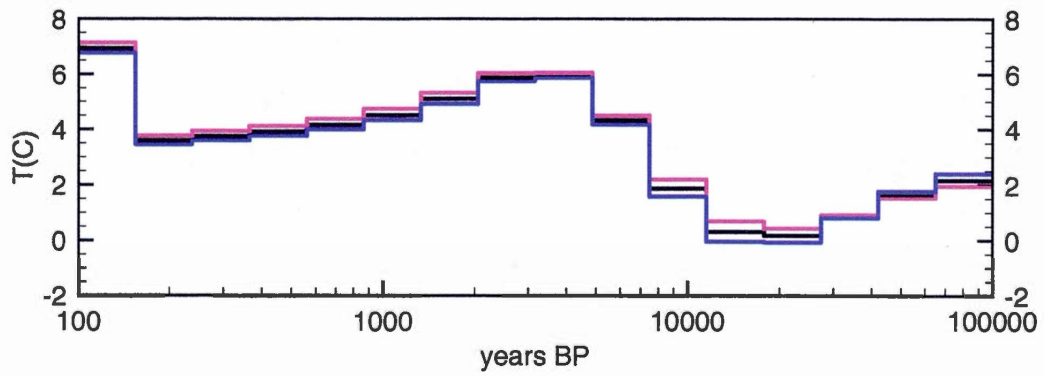

Figure A.8 GST history for Falconbridge (Sudbury), where 4 eigenvalues are retained. The pink and blue lines represent the inversion of the upper and lower bounds of the geothermal quasi-steady state or the extremal steady states.

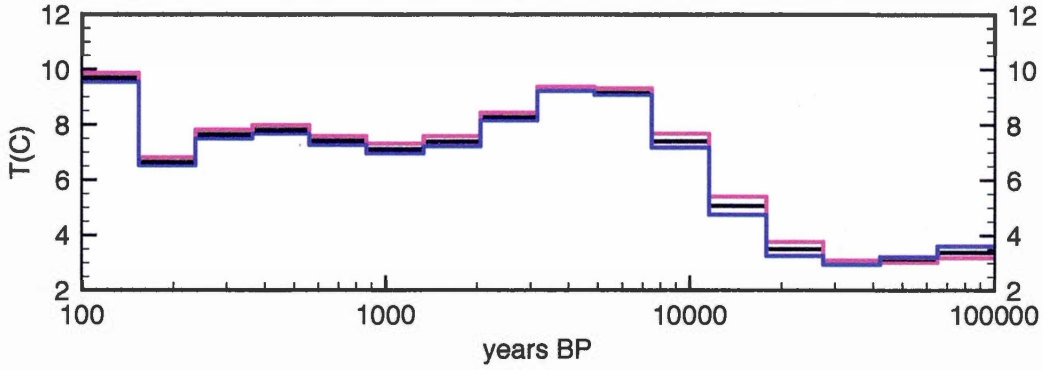

Figure A.9 GST history for Lockerby (Sudbury), where 4 eigenvalues are retained. The pink and blue lines represent the inversion of the upper and lower bounds of the geothermal quasi-steady state or the extremal steady states.

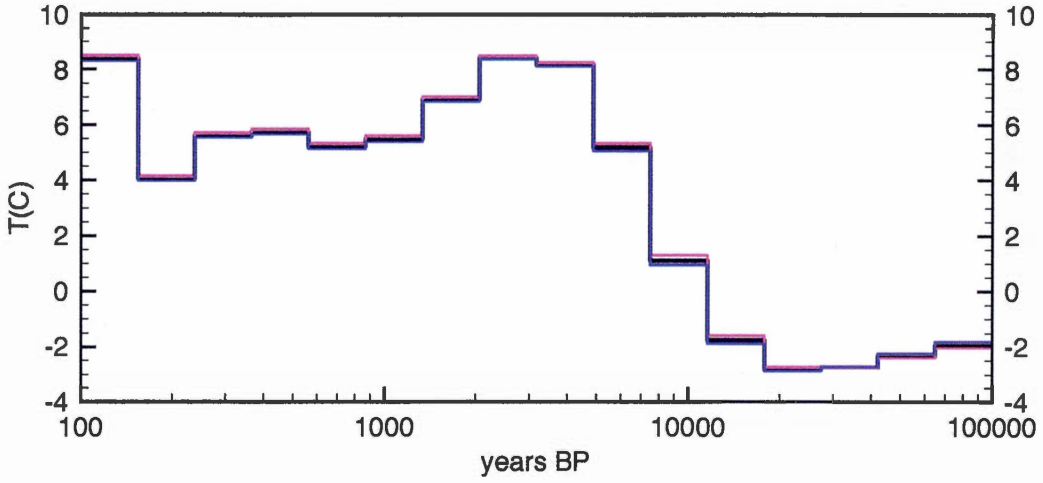

Figure A.10 GST history for Craig Mine (Sudbury), where 4 eigenvalues are retained. The pink and blue lines represent the inversion of the upper and lower bounds of the geothermal quasi-steady state or the extremal steady states.

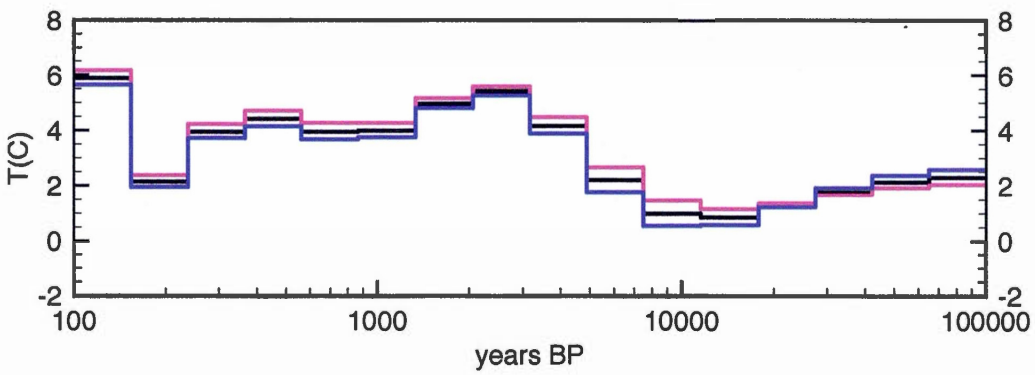

Figure A.11 GST history for Val d'Or, where 4 eigenvalues are retained. The pink and blue lines represent the inversion of the upper and lower bounds of the geothermal quasi-steady state or the extremal steady states.

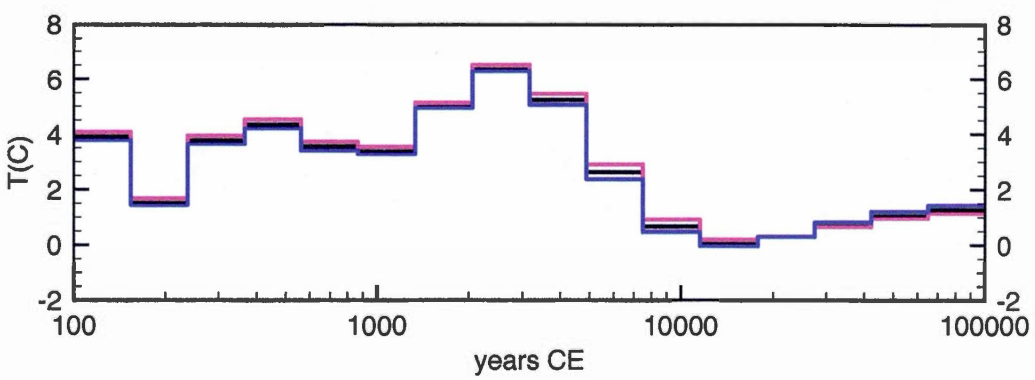

Figure A.12 GST history for Matagami, where 4 eigenvalues are retained. The pink and blue lines represent the inversion of the upper and lower bounds of the geothermal quasi-steady state or the extremal steady states.

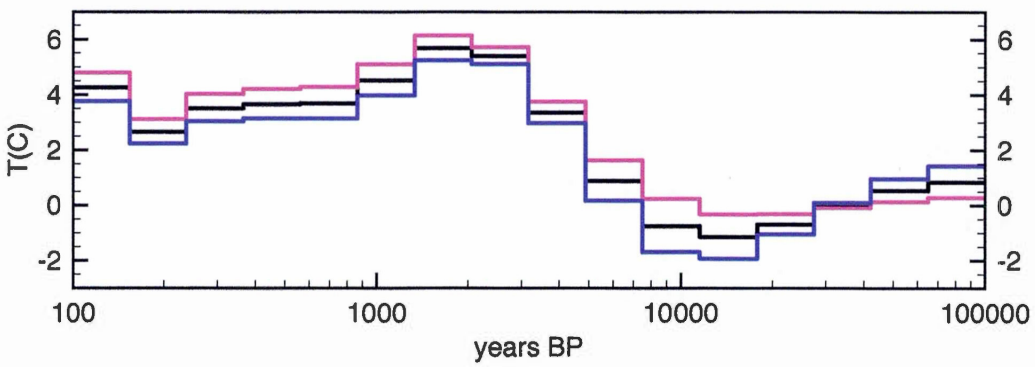

Figure A.13 GST history for Sept Iles, where 4 eigenvalues are retained. The pink and blue lines represent the inversion of the upper and lower bounds of the geothermal quasi-steady state or the extremal steady states.

Table A.1 Comparison of GST histories reconstructed from the temperature anomaly (anom) and the full profile (full) where $T_{min}(anom)$ is the minimum temperature obtained by inverting the temperature anomaly, $t_{min}(anom)$ is the timing of the minimal temperature obtained by inverting the temperature anomaly, $T_{min}(full)$ is the minimum temperature obtained by inverting the full profile, and $t_{min}(full)$ is the timing of the minimum temperature obtained from the inversion of the full profile. Parentheses indicate sites where the GST history is not reliable.

Site	$T_{min}(anom)$ ($^{\circ}C$)	$t_{min}(anom)$ ka	$T_{min}(full)$ ($^{\circ}C$)	$t_{min}(full)$ ka
FlinFlon	-0.21±0.2	7.5-10	-0.25	10-20
Pipe	0.20±0.17	0.15-0.2	0.27	0.15-0.2
(Owl)[a]	-2.67±0.30	5-7.5	-2.36	5-7.5
Balmertown	1.53±0.25	5-10	1.65	5-7.5
Manitouwadge 0610	0.87±0.24	10-20	0.95	10-20
(Manitouwadge 0611)[b]	-2.85±0.75	10-30	-2.83	20-30
Victor Mine	2.21±0.16	10-30	3.00	10-30
Falconbridge	0.18±0.24	20-30	-0.20	20-30
Lockerby	3.00±0.08	30-40	2.84	10-30
(Craig Mine)[c]	2.80±0.06	20-30	3.0	20-30
Val d'Or	0.85±0.31	7-20	0.58	10-20
Matagami	0.08±0.12	10-20	0.34	10-20
Sept Iles	-1.14±0.80	10-20	-1.42	10-20

[a]The temperature profile at this site may be distorted by horizontal contrasts in thermal conductivity, [b]The temperature profile in the lowermost part of the hole may be affected by subvertical layering and thermal conductivity contrasts, [c]The temperature profile may be affected by waterflow caused by pumping in the nearby mine.

APPENDIX B

INDIVIDUAL GST RECONSTRUCTIONS FOR NORTHERN ONTARIO AND QUÉBEC

In the second chapter, "Climate trends in northern Ontario and Québec from borehole temperature profiles", twenty-five borehole temperature-depth profiles were measured to reconstruct the climate trends for the past 500 years in northern Ontario and Québec. Only eighteen boreholes from ten sites were deemed suitable for climate studies. The GST histories for sites with multiple boreholes (Thierry Mine, Noront, Eastmain, and Camp Coulon) were determined using simultaneous inversion. Here, we present the individual GST histories for the boreholes from these sites (Figures B.2-B.12).

The individual GST histories were calculated from the temperature-depth profiles for the last 500 years for intervals of 20 years with 3 eigenvalues retained. The temperature-depth profiles were truncated at the same depth used for the simultaneous inversion to ensure comparison of the same time period (530 m at Thierry Mine, 400 m at Noront, 400 m at Eastmain, and 400 m at Camp Coulon) (Beltrami *et al.*, 2011). Table B.1 summarizes the results of the inversions. The individual reconstructions are noisier than those obtained from simultaneous inversion, illustrating the increase in signal to noise ratio when utilizing the latter technique. No LIA signal is observed at any site. All sites, except 1014 (Noront),

infer a warming of ~1-2 K for the past ~150-200 years. It appears that 1014 (Noront) has not recorded a warming or cooling signal. Furthermore, the individual GST histories suggest that the regions were free of permafrost for the last 500 years, agreeing with the GST histories obtained from simultaneous inversion.

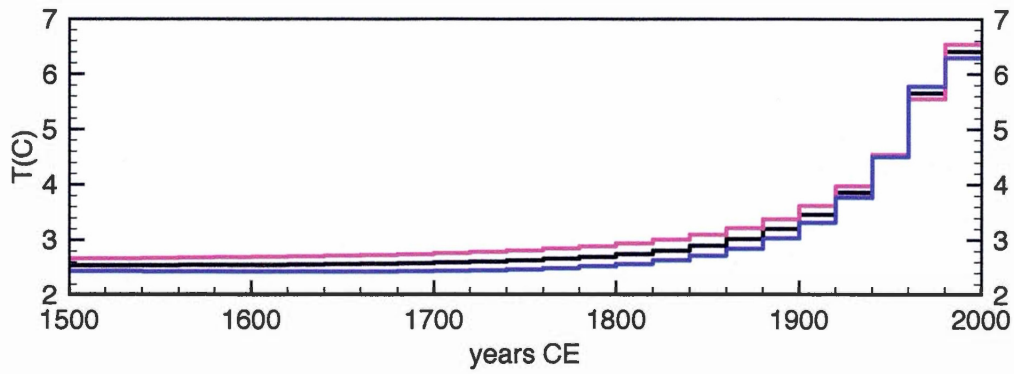

Figure B.1 GST history for 0605 (Thierry Mine), where 3 eigenvalues are retained. The pink and blue lines represent the inversion of the upper and lower bounds of the geothermal quasi-steady state or the extremal steady states.

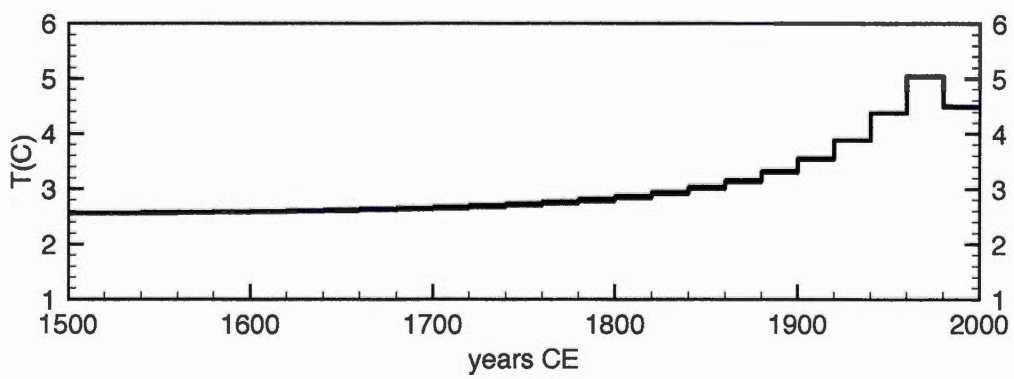

Figure B.2 GST history for 0606 (Thierry Mine), where 3 eigenvalues are retained. The extremal steady states are not visible because the three lines are superimposed.

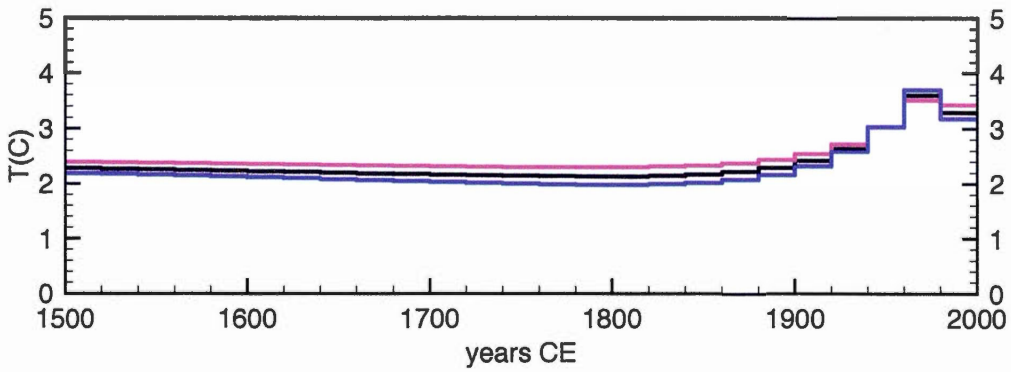

Figure B.3 GST history for 0608 (Thierry Mine), where 3 eigenvalues are retained. The pink and blue lines represent the inversion of the upper and lower bounds of the geothermal quasi-steady state or the extremal steady states.

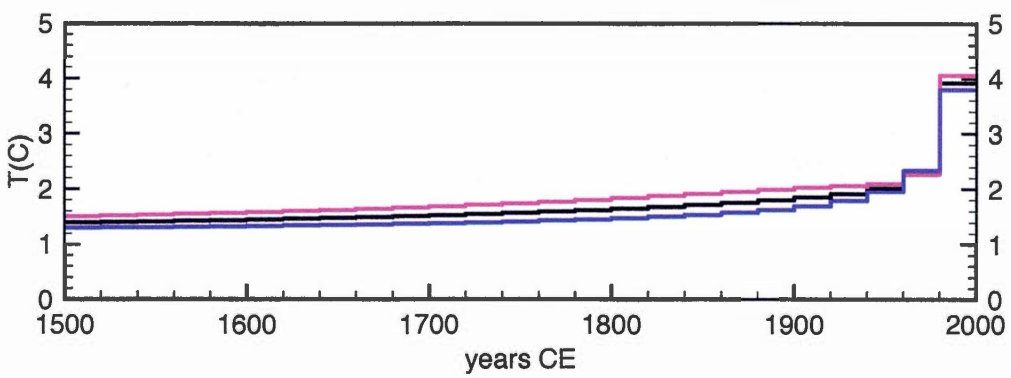

Figure B.4 GST history for 1012 (Noront), where 3 eigenvalues are retained. The pink and blue lines represent the inversion of the upper and lower bounds of the geothermal quasi-steady state or the extremal steady states.

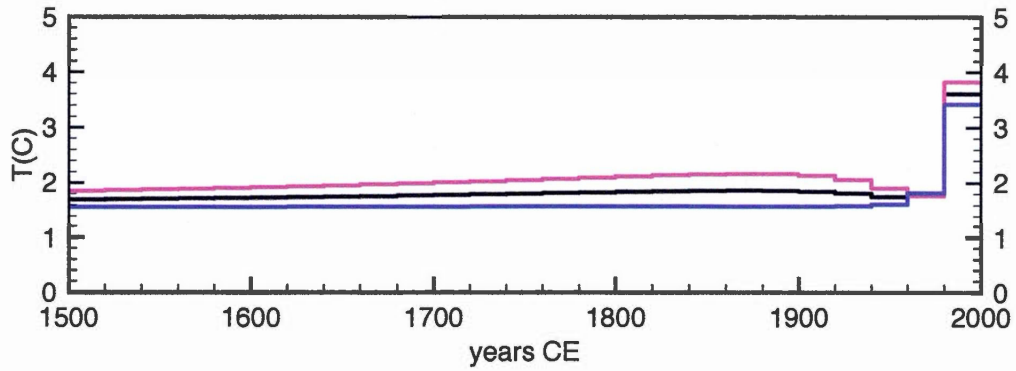

Figure B.5 GST history for 1013 (Noront), where 3 eigenvalues are retained. The pink and blue lines represent the inversion of the upper and lower bounds of the geothermal quasi-steady state or the extremal steady states.

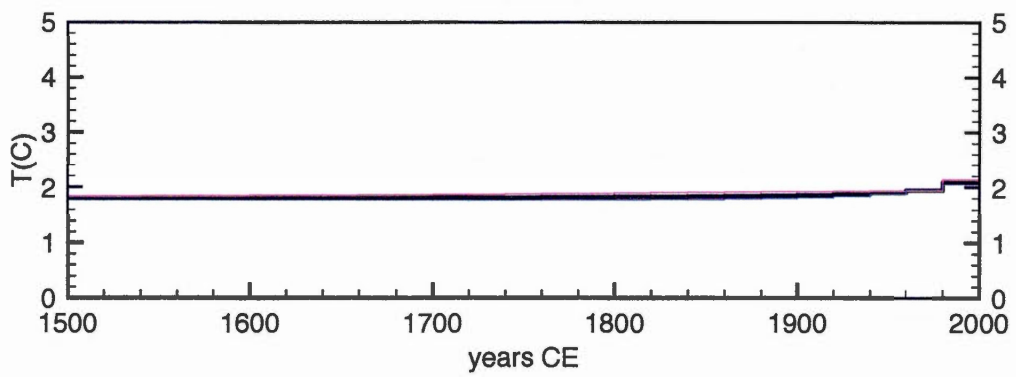

Figure B.6 GST history for 1014 (Noront), where 3 eigenvalues are retained. The pink and blue lines represent the inversion of the upper and lower bounds of the geothermal quasi-steady state or the extremal steady states.

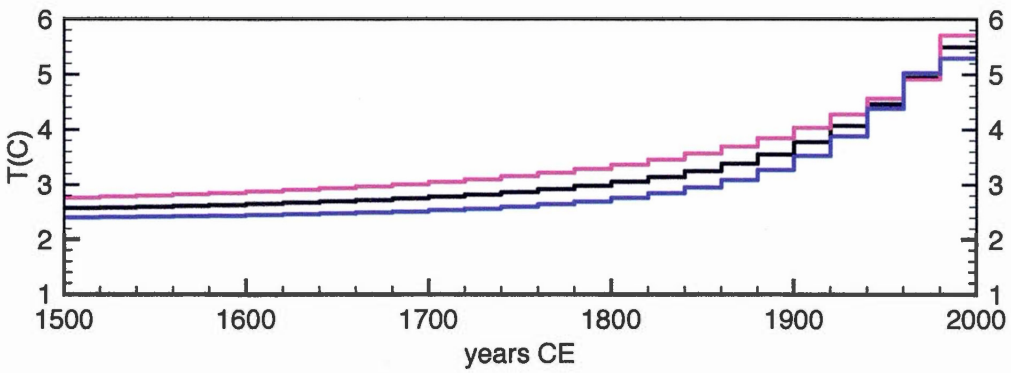

Figure B.7 GST history for 1015 (Noront), where 3 eigenvalues are retained. The pink and blue lines represent the inversion of the upper and lower bounds of the geothermal quasi-steady state or the extremal steady states.

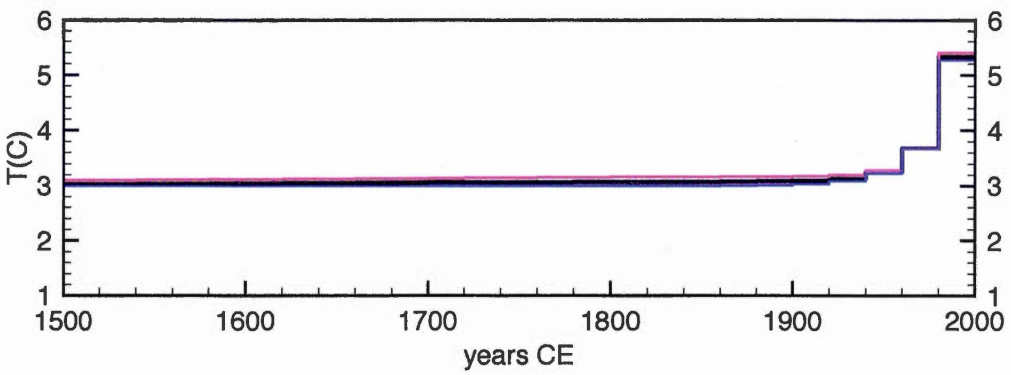

Figure B.8 GST history for 0803 (Eastmain), where 3 eigenvalues are retained. The pink and blue lines represent the inversion of the upper and lower bounds of the geothermal quasi-steady state or the extremal steady states.

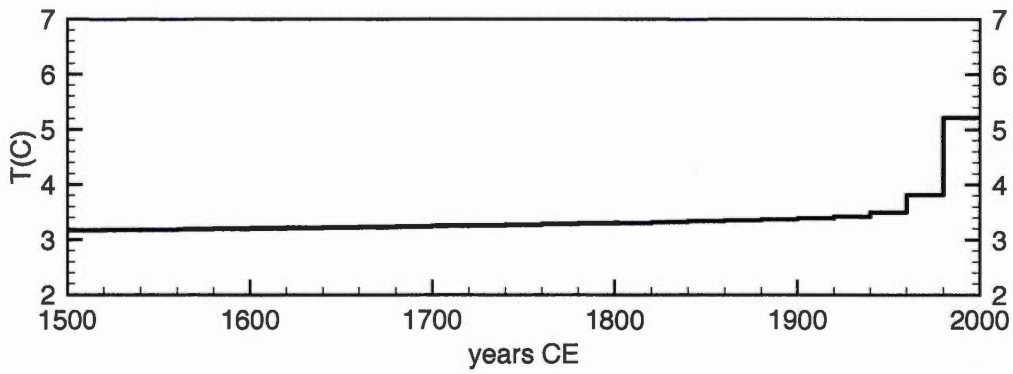

Figure B.9 GST history for 0804 (Eastmain), where 3 eigenvalues are retained. The extremal steady states are not visible because the three lines are superimposed.

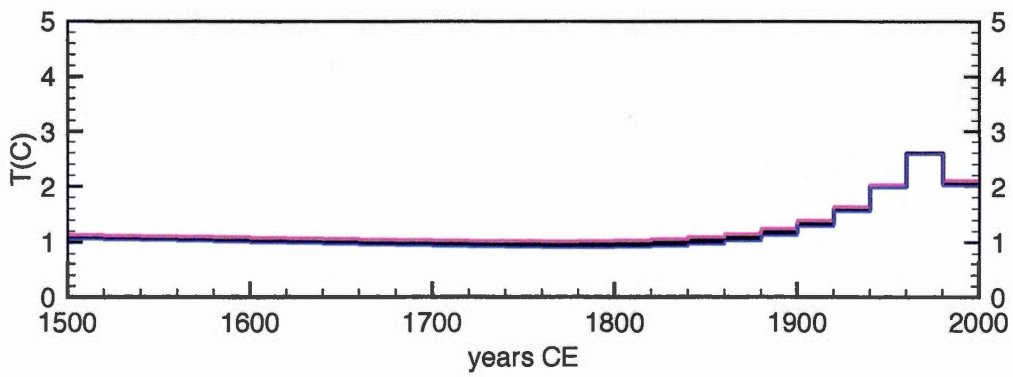

Figure B.10 GST history for 0712 (Camp Coulon), where 3 eigenvalues are retained. The pink and blue lines represent the inversion of the upper and lower bounds of the geothermal quasi-steady state or the extremal steady states.

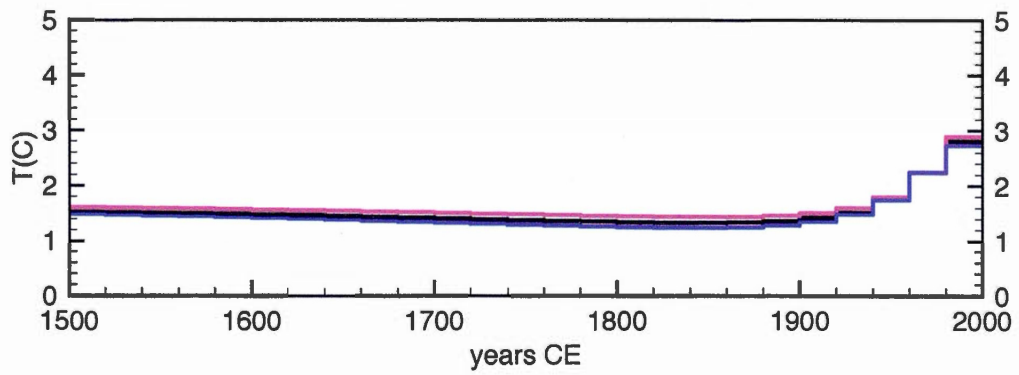

Figure B.11 GST history for 0713 (Camp Coulon), where 3 eigenvalues are retained. The pink and blue lines represent the inversion of the upper and lower bounds of the geothermal quasi-steady state or the extremal steady states.

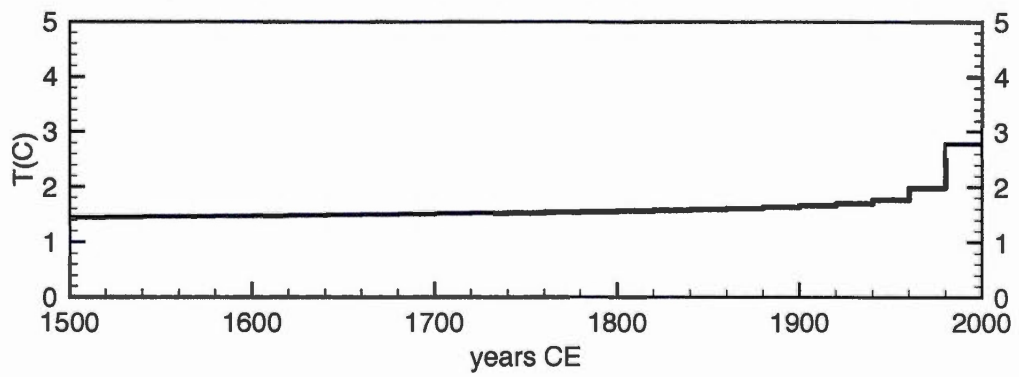

Figure B.12 GST history for 0714 (Camp Coulon), where 3 eigenvalues are retained. The extremal steady states are not visible because the three lines are superimposed.

Table B.1 Summary of GST results where T_o is the long-term surface temperature, q_o is the quasi-steady state heat flux, ΔT is the difference between the maximal temperature and the reference temperature at 500 years BP.

Site	Log ID	year	T_o (°C)	q_o (mW m^{-2})	ΔT (K)	LIA
Thierry Mine					2.85	no
	0605	2006	2.63±0.01	25.9±0.5	3.87	no
	0606	2006	2.55±0.01	23.5±0.7	2.48	no
	0608	2006	2.62±0.01	23.9±0.3	1.32	no
Noront					1.85	no
	1012	2010	1.16±0.01	35.5±0.9	2.52	no
	1013	2010	1.51±0.02	31.3±1.5	1.91	no
	1014	2010	1.78±0.004	32.2±0.3	0.29	no
	1015	2010	2.35±0.02	27.6±1.4	2.91	no
Eastmain					2.15	no
	0803	2008	2.98±0.01	27.3±0.4	2.29	no
	0804	2008	3.01±0.003	27.0±0.2	2.05	no
Camp Coulon					1.34	no
	0712	2007	1.46±0.01	26.6±0.4	1.50	no
	0713	2007	1.83±0.01	24.2±0.6	1.26	no
	0714	2007	1.33±0.004	-	1.33	no

APPENDIX C

INDIVIDUAL GST RECONSTRUCTIONS FOR NORTHERN CHILE

In the third chapter, thirty-one borehole temperature-depth profiles were collected to determine the GST histories in northern Chile for the past 500 years. Nine profiles from four sites were deemed suitable for inversion. For sites with multiple borehole temperature-depth profiles, the GST histories were determined using simultaneous inversion. Three boreholes (na12, p398, z197) are found at Michilla, and four boreholes (DDH2457, 1501, 1504, 1505) are at Inca de Oro. The profiles were cut at 300 m to ensure comparison of the same time period (Beltrami *et al.*, 2011). The individual GST histories for boreholes from these sites were reconstructed for the past 500 years for 20 year intervals with 3 eigenvalues retained (Figures C.2-C.7).

Contrasting trends are observed in the GST histories of the three Michilla boreholes (Figures C.2-C.3). A warming is inferred at two sites (na12, p398) and a cooling at the other (z197). The small amplitude and inconsistencies between these inversions point to the absence of a signal above the level of noise and explains the lack of signal in the Michilla GST history.

Differing trends are also observed in the individual GST histories of Inca de Oro (Figures C.4-C.6). The GSTs of three Inca de Oro sites (DDH2457, 1501, 1504)

show a cooling of ~0.5-1 K from ~40-150 years BP. This is agrees with the Inca de Oro GST reconstruction from simultaneous inversion. However, this cooling is not present in the GST history of 1505 (Figure C.7). A very recent warming at ~20-40 years BP of ~1-2.5 K is inferred for the Inca de Oro sites. The timing and amplitude of this warming are consistent with the Inca de Oro GST history.

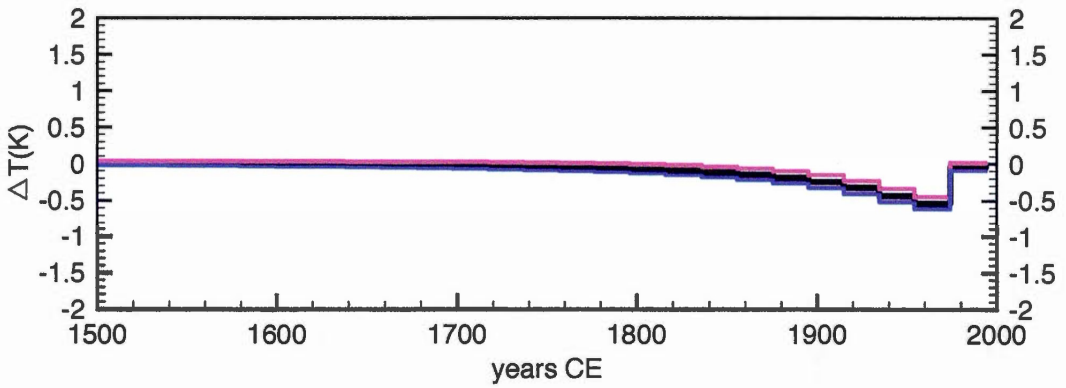

Figure C.1 GST changes for na12 (Michilla), where 3 eigenvalues are retained. The pink and blue lines represent the inversion of the upper and lower bounds of the geothermal quasi-steady state or the extremal steady states.

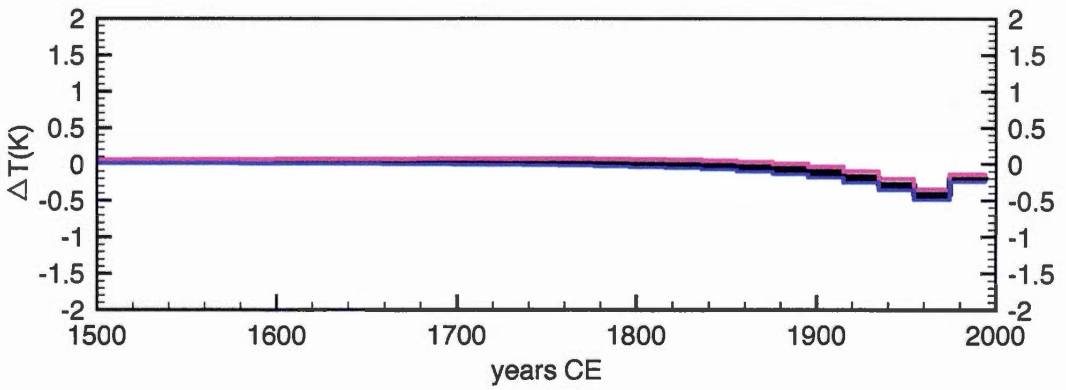

Figure C.2 GST changes for p398 (Michilla), where 3 eigenvalues are retained. The pink and blue lines represent the inversion of the upper and lower bounds of the geothermal quasi-steady state or the extremal steady states.

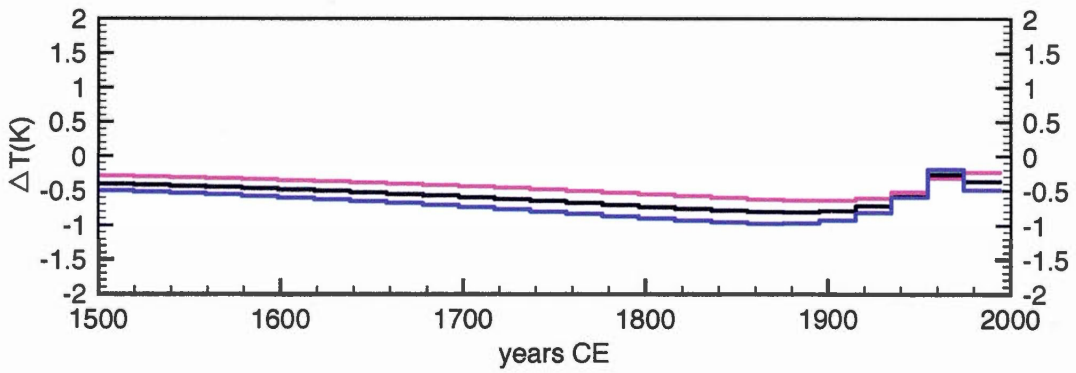

Figure C.3 GST changes for z197 (Michilla), where 3 eigenvalues are retained. The pink and blue lines represent the inversion of the upper and lower bounds of the geothermal quasi-steady state or the extremal steady states.

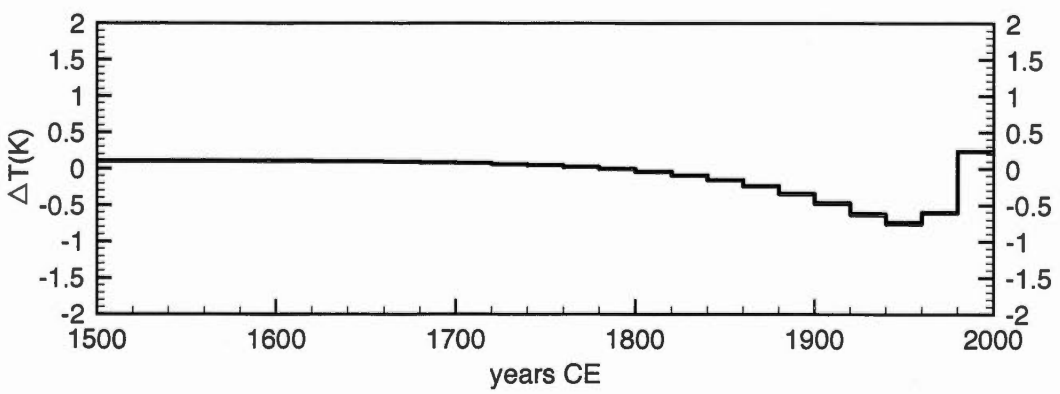

Figure C.4 GST changes for DDH2457(Inca de Oro), where 3 eigenvalues are retained. The extremal steady states are not visible because the three lines are superimposed.

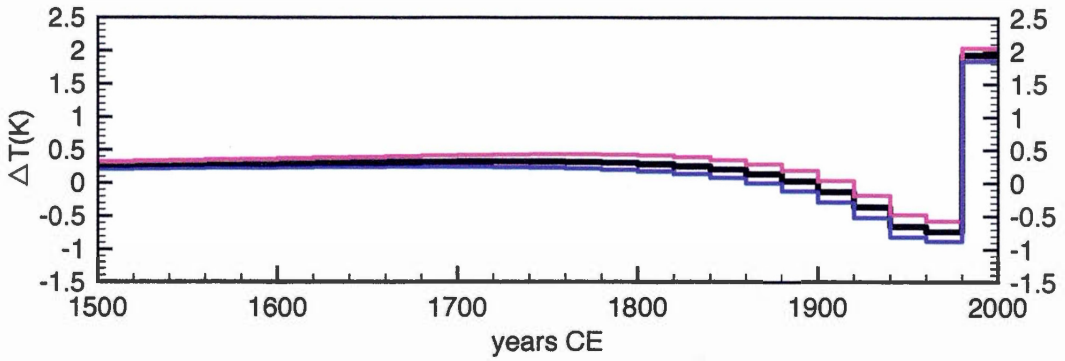

Figure C.5 GST changes for 1501(Inca de Oro), where 3 eigenvalues are retained. The pink and blue lines represent the inversion of the upper and lower bounds of the geothermal quasi-steady state or the extremal steady states.

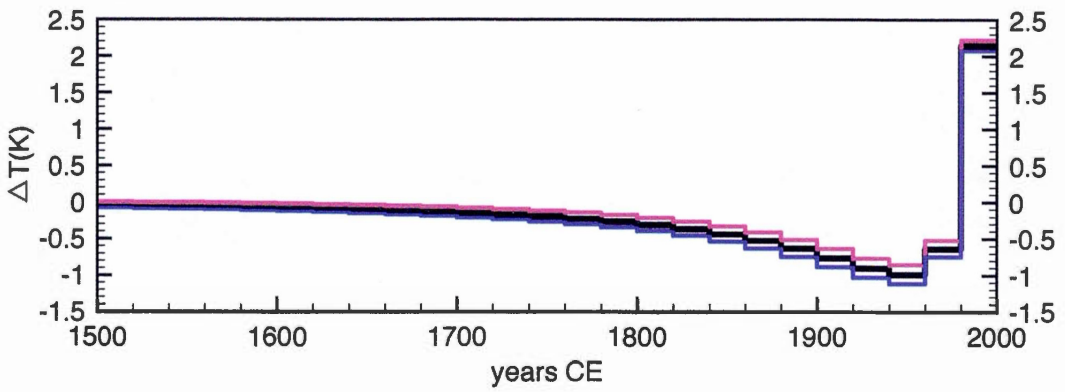

Figure C.6 GST changes for 1504 (Inca de Oro), where 3 eigenvalues are retained. The pink and blue lines represent the inversion of the upper and lower bounds of the geothermal quasi-steady state or the extremal steady states.

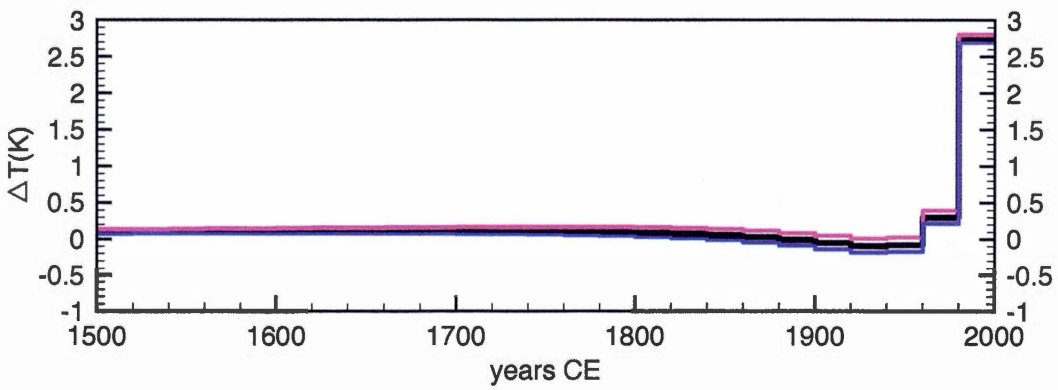

Figure C.7 GST changes for 1505 (Inca de Oro), where 3 eigenvalues are retained. The pink and blue lines represent the inversion of the upper and lower bounds of the geothermal quasi-steady state or the extremal steady states.

REFERENCES

Archambault, S. and Bergeron, Y. (1992). An 802-year tree-ring chronology from the Quebec boreal forest. *Canadian Journal of Forest Research*, *22*(5), 674–682. http://dx.doi.org/10.1139/x92-090

Bartlett, M. G., Chapman, D. S. and Harris, R. N. (2005). Snow effect on North American ground temperatures, 1950–2002. *Journal of Geophysical Research: Earth Surface (2003–2012)*, *110*(F03008). http://dx.doi.org/10.1029/2005JF000293

Beck, A. (1977). Climatically perturbed temperature gradient and their effect on regional and continental heat-flow means. *Tectonophysics*, *41*(1-3), 17–39. http://dx.doi.org/10.1016/0040-1951(77)90178-0

Bégin, Y. (2000). Reconstruction of subarctic lake levels over past centuries using tree rings. *Journal of Cold Regions Engineering*, *14*(4), 192–212. http://dx.doi.org/10.1061/(ASCE)0887-381X(2000)14:4(192)

Beltrami, H. (2001). On the relationship between ground temperature histories and meteorological records: a report on the pomquet station. *Global and Planetary Change*, *29*(3), 327–348. http://dx.doi.org/10.1016/S0921-8181(01)00098-4

Beltrami, H. and Bourlon, E. (2004). Ground warming patterns in the Northern Hemisphere during the last five centuries. *Earth and Planetary Science Letters*, *227*(3), 169–177. http://dx.doi.org/10.1016/j.epsl.2004.09.014

Beltrami, H., Cheng, L. and Mareschal, J. C. (1997). Simultaneous inversion of borehole temperature data for determination of ground surface temperature history. *Geophysical Journal International*, *129*(2), 311–318. http://dx.doi.org/10.1111/j.1365-246X.1997.tb01584.x

Beltrami, H. and Mareschal, J.-C. (1992). Ground temperature histories for central and eastern Canada from geothermal measurements: Little Ice Age signature. *Geophysical research letters*, *19*(7), 689–692. http://dx.doi.org/10.1029/92GL00671

Beltrami, H. and Mareschal, J.-C. (1995). Resolution of ground temperature histories inverted from borehole temperature data. *Global and Planetary Change*, *11*(1-2), 57–70. http://dx.doi.org/10.1016/0921-8181(95)00002-9

Beltrami, H., Smerdon, J., G.S.Matharoo and N.Nickerson (2011). Impact of maximum borehole depths on inverted temperature histories in borehole paleoclimatology. *Climate of the Past*, *7*, 715–748. http://dx.doi.org/10.5194/cp-7-745-2011

Beltrami, H. and Taylor, A. E. (1995). Records of climatic change in the Canadian Arctic: towards calibrating oxygen isotope data with geothermal data. *Global and Planetary Change*, *11*(3), 127–138. http://dx.doi.org/10.1016/0921-8181(95)00006-2

Benfield, A. (1949). The effect of uplift and denudation on underground temperatures. *Journal of Applied Physics*, *20*(1), 66–70. http://dx.doi.org/10.1063/1.1698238

Betancourt, J., Latorre, C., Rech, J., Quade, J. and Rylander, K. (2000). A 22,000-year record of monsoonal precipitation from northern Chile's Ata-

cama Desert. *Science*, *289*(5484), 1542–1546. http://dx.doi.org/10.1126/science.289.5484.1542

Birch, A. F. (1948). The effects of Pleistocene climatic variations upon geothermal gradients. *American Journal of Science*, *246*(12), 729–760. http://dx.doi.org/10.2475/ajs.246.12.729

Blackwell, D. D., Steele, J. L. and Brott, C. A. (1980). The terrain effect on terrestrial heat flow. *Journal of Geophysical Research: Solid Earth*, *85*(B9), 4757–4772. http://dx.doi.org/10.1029/JB085iB09p04757

Bobst, A. L., Lowenstein, T. K., Jordan, T. E., Godfrey, L. V., Ku, T.-L. and Luo, S. (2001). A 106ka paleoclimate record from drill core of the Salar de Atacama, northern Chile. *Palaeogeography, Palaeoclimatology, Palaeoecology*, *173*(1), 21–42. http://dx.doi.org/10.1016/S0031-0182(01)00308-X

Bodri, L. and Cermak, V. (2007). *Borehole Climatology*. Amsterdam: Elsevier.

Boninsegna, J. A., Argollo, J., Aravena, J., Barichivich, J., Christie, D., Ferrero, M., Lara, A., Le Quesne, C., Luckman, B., Masiokas, M. *et al.* (2009). Dendroclimatological reconstructions in South America: a review. *Palaeogeography, Palaeoclimatology, Palaeoecology*, *281*(3), 210–228. http://dx.doi.org/10.1016/j.palaeo.2009.07.020

Boudreau, R., Galloway, J., Patterson, R., Kumar, A. and Michel, F. (2005). A paleolimnological record of Holocene climate and environmental change in the Temagami region, northeastern Ontario. *Journal of Paleolimnology*, *33*(4), 445–461. http://dx.doi.org/10.1007/s10933-004-7616-7

Braconnot, P., Harrison, S. P., Kageyama, M., Bartlein, P. J., Masson-Delmotte, V., Abe-Ouchi, A., Otto-Bliesner, B. and Zhao, Y. (2012). Evaluation of climate

models using palaeoclimatic data. *Nature Climate Change*, *2*(6), 417–424. http://dx.doi.org/10.1038/nclimate1456

Bradley, R. (1999). *Paleoclimatology: Reconstructing Climates of the Quaternary* (second éd.). Elsevier.

Brown, J., Ferrians, O., Heginbottom, J. A. and Melnikov, E. (2002). *Circum-Arctic Map of Permafrost and Ground-Ice Conditions, Version 2.* Map, National Snow and Ice Data Center, Boulder (CO).

Brown, R. D. (2010). Analysis of snow cover variability and change in Québec, 1948–2005. *Hydrological Processes*, *24*(14), 1929–1954. http://dx.doi.org/10.1002/hyp.7565

Brown, R. D. and Mote, P. W. (2009). The response of Northern Hemisphere snow cover to a changing climate. *Journal of Climate*, *22*(8), 2124–2145. http://dx.doi.org/10.1175/2008JCLI2665.1

Brown, R. J. (1979). Permafrost distribution in the southern part of the discontinuous zone in Quebec and Labrador. *Géographie physique et Quaternaire*, *33*(3-4), 279–289. http://dx.doi.org/10.7202/1000364ar

Bullard, E. (1939). Heat Flow in South Africa. *Proceedings of the Royal Society London A*, *173*(955), 474–502.

Bunbury, J., Finkelstein, S. A. and Bollmann, J. (2012). Holocene hydro-climatic change and effects on carbon accumulation inferred from a peat bog in the Attawapiskat River watershed, Hudson Bay Lowlands, Canada. *Quaternary Research*, *78*(2), 275–284. http://dx.doi.org/10.1016/j.yqres.2012.05.013

Carlson, A. E., LeGrande, A. N., Oppo, D. W., Came, R. E., Schmidt, G. A., Anslow, F. S., Licciardi, J. M. and Obbink, E. A. (2008). Rapid early Holocene

deglaciation of the Laurentide ice sheet. *Nature Geosci*, *1*(9), 620–624. http://dx.doi.org/10.1038/ngeo285

Carslaw, H. and Jaeger, J. (1959). *Conduction of Heat in Solids*. New York: Oxford Science Publications.

Cermak, V. (1971). Underground temperature and inferred climatic temperature of the past millennium. *Palaeogeography, Palaeoclimatology, Palaeoecology*, *10*(1), 1–19. http://dx.doi.org/10.1016/0031-0182(71)90043-5

Chouinard, C., Fortier, R. and Mareschal, J.-C. (2007). Recent climate variations in the subarctic inferred from three borehole temperature profiles in northern Quebec, Canada. *Earth and Planetary Science Letters*, *263*(3-4), 355–369. http://dx.doi.org/10.1016/j.epsl.2007.09.017

Chouinard, C. and Mareschal, J.-C. (2007). Selection of borehole temperature depth profiles for regional climate reconstructions. *Climate of the Past*, *3*, 297–313. http://dx.doi.org/10.5194/cp-3-297-2007

Chouinard, C. and Mareschal, J.-C. (2009). Ground surface temperature history in southern Canada: Temperatures at the base of the Laurentide ice sheet and during the Holocene. *Earth and Planetary Science Letters*, *277*(1–2), 280 – 289. http://dx.doi.org/10.1016/j.epsl.2008.10.026

Church, J. A., White, N. J., Konikow, L. F., Domingues, C. M., Cogley, J. G., Rignot, E., Gregory, J. M., van den Broeke, M. R., Monaghan, A. J. and Velicogna, I. (2011). Revisiting the Earth's sea-level and energy budgets from 1961 to 2008. *Geophysical Research Letters*, *38*(18). http://dx.doi.org/10.1029/2011GL048794

Clark, P. U. (1994). Unstable behavior of the Laurentide Ice Sheet over deforming

sediment and its implications for climate change. *Quaternary Research*, *41*(1), 19–25. http://dx.doi.org/10.1006/qres.1994.1002

Clark, P. U., Alley, R. B. and Pollard, D. (1999). Northern Hemisphere Ice-Sheet Influences on Global Climate Change. *Science*, *286*(5442), 1104–1111. http://dx.doi.org/10.1126/science.286.5442.1104

Clark, P. U. and Pollard, D. (1998). Origin of the Middle Pleistocene Transition by ice sheet erosion of regolith. *Paleoceanography*, *13*(1), 1–9. http://dx.doi.org/10.1029/97PA02660

Clauser, C. and Mareschal, J.-C. (1995). Ground temperature history in central Europe from borehole temperature data. *Geophysical Journal International*, *121*(3), 805–817. http://dx.doi.org/10.1111/j.1365-246X.1995.tb06440.x

Dahl-Jensen, D., Mosegaard, K., Gundestrup, N., Clow, G. D., Johnsen, S. J., Hansen, A. W. and Balling, N. (1998). Past Temperatures Directly from the Greenland Ice Sheet. *Science*, *282*(5387), 268–271. http://dx.doi.org/10.1126/science.282.5387.268

Davis, M., Douglas, C., Calcote, R., Cole, K., Green Winkler, M. and Flakne, R. (2000). Holocene climate in the Western Great Lakes national park and lakeshores: implications for future climate change. *Conservation Biology*, *14*(4), 968–983. http://dx.doi.org/10.1046/j.1523-1739.2000.99219.x

Demezhko, D. and Gornostaeva, A. (2015). Late Pleistocene-Holocene ground surface heat flux changes reconstructed from borehole tempeature data (the Urals, Russia). *Climate of the Past*, *11*, 647–653. http://dx.doi.org/10.5194/cp-11-647-2015

Demezhko, D. and Shchapov, V. (2001). 80,000 years ground surface temperature history inferred from the temperature-depth log measured in the superdeep hole SG-4 (the Urals, Russia). *Global and Planetary Change*, *20*(3-4), 219–230. http://dx.doi.org/10.1016/S0921-8181(01)00091-1

Demezhko, D. Y., Gornostaeva, A. A., Tarkhanov, G. V. and Esipko, O. A. (2013). 30,000 years of ground surface temperature and heat flux changes in Karelia reconstructed from borehole temperature data. *Bulletin of Geography. Physical Geography Series*, *6*(1), 7–25. http://dx.doi.org/10.2478/bgeo-2013-0001

Denton, G. and Hughes, T. (dir.) (1981). *The Last Great Ice Sheets*. New York: Wiley-Interscience.

Dyke, A., Andrews, J., Clark, P., England, J., Miller, G., Shaw, J. and Veillette, J. (2002). The Laurentide and Innuitian ice sheets during the Last Glacial Maximum. *Quaternary Science Reviews*, *21*(1–3), 9 – 31. http://dx.doi.org/10.1016/S0277-3791(01)00095-6

Environment Canada (2010). Canadian climate normals or averages 1981-2010. *National Climate Data and Information Archive*.

Fahnestock, M., Abdalati, W., Luo, S. and Gogineni, S. (2001). Internal layer tracing and age-depth-accumulation relationships for the northern Greenland ice sheet. *Journal of Geophysical Research: Atmospheres (1984–2012)*, *106*(D24), 33789–33797. http://dx.doi.org/10.1029/2001JD900200

Fisher, D. A. and Koerner, R. M. (1994). Signal and noise in four ice-core records from the Agassiz Ice Cap, Ellesmere Island, Canada: details of the last millennium for stable isotopes, melt and solid conductivity. *The Holocene*, *4*(2), 113–120. http://dx.doi.org/10.1177/095968369400400201

Flantua, S. G. A., Hooghiemstra, H., Vuille, M., Behling, H., Carson, J. F., Gosling, W. D., Hoyos, I., Ledru, M. P., Montoya, E., Mayle, F., Maldonado, A., Rull, V., Tonello, M. S., Whitney, B. S. and González-Arango, C. (2016). Climate variability and human impact in South America during the last 2000 years: synthesis and perspectives from pollen records. *Climate of the Past*, *12*(2), 483–523. http://dx.doi.org/10.5194/cp-12-483-2016

Förster, A. and Schrötter, J. (1997). Distributed optic-fibre temperature sensing (DTS): a new tool for determining subsurface temperature changes and reservoir characteristics. *Proceedings of the 22nd Workshop in Geothermal Reservoir Engineering*, 27–29.

Förster, A., Schrötter, J., Merriam, D. and Blackwell, D. D. (1997). Application of optical-fiber temperature logging—An example in a sedimentary environment. *Geophysics*, *62*(4), 1107–1113.

Gajewski, K. (1988). Late Holocene climate changes in eastern North America estimated from pollen data. *Quaternary Research*, *29*(3), 255–262. http://dx.doi.org/10.1016/0033-5894(88)90034-8

García-García, A., Cuesta-Valero, F., Beltrami, H. and Smerdon, J. (2016). Simulation of Air and Ground Temperatures in PIMIP3/CMIP5 Last Millenium Simulation: Implications for Climate Reconstructions from Borehole Temperature Profiles. *Environmental Research Letters*, *11*(4). http://dx.doi.org/10.1088/1748-9326/11/4/044022

Gent, P. R., Danabasoglu, G., Donner, L. J., Holland, M. M., Hunke, E. C., Jayne, S. R., Lawrence, D. M., Neale, R. B., Rasch, P. J., Vertenstein, M., Worley, P. H., Yang, Z.-L. and Zhang, M. (2011). The community climate system model version 4. *Journal of Climate*, *24*(19), 4973–4991. http://dx.doi.org/10.1175/2011JCLI4083.1

Giorgetta, M. A., Jungclaus, J., Reick, C. H., Legutke, S., Bader, J., Böttinger, M., Brovkin, V., Crueger, T., Esch, M., Fieg, K., Glushak, K., Gayler, V., Haak, H., Hollweg, H.-D., Ilyina, T., Kinne, S., Kornblueh, L., Matei, D., Mauritsen, T., Mikolajewicz, U., Mueller, W., Notz, D., Pithan, F., Raddatz, T., Rast, S., Redler, R., Roeckner, E., Schmidt, H., Schnur, R., Segschneider, J., Six, K. D., Stockhause, M., Timmreck, C., Wegner, J., Widmann, H., Wieners, K.-H., Claussen, M., Marotzke, J. and Stevens, B. (2013). Climate and carbon cycle changes from 1850 to 2100 in mpi-esm simulations for the coupled model intercomparison project phase 5. *Journal of Advances in Modeling Earth Systems*, *5*(3), 572–597. `http://dx.doi.org/10.1002/jame.20038`

Gomez, N., Mitrovica, J. X., Tamisiea, M. E. and Clark, P. U. (2010). A new projection of sea level change in response to collapse of marine sectors of the Antarctic Ice Sheet. *Geophysical Journal International*, *180*(2), 623–634. `http://dx.doi.org/10.1111/j.1365-246X.2009.04419.x`

González-Rouco, J., Beltrami, H., Zorita, E. and Stevens, M. (2009). Borehole climatology: a discussion based on contributions from climate modeling. *Climate of the Past*, *5*(1), 97–127. `http://dx.doi.org/10.5194/cp-5-97-2009`

González-Rouco, J., Beltrami, H., Zorita, E. and Von Storch, H. (2006). Simulation and inversion of borehole temperature profiles in surrogate climates: Spatial distribution and surface coupling. *Geophysical Research Letters*, *33*(1). `http://dx.doi.org/10.1029/2005GL024693`

Gosselin, C. and Mareschal, J.-C. (2003). Recent warming in northwestern Ontario inferred from borehole temperature profiles. *Journal of Geophysical Research: Solid Earth*, *108*(B9). `http://dx.doi.org/10.1029/2003JB002447`

Greve, R. (2005). Relation of measured basal temperatures and the spatial distribution of the geothermal heat flux for the Greenland ice

sheet. *Annals of Glaciology*, *42*(1), 424–432. http://dx.doi.org/10.3189/172756405781812510

Grosjean, M., Cartajena, I., Geyh, M. A. and Núñez, L. (2003). From proxy data to paleoclimate interpretation: the mid-Holocene paradox of the Atacama Desert, northern Chile. *Palaeogeography, Palaeoclimatology, Palaeoecology*, *194*(1), 247–258.

Grosjean, M., Van Leeuwen, J., Van der Knaap, W., Geyh, M., Ammann, B., Tanner, W., Messerli, B., Núñez, L., Valero-Garcés, B. and Veit, H. (2001). A 22,000 14 C year BP sediment and pollen record of climate change from Laguna Miscanti (23 S), northern Chile. *Global and Planetary Change*, *28*(1), 35–51. http://dx.doi.org/10.1016/S0921-8181(00)00063-1

Grosse, G., Goetz, S., McGuire, A. D., Romanovsky, V. E. and Schuur, E. A. (2016). Changing permafrost in a warming world and feedbacks to the earth system. *Environmental Research Letters*, *11*(4), 040201. http://dx.doi.org/10.1088/1748-9326/11/4/040201

Gruber, S. (2012). Derivation and analysis of a high-resolution estimate of global permafrost zonation. *The Cryosphere*, *6*, 221–233. http://dx.doi.org/10.5194/tc-6-221-2012

Guillou-Frottier, L., Jaupart, C., Mareschal, J. C., Gariépy, C., Bienfait, G., Cheng, L. Z. and Lapointe, R. (1996). High heat flow in the trans-Hudson Orogen, Central Canadian Shield. *Geophysical Research Letters*, *23*(21), 3027–3030. http://dx.doi.org/10.1029/96GL02895

Guillou-Frottier, L., Mareschal, J. C. and Musset, J. (1998). Ground surface temperature history in central Canada inferred from 10 selected borehole

temperature profiles. *Journal of Geophysical Research, 103*(B4), 7385–7397. http://dx.doi.org/10.1029/98JB00021

Gurza Fausto, E. (2014). *Borehole Climatology in South America.* (Mémoire de maîtrise). St. Francis Xavier University.

Halsey, L. A., Vitt, D. H. and Zoltai, S. C. (1995). Disequilibrium response of permafrost in boreal continental western Canada to climate change. *Climatic Change, 30*(1), 57–73. http://dx.doi.org/10.1007/BF01093225

Hamza, V., Frangipani, A. and Becker, E. (1987). *Mapas geotermais do Brasil.* Rapport technique 25305, Instituto de Pesquisas Tecnólogicas.

Hamza, V. M. and Muñoz, M. (1996). Heat flow map of South America. *Geothermics, 25*(6), 599623–621646. http://dx.doi.org/10.1016/S0375-6505(96)00025-9

Hamza, V. M. and Vieira, F. P. (2011). *Climate changes of the recent past in the South American continent: inferences based on analysis of borehole temperature profiles.* INTECH Open Access Publisher. http://dx.doi.org/10.5772/23363

Harris, R. N. and Chapman, D. S. (1998). Geothermics and climate change: 2. Joint analysis of borehole temperature and meteorological data. *Journal of Geophysical Research: Solid Earth, 103*(B4), 7371–7383. http://dx.doi.org/10.1029/97JB03296

Harris, R. N. and Chapman, D. S. (2001). Mid-latitude (30–60 N) climatic warming inferred by combining borehole temperatures with surface air temperatures. *Geophysical Research Letters, 28*(5), 747–750. http://dx.doi.org/10.1029/2000GL012348

Hausner, M. B., Suárez, F., Glander, K. E., Giesen, N. v. d., Selker, J. S. and Tyler, S. W. (2011). Calibrating single-ended fiber-optic raman spectra distributed temperature sensing data. *Sensors*, *11*(11), 10859–10879. http://dx.doi.org/10.3390/s111110859

Heginbottom, J. A. (2002). Permafrost mapping: a review. *Progress in Physical Geography*, *26*(4), 623–642. http://dx.doi.org/10.1191/0309133302pp355ra

Hotchkiss, W. and Ingersoll, L. (1934). Post-glacial time calculations from recent geothermal measurements in the Calumet Copper Mines. *Journal of Geology*, *42*(2), 113–142.

Huang, S., Pollack, H. N. and Shen, P.-Y. (2000). Temperature trends over the past five centuries reconstructed from borehole temperatures. *Nature*, *403*(6771), 756–758. http://dx.doi.org/10.1038/35001556

Hughes, T. (2009). Modeling ice sheets from the bottom up. *Quaternary Science Reviews*, *28*(19-20), 1831–1849. http://dx.doi.org/10.1016/j.quascirev.2009.06.004

IPCC. (2013). *Climate Change 2013: The Physical Science Basis*. Cabridge, United Kingdom and New York, NY, USA: Cambridge University Press.

Jackson, D. (1972). Interpretation of inaccurate, insufficient, and inconsistent data. *Geophysical Journal International*, *28*(2), 97–109. http://dx.doi.org/10.1111/j.1365-246X.1972.tb06115.x

Jaume-Santero, F., Pickler, C., Beltrami, H. and Mareschal, J.-C. (2016). North American regional climate reconstruction from Ground Surface Temperature Histories. *Climate of the Past Discussion*. http://dx.doi.org/10.5194/cp-2016-85

Jaupart, C., Mareschal, J., Bouquerel, H. and Phaneuf, C. (2014). The building and stabilization of an Archean Craton in the Superior Province, Canada, from a heat flow perspective. *Journal of Geophysical Research: Solid Earth*, *119*(12), 9130–9155. http://dx.doi.org/10.1002/2014JB011018

Jaupart, C. and Mareschal, J.-C. (2011). *Heat generation and transport in the Earth*. Cambridge, United Kingdom: Cambridge University Press.

Jeffreys, H. (1938). The Disturbance of the Temperature Gradient in the Earth's Crust by Inequalities of Height. *Monthly Notices R Astron. Soc., Geophys. Suppl.*, *4*, 309–312. http://dx.doi.org/10.1111/j.1365-246X.1938.tb01752.x

Jessop, A. (1971). The Distribution of Glacial Perturbation of Heat Flow in Canada. *Canadian Journal of Earth Sciences*, *8*(1), 162–166. http://dx.doi.org/10.1139/e71-012

Jessop, A. and Lewis, T. (1978). Heat flow and heat generation in the Superior province of the Canadian Shield. *Tectonophysics*, *50*(1), 55–57. http://dx.doi.org/10.1016/0040-1951(78)90199-3

Jessop, A. M. (1968). Three measurements of heat flow in eastern Canada. *Canadian Journal of Earth Sciences*, *5*(1), 61–68. http://dx.doi.org/10.1139/e68-006

Jones, P., Lister, D., Osborn, T., Harpham, C., Salmon, M. and Morice, C. (2012). Hemispheric and large-scale land-surface air temperature variations: An extensive revision and an update to 2010. *Journal of Geophysical Research: Atmospheres*, *117*(D5). http://dx.doi.org/10.1029/2011JD017139

Joughin, I., Smith, B. and Medley, B. (2014). Marine Ice Sheet Collapse Poten-

tially Under Way for the Thwaites Glacier Basin, West Antarctica. *Science*, *344*(6185), 735–738. http://dx.doi.org/10.1126/science.1249055

Kukkonen, I. T. and Jõeleht, A. (2003). Weichselian temperatures from geothermal heat flow data. *Journal of Geophysical Research: Solid Earth*, *108*(B3). http://dx.doi.org/10.1029/2001JB001579

Lachenbruch, A. and Marshall, B. (1986). Changing climate: Geothermal evidence from permafrost in the Alaskan Arctic. *Science*, *234*(4777), 689–696. http://dx.doi.org/10.1126/science.234.4777.689

Lachenbruch, A. H. (1988). Permafrost, the active layer and changing climate. *Global and Planetary Change*, *29*, 259–273.

Lamb, H. (1995). *Climate, History and the Modern World* (2 éd.). Routledge.

Lanczos, C. (1961). *Linear Differential Operators*. Princeton, N.J.: D. Van Nostrand.

Latorre, C., Betancourt, J., Rylander, K. and Quade, J. (2002). Vegetation invasion into absolute desert: A 45 k.y. rodent midden record from the Calama-Salar de Atacama basins, northern Chile (lat 22-24S). *Geological Society of America Bulletin*, *114*(3), 349–366. http://dx.doi.org/10.1130/0016-7606(2002)114<0349:VIIADA>2.0.CO;2

Lavoie, C. and Payette, S. (1992). Black spruce growth forms as a record of a changing winter environment at treeline, Quebec, Canada. *Arctic and Alpine Research*, *24*(1), 40–49. http://dx.doi.org/10.2307/1551318

Lévy, F., Jaupart, C., Mareschal, J.-C., Bienfait, G. and Limare, A. (2010). Low heat flux and large variations of lithospheric thickness in the Canadian Shield. *Journal of Geophysical Research: Solid Earth (1978–2012)*, *115*(B06404). http://dx.doi.org/10.1029/2009JB006470

Lewis, T. (1998). The effect of deforestation on ground surface temperatures. *Global and Planetary Change*, *18*(1), 1–13. http://dx.doi.org/10.1016/S0921-8181(97)00011-8

Lewis, T. J. and Wang, K. (1992). Influence of terrain on bedrock temperatures. *Palaeogeography, Palaeoclimatology, Palaeoecology*, *98*(2-4), 87–100. http://dx.doi.org/10.1016/0031-0182(92)90190-G

Lewis, T. J. and Wang, K. (1998). Geothermal evidence for deforestation induced warming: Implications for the climatic impact of land development. *Geophysical Research Letters*, *25*(4), 535–538. http://dx.doi.org/10.1029/98GL00181

Li, L. *et al.* (2014). An overview of BCC climate system model development and application for climate change studies. *Journal of Meteorological Research*, *28*(1), 34–56. http://dx.doi.org/10.1007/s13351-014-3041-7

Llubes, M., Lanseau, C. and Rémy, F. (2006). Relations between basal condition, subglacial hydrological networks and geothermal flux in Antarctica. *Earth and Planetary Science Letters*, *241*(3), 655–662. http://dx.doi.org/10.1016/j.epsl.2005.10.040

Majorowicz, J., Chan, J., Crowell, J., Gosnold, W., Heaman, L. M., Kück, J., Nieuwenhuis, G., Schmitt, D. R., Unsworth, M., Walsh, N. and Weides, S. (2014). The first deep heat flow determination in crystalline basement rocks beneath the Western Canadian Sedimentary Basin. *Geophysical Journal International*, *197*(2), 731–747. http://dx.doi.org/10.1093/gji/ggu065

Majorowicz, J. and Šafanda, J. (2015). Effect of postglacial warming seen in high precision temperature log deep into the granites in NE Alberta. *International Journal of Earth Sciences*, *104*, 1563–1571. http://dx.doi.org/10.1007/s00531-014-1075-9

Majorowicz, J., Šafanda, J. and Group, T.-. W. (2008). Heat flow variation with depth in Poland: evidence from equilibrium temperature logs in 2.9-km-deep well Torun-1. *International Journal of Earth Sciences*, *97*(2), 307–315. http://dx.doi.org/10.1007/s00531-007-0210-2

Majorowicz, J. A., Skinner, W. R. and Safanda, J. (2004). Large ground warming in the Canadian Arctic inferred from inversions of temperature logs. *Earth and Planetary Science Letters*, *221*(1-4), 15–25. http://dx.doi.org/10.1016/S0012-821X(04)00106-2

Mann, M. E., Bradley, R. S. and Hughes, M. K. (1999). Northern hemisphere temperatures during the past millennium: inferences, uncertainties, and limitations. *Geophysical research letters*, *26*(6), 759–762. http://dx.doi.org/10.1029/1999GL900070

Mann, M. E. and Jones, P. D. (2003). Global surface temperatures over the past two millennia. *Geophysical Research Letters*, *30*(15). http://dx.doi.org/10.1029/2003GL017814

Mareschal, J., Poirier, A., Rolandone, F., Bienfait, G., Gariépy, C., Lapointe, R. and Jaupart, C. (2000). Low mantle heat flow at the edge of the North American continent, Voisey Bay, Labrador. *Geophysical Research Letters*, *27*(6), 823–826. http://dx.doi.org/10.1029/1999GL011069

Mareschal, J.-C. and Beltrami, H. (1992). Evidence for recent warming from perturbed geothermal gradients: examples from eastern Canada. *Climate Dynamics*, *6*(3-4), 135–143. http://dx.doi.org/10.1007/BF00193525

Mareschal, J. C., Jaupart, C., Cheng, L. Z., Rolandone, F., Gariépy, C., Bienfait, G., Guillou-Frottier, L. and Lapointe, R. (1999a). Heat flow in the Trans-Hudson Orogen of the Canadian Shield: Implications for Proterozoic continental

growth. *Journal of Geophysical Research*, *104*(B12), 7–29. http://dx.doi.org/10.1029/1998JB900209

Mareschal, J. C., Pinet, C., Gariépy, C., Jaupart, C., Bienfait, G., Coletta, G. D., Jolivet, J. and Lapointe, R. (1989). New heat flow density and radiogenic heat production data in the Canadian Shield and the Quebec Appalachians. *Canadian Journal of Earth Sciences*, *26*, 845–852. http://dx.doi.org/10.1139/e89-068

Mareschal, J.-C., Rolandone, F. and Bienfait, G. (1999b). Heat flow variations in a deep borehole near Sept-Iles, Québec, Canada: Paleoclimatic interpretation and implications for regional heat flow estimates. *Geophysical Research Letters*, *26*(14), 2049–2052. http://dx.doi.org/10.1029/1999GL900489

Marshall, S. (2005). Recent advances in understanding ice sheet dynamics. *Earth and Planetary Science Letters*, *240*(2), 191–204.

Marshall, S. and Clark, P. (2002). Basal temperature evolution of North American ice sheets and implications for the 100-kyr cycle. *Geophysical Research Letters*, *29*(24), 67–1–67–4. http://dx.doi.org/10.1029/2002GL015192

Matthews, J. A. and Briffa, K. R. (2005). The 'little ice age': Re-evaluation of an evolving concept. *Geografiska Annaler: Series A, Physical Geography*, *87*(1), 17–36. http://dx.doi.org/10.1111/j.0435-3676.2005.00242.x

Menke, W. (1989). *Geophysical Data Analysis: Discrete Inverse Theory*, volume 4. San Diego: Academic Press.

Messerli, B., Grosjean, M. and Vuille, M. (1997). Water availability, protected areas, and natural resources in the andean desert altiplano. *Mountain research and development*, *17*(3), 229–238. http://dx.doi.org/10.2307/3673850

Mignot, J. and Bony, S. (2013). Presentation and analysis of the IPSL and CNRM climate models used in CMIP5. *Climate Dynamics*, *40*, 2089. http://dx.doi.org/10.10007/s00382-013-1720-1

Misener, A. and Beck, A. (1960). *The measurement of heat flow over land.* New York: Interscience.

Mitrovica, J. X., Gomez, N. and Clark, P. U. (2009). The Sea-Level Fingerprint of West Antarctic Collapse. *Science*, *323*(5915), 753–753. http://dx.doi.org/10.1126/science.1166510

Moberg, A., Sonechkin, D. M., Holmgren, K., Datsenko, N. M. and Karlén, W. (2005). Highly variable Northern Hemisphere temperatures reconstructed from low-and high-resolution proxy data. *Nature*, *433*(7026), 613–617. http://dx.doi.org/10.1038/nature03265

Moy, C. M., Moreno, P. I., Dunbar, R. B., Kaplan, M. R., Francois, J.-P., Villalba, R. and Haberzettl, T. (2009). Climate change in southern South America during the last two millennia. In *Past climate variability in South America and surrounding regions* 353–393. Springer

Neukom, R. and Gergis, J. (2012). Southern Hemisphere high-resolution palaeoclimate records of the last 2000 years. *The Holocene*, *22*(5), 501–524. http://dx.doi.org/10.1177/0959683611427335

Neukom, R., Gergis, J., Karoly, D. J., Wanner, H., Curran, M., Elbert, J., González-Rouco, F., Linsley, B. K., Moy, A. D., Mundo, I. *et al.* (2014). Inter-hemispheric temperature variability over the past millennium. *Nature Climate Change*, *4*(5), 362–367. http://dx.doi.org/10.1038/nclimate2174

Neukom, R., Luterbacher, J., Villalba, R., Küttel, M., Frank, D., Jones, P., Grosjean, M., Esper, J., Lopez, L. and Wanner, H. (2010). Multi-centennial summer

and winter precipitation variability in southern South America. *Geophysical Research Letters*, *37*(14). http://dx.doi.org/10.1029/2010GL043680

Nicault, A., Boucher, E., Tapsoba, D., Arseneault, D., Berninger, F., Bégin, C., DesGranges, J., Guiot, J., Marion, J., Wicha, S. and Begin, Y. (2014). Spatial analysis of black spruce (Picea mariana (Mill.) BSP) radial growth response to climate in northern Québec–Labrador Peninsula, Canada. *Canadian Journal of Forest Research*, *45*(3), 343–352. http://dx.doi.org/10.1139/cjfr-2014-0080

Nielsen, S. and Beck, A. (1989). Heat flow density values and paleoclimate determined from stochastic inversion of four temperature-depth profiles from the Superior Province of the Canadian Shield. *Tectonophysics*, *164*(2–4), 345 – 359. http://dx.doi.org/10.1016/0040-1951(89)90026-7

Oerlemans, J. and van der Veen, C. (1984). *Ice Sheets and Climate.* Dordrecht, Boston, Lancaster: D. Reidel Publishing Company.

PAGES-2K Network (2013). Continental-scale temperature variability during the past two millennia. *Nature Geoscience*, *6*(5), 339–346. http://dx.doi.org/10.1038/ngeol1797

Pattyn, F. (2010). Antarctic subglacial conditions inferred from a hybrid ice sheet/ice stream model. *Earth and Planetary Science Letters*, *295*(3-4), 451–461. http://dx.doi.org/10.1016/j.epsl.2010.04.025

Peltier, W. (2004). Global glacial isostasy and the surface of the ice-age earth: The ICE-5G (VM2) Model and GRACE. *Annual Review of Earth and Planetary Sciences*, *32*(1), 111–149. http://dx.doi.org/10.1146/annurev.earth.32.082503.144359

Peltier, W. R. (2002). Global glacial isostatic adjustment: palaeogeodetic and space-geodetic tests of the ICE-4G (VM2) model. *Journal of Quaternary Science*, *17*(5-6), 491–510. http://dx.doi.org/10.1002/jqs.713

Perry, H., Jaupart, C., Mareschal, J. and Bienfait, G. (2006). Crustal heat production in the Superior Province, Canadian Shield, and in North America inferred from heat flow data. *Journal of Geophysical Research: Solid Earth*, *111*(B04401). http://dx.doi.org/10.1029/2005JB003893

Perry, H., Mareschal, J. C. and Jaupart, C. (2009). Enhanced crustal geo-neutrino production near the Sudbury Neutrino Observatory, Ontario, Canada. *Earth and Planetary Science Letters*, *288*(1-2), 301–308. http://dx.doi.org/10.1016/j.epsl.2009.09.033

Phillips, D. (2002). *Climatic Atlas of Canada series 1.* Rapport technique, Canadian Climate Center, Ottawa (ON).

Pickler, C., Beltrami, H. and Mareschal, J.-C. (2016a). Climate trends in northern Ontario and Québec from borehole temperature profiles. *Climate of the Past*, *12*(12), 2215–2227. http://dx.doi.org/10.5194/cp-12-2215-2016

Pickler, C., Beltrami, H. and Mareschal, J.-C. (2016b). Laurentide Ice Sheet basal temperatures during the last glacial cycle as inferred from borehole data. *Climate of the Past*, *12*(1), 115–127. http://dx.doi.org/10.5194/cp-12-115-2016

Pollack, H. N. and Smerdon, J. E. (2004). Borehole climate reconstructions: Spatial structure and hemispheric averages. *Journal of Geophysical Research: Atmospheres*, *109*(D11). http://dx.doi.org/10.1029/2004JD005056

Pollard, D., DeConto, R. and Nyblabe, A. (2005). Sensitivity of Cenozoic Antarc-

tic ice sheet variations to geothermal heat flux. *Global and Planetary Change*, *49*(1-2), 63–74. http://dx.doi.org/10.1016/j.gloplacha.2005.05.003

Pritchard, H. D., Ligtenberg, S. R. M., Fricker, H. A., Vaughan, D. G., van den Broeke, M. R. and Padman, L. (2012). Antarctic ice-sheet loss driven by basal melting of ice shelves. *Nature*, *484*(7395), 502–505. http://dx.doi.org/10.1038/nature10968

Rignot, E., Mouginot, J., Morlighem, M., Seroussi, H. and Scheuchl, B. (2014). Widespread, rapid grounding line retreat of Pine Island, Thwaites, Smith, and Kohler glaciers, West Antarctica, from 1992 to 2011. *Geophysical Research Letters*, *41*(10), 3502–3509. http://dx.doi.org/10.1002/2014GL060140

Rolandone, F., Jaupart, C., Mareschal, J., Gariépy, C., Bienfait, G., Carbonne, C. and Lapointe, R. (2002). Surface heat flow, crustal temperatures and mantle heat flow in the Proterozoic Trans-Hudson Orogen, Canadian Shield. *Journal of Geophysical Research: Solid Earth*, *107*(B12), 1978–2012. http://dx.doi.org/10.1029/2001JB000698

Rolandone, F., Mareschal, J., Jaupart, C., Gosselin, C., Bienfait, G. and Lapointe, R. (2003a). Heat flow in the western Superior Province of the Canadian Shield. *Geophysical Research Letters*, *30*(12). http://dx.doi.org/10.1029/2003GL017386

Rolandone, F., Mareschal, J.-C. and Jaupart, C. (2003b). Temperatures at the base of the Laurentide Ice Sheet inferred from borehole temperature data. *Geophysical Research Letters*, *30*(18). http://dx.doi.org/10.1029/2003GL018046

Rutherford, S., Mann, M., Osborn, T., Briffa, K., Jones, P. D., Bradley, R. and Hughes, M. (2005). Proxy-based Northern Hemisphere surface temperature

reconstructions: sensitivity to method, predictor network, target season, and target domain. *Journal of Climate*, *18*(13), 2308–2329. http://dx.doi.org/http://dx.doi.org/10.1175/JCLI3351.1

Šafanda, J., Szewczyk, J. and Majorowicz, J. (2004). Geothermal evidence of very low glacial temperatures on a rim of the Fennoscandian ice sheet. *Geophysical Research Letters*, *31*(L07211). http://dx.doi.org/10.1029/2004GL019547

Sass, J. H., Lachenbruch, A. H. and Jessop, A. M. (1971). Uniform heat flow in a deep hole in the Canadian Shield and its paleoclimatic implications. *Journal of Geophysical Research*, *76*(35), 8586–8596. http://dx.doi.org/10.1029/JB076i035p08586

Schmidt, G. A., Kelley, M., Nazarenko, L., Ruedy, R., Russell, G. L., Aleinov, I., Bauer, M., Bauer, S. E., Bhat, M. K., Bleck, R., Canuto, V., Chen, Y.-H., Cheng, Y., Clune, T. L., Del Genio, A., de Fainchtein, R., Faluvegi, G., Hansen, J. E., Healy, R. J., Kiang, N. Y., Koch, D., Lacis, A. A., LeGrande, A. N., Lerner, J., Lo, K. K., Matthews, E. E., Menon, S., Miller, R. L., Oinas, V., Oloso, A. O., Perlwitz, J. P., Puma, M. J., Putnam, W. M., Rind, D., Romanou, A., Sato, M., Shindell, D. T., Sun, S., Syed, R. A., Tausnev, N., Tsigaridis, K., Unger, N., Voulgarakis, A., Yao, M.-S. and Zhang, J. (2014). Configuration and assessment of the GISS ModelE2 contributions to the CMIP5 archive. *Journal of Advances in Modeling Earth Systems*, *6*(1), 141–184. http://dx.doi.org/10.1002/2013MS000265

Schneider, D. P., Steig, E. J., van Ommen, T. D., Dixon, D. A., Mayewski, P. A., Jones, J. M. and Bitz, C. M. (2006). Antarctic temperatures over the past two centuries from ice cores. *Geophysical Research Letters*, *33*(L16707). http://dx.doi.org/10.1029/2006GL027057

Schuur, E. A., Bockheim, J., Canadell, J. G., Euskirchen, E., Field, C. B., Gory-

achkin, S. V., Hagemann, S., Kuhry, P., Lafleur, P. M., Lee, H., Mazhitova, G., Nelson, F. E., Rinke, A., Romanovsky, V., Shiklomanov, N., Tarnocai, C., Venevsky, S., Vogel, J. G. and Zimov, S. A. (2008). Vulnerability of permafrost carbon to climate change: implications for the global carbon cycle. *BioScience*, *58*(8), 701–714. http://dx.doi.org/10.1641/B580807

Shen, P. and Beck, A. (1992). Paleoclimate change and heat flow density inferred from temperature data in the Superior Province of the Canadian Shield. *Palaeogeography, Palaeoclimatology, Palaeoecology*, *98*(2), 143–165. http://dx.doi.org/10.1016/0031-0182(92)90194-A

Shen, P. Y. and Beck, A. E. (1983). Determination of surface temperature history from borehole temperature gradients. *Journal of Geophysical Research: Solid Earth*, *88*(B9), 7485–7493. http://dx.doi.org/10.1029/JB088iB09p07485

Shen, P. Y. and Beck, A. E. (1991). Least squares inversion of borehole temperature measurements in functional space. *Journal of Geophysical Research: Solid Earth*, *96*(B12), 19965–19979. http://dx.doi.org/10.1029/91JB01883

Springer, M. (1997). *Die regionale Oberflachenwarmeflussdichte-Verteilung in den zentralen Anden und daraus abgeleitete Temperaturmodelle der Lithosphare.* (Thèse de doctorat). Friene Universität Berlin.

Springer, M. and Förster, A. (1998). Heat-flow density across the Central Andean subduction zone. *Tectonophysics*, *291*(1), 123–139. http://dx.doi.org/doi:10.1016/S0040-1951(98)00035-3

Straneo, F. and Heimbach, P. (2013). North Atlantic warming and the retreat of Greenland's outlet glaciers. *Science*, *504*, 36–43. http://dx.doi.org/10.1038/nature12854

Suárez, F., Dozier, J., Selker, J. S., Hausner, M. B. and Tyler, S. W. (2011). *Heat transfer in the environment: Development and use of fiber-optic distributed temperature sensing.* INTECH Open Access Publisher. http://dx.doi.org/10.5572/19474

Taylor, A., Wang, K., Smith, S., Burgess, M. and Judge, A. (2006). Canadian Arctic Permafrost Observatories: detecting contemporary climate change through inversion of subsurface temperature time series. *Journal of Geophysical Research, 111*(B2). http://dx.doi.org/10.1029/2004JB003208

Taylor, K. E., Stouffer, R. J. and Meehl, G. A. (2012). An overview of CMIP5 and the experiment design. *Bulletin of the American Meteorological Society, 93*(4), 485. http://dx.doi.org/10.1175/BAMS-D-11-00094.1

Thibault, S. and Payette, S. (2009). Recent permafrost degradation in bogs of the James Bay area, northern Quebec, Canada. *Permafrost and Periglacial Processes, 20*(4), 383–389. http://dx.doi.org/10.1002/ppp.660

Uyeda, S. and Watanabe, T. (1970). Preliminary report of terrestrial heat flow study in the South American continent; distribution of geothermal gradients. *Tectonophysics, 10*(1-3), 235–242. http://dx.doi.org/10.1016/0040-1951(70)90109-5

Uyeda, S. and Watanabe, T. (1982). Terrestrial heat flow in western South America. *Tectonophysics, 83*(1-2), 63–70. http://dx.doi.org/10.1016/0040-1951(82)90007-5

Vasseur, G., Bernard, P., de Meulebrouck, J. V., Kast, Y. and Jolivet, J. (1983). Holocene paleotemperatures deduced from geothermal measurements. *Palaeogeography, Palaeoclimatology, Palaeoecology, 43*(3–4), 237 – 259. http://dx.doi.org/10.1016/0031-0182(83)90013-5

Velicogna, I. and Wahr, J. (2013). Time-variable gravity observations of ice sheet mass balance: Precision and limitations of the GRACE satellite data. *Geophysical Research Letters*, *40*(12), 3055–3063. http://dx.doi.org/10.1002/grl.50527

Viau, A. and Gajewski, K. (2009). Reconstructing millennial-scale, regional paleoclimates of boreal Canada during the Holocene. *Journal of Climate*, *22*(2), 316–330. http://dx.doi.org/10.1175/2008JCLI2342.1

Viau, A. E., Ladd, M. and Gajewski, K. (2012). The climate of North America during the past 2000 years reconstructed from pollen data. *Global and Planetary Change*, *84*, 75–83. http://dx.doi.org/10.1016/j.gloplacha.2011.09.010

Villalba, R., Grosjean, M. and Kiefer, T. (2009). Long-term multi-proxy climate reconstructions and dynamics in South America (LOTRED-SA): state of the art and perspectives. *Palaeogeography, Palaeoclimatology, Palaeoecology*, *281*(3), 175–179. http://dx.doi.org/10.1016/j.palaeo.2009.08.007

Vitorello, I., Hamza, V. and Pollack, H. N. (1980). Terrestrial heat flow in the Brazilian highlands. *Journal of Geophysical Research: Solid Earth*, *85*(B7), 3778–3788. http://dx.doi.org/10.1029/JB085iB07p03778

von Gunten, L., Grosjean, M., Rein, B., Urrutia, R. and Appleby, P. (2009). A quantitative high-resolution summer temperature reconstruction based on sedimentary pigments from Laguna Aculeo, central Chile, back to AD 850. *The Holocene*, *19*(6), 873–881. http://dx.doi.org/10.1177/0959683609336573

Wang, K. (1992). Estimation of ground surface temperatures from borehole temperature data. *Journal of Geophysical Research: Solid Earth*, *97*(B2), 2095–2106. http://dx.doi.org/10.1029/91JB02716

Wang, K. and Lewis, T. J. (1992). Geothermal evidence from Canada for a cold period before recent climatic warming. *Science*, *256*(5059), 1003–1005. http://dx.doi.org/10.1126/science.256.5059.1003

Wang, K., Lewis, T. J. and Jessop, A. M. (1992). Climatic changes in central and eastern Canada inferred from deep borehole temperature data. *Global and planetary change*, *6*(2), 129–141. http://dx.doi.org/10.1016/0921-8181(92)90031-5

Watanabe, T., Uyeda, S., Guzman Roa, J., Cabré, R. and Kuronuma, H. (1980). Report of Heat Flow Measurements in Bolivia. *Bulletin of the Earthquake Research Institute*, *55*, 43–54.

Wisian, K. W., Blackwell, D. D., Bellani, S., Henfling, J. A., Normann, R. A., Lysne, P. C., Förster, A. and Schrötter, J. (1997). How hot is it? (A comparison of advanced technology temperature logging systems). *Geothermal Resources Council Transactions*, *20*, 427–434.

Yukimoto, S., Adachi, Y., Hosaka, M., Sakami, T., Yoshimura, H., Hirabara, M., Tanaka, T. Y., Shindo, E., Tsujino, H., Deushi, M., Mizuta, R., Yabu, S., Obata, A., Nakano, H., Koshiro, T., Ose, T. and Kitoh, A. (2012). A new global climate model of the Meteorological Research Institute: MRI-CGCM3—model description and basic performance. *Journal of the Meteorological Society of Japan*, *90A*, 23–64. http://dx.doi.org/10.2151/jmsj.2012-A02

Zhang, T. (2005). Influence of the seasonal snow cover on the ground thermal regime: An overview. *Reviews of Geophysics*, *43*(4). http://dx.doi.org/10.1029/2004RG000157

Zwally, H. J., Abdalati, W., Herring, T., Larson, K., Saba, J. and Steffen, K.

(2002). Surface Melt-Induced Acceleration of Greenland Ice-Sheet Flow. *Science*, *297*(5579), 218–22. http://dx.doi.org/10.1126/science.1072708

Zweck, C. and Huybrechts, P. (2005). Modeling of the Northern Hemisphere ice sheets during the last glacial cycle and glaciological sensitivity. *Journal of Geophysical Research*, *110*(D07103), 1984–2012. http://dx.doi.org/10.1029/2004JD005489